nagra

Arbeitsbericht NAB 23-09

Aqueous Corrosion of Vitrified Nuclear Waste:

Current Process Understanding, Literature Review and Recommended Rates

November 2022

E. Curti

National Cooperative
for the Disposal of
Radioactive Waste

Hardstrasse 73
P.O. Box
5430 Wettingen
Switzerland
Tel. +41 56 437 11 11

nagra.ch

nagra.

Arbeitsbericht NAB 23-09

Aqueous Corrosion of Vitrified Nuclear Waste:

Current Process Understanding, Literature Review and Recommended Rates

November 2022

E. Curti

Laboratoryfor Waste Management (LES),
Paul Scherrer Institut (PSI)

KEYWORDS
Borosilicate glass, corrosion rate, alteration, durability

National Cooperative
for the Disposal of
Radioactive Waste

Hardstrasse 73
P.O. Box
5430 Wettingen
Switzerland
Tel. +41 56 437 11 11

nagra.ch

Nagra Arbeitsberichte ("Working Reports") present the results of work in progress that have not necessarily been subject to a comprehensive review. They are intended to provide rapid dissemination of current information.

Table of Contents

List of Tables

List of Figures

List of Acronyms

AREVA	former ORANO
AVM	French vitrified waste from graphite-moderated natural U reactors
BNFL	former BNGS, now Sellafield Ltd.
BNGS	British Nuclear Group Sellafield (formerly BNFL)
CASH	Calcium Alumina Silicate Hydrates
CEA	Commissariat à l'Energie Atomique et aux énergies alternatives
COGEMA	former ORANO
COx	Callovian-Oxfordian claystone formation
CORALUS	Underground laboratory experimental program (Belgium)
CSH	Calcium Silicate Hydrates
EDS	Energy Dispersive X-ray Spectroscopy (X-ray emission detection system)
FIB	Focused Ion Beam
GLADIS	GLAss DISsolution integrated model
GRAAL	Glass Reactivity with Allowance for the Alteration Layer Model
HAADF	High-Angle Annular Dark-Field imaging
HLW	High-Level Waste (spent fuel and vitrified waste from reprocessing)
HRTEM	High Resolution Transmission Electron Microscopy
IDA	Inter-Diffusion-Affinity (glass dissolution model)
IDP	Interfacial-Dissolution-Precipitation (glass dissolution model)
IRF	Instant Release Fraction
ISG	International Simple Glass
JSS	joint Japanese (CRIEPI), Swiss (NAGRA), Swedish (SKB) project
LA-ICPMS	Laser Ablation- Inductively Coupled Plasma Mass Spectrometry
LES	Laboratory for Waste Management (Paul Scherrer Institut)
MCC	Materials Characterization Center (glass leach tests)
MW	Magnox Waste glass inactive simulant (BNFL, U.K.)
NAB	Nagra Working Report (Nagra Arbeitsbericht)
NL	Normalized Mass Loss (of corroded glass)
NTB	Nagra Technical Report (Nagra Technischer Bericht)
OPC	Ordinary Portland Cement
ORANO	Multinational nuclear fuel cycle company, formerly AREVA, COGEMA

PNNL	Pacific Northwest National Laboratory
PRI	Passivating Reactive Interface
PSI	Paul Scherrer Institut
R7T7	French vitrified waste from UO_2 fuel (ORANO, F)
SGT	Sachplan Geologische Tiefenlager (Sectoral Plan)
SEM	Scanning Electron Microscopy
SON68	non-radioactive simulant of R7T7 glass (ORANO, F)
S/V	glass Surface area to solution Volume ratio
STRENG	Source term model for vitrified HLW
TEM-EDX	Transmission Electron Microscopy – Energy Dispersive X-ray Spectroscopy
Tof-SIMS	Time of flight secondary ion mass spectrometry
XANES	X-ray Absorption Near Edge Spectroscopy
XRD	X-Ray Diffraction
XRF	X-Ray Fluorescence
YCPW	Young Cement Pore Water
ZWILAG	Zwischenlager Würenlingen AG

1 Introduction

1.1 Vitrified radioactive waste in Switzerland

In the early stage of the Swiss disposal program, reprocessing and vitrification of all spent nuclear fuel was the option chosen for the disposal of high-level radioactive waste in a deep geological repository. To this aim, long-term contracts were stipulated with ORANO (formerly AREVA/COGEMA) in France and with Sellafield Ltd. (formerly BNFL/BNGS) in the United Kingdom (Nagra 2014a). The vitrified reprocessed waste was then returned, after separation of U and Pu, from the two reprocessing plants in La Hague and Sellafield and are currently stored in the ZWILAG interim storage facility in Würenlingen. The vitrified waste packages consist of stainless steel coquilles (a few mm-thick), each enclosing 182 L of solidified borosilicate glass. The contractors provided distinct specifications, resulting in two reference borosilicate glass compositions and inventories. These are defined in Nagra's most recent inventory catalogue (Nagra 2023) as waste sorts WA-F-KG-K1-HAA and WA-U-KG-K1-HAA, respectively.

In 2006, the Swiss federal government enforced a reprocessing moratorium. From that date on, reprocessing of waste arising from Swiss reactors was dismissed and Nagra had to pursue a strategy involving, in addition to vitrified waste, the direct disposal of untreated spent fuel. Consequently, both types of high-level waste will have to be disposed of in the planned Swiss repository. According to current projections, about 1/3 of the total activity will be in the form of borosilicate glass and the remaining 2/3 as spent fuel. This implies that the safety case for a geological repository requires robust scientific knowledge for both types of waste. Although after the moratorium research efforts in the field of glass corrosion have been reduced in Switzerland in favour of spent fuel research, sufficient knowledge is provided by the intense research conducted by the international scientific community in recent years. The recent studies carried out in France, Belgium and United Kingdom are particularly relevant for the Swiss program, as they investigate the same types of borosilicate glass returned to Switzerland.

1.2 Summary of previous work conducted at PSI

Work on nuclear waste glass corrosion started at PSI in the early eighties of the past century. At that time, the knowledge on degradation processes of borosilicate glass in aqueous media was quite limited, calling for extensive experimental glass corrosion studies to provide a sufficiently large basis of data. A major step in this direction was the so-called "JSS project[1]" carried out between 1984 and 1988. During this project (co-financed by Nagra and other waste management organisations), a large number of glass corrosion tests with both active and non-active glasses were carried out under a wide variety of conditions in the laboratories of PSI and Studsvik (Sweden). A synthesis of results from the JSS project can be found in a technical note (Curti 2018) complemented by an electronic database. Both documents are freely available in electronic form under https://www.psi.ch/de/les/glassdatabase).

The "JSS project" set the basis for the empirical understanding of the corrosion kinetics of the two reference borosilicate glasses, denoted SON68 and MW[2], corresponding to the specifications of ORANO (F) and Sellafield Ltd. (UK), respectively (see simplified compositions in Tab. 1-1).

---

[1] joint **J**apanese (CRIEPI), **S**wiss (Nagra), **S**wedish (SKB) project

[2] The two glasses are non-radioactive simulations of the actual HLW glasses. The acronym MW stays for Magnox-Waste. Although no Swiss reactor is of Magnox type, Sellafield Ltd. returns to Switzerland vitrified Magnox waste with a total activity equivalent to the spent fuel activity delivered for reprocessing. Because Magnox reactors operate with natural uranium rods inserted in an Mg-alloy cladding, the MW glass is enriched in Mg.

For static experiments with no refill of water, a large body of data at 90 °C clearly showed initial fast dissolution rates in the order of about 0.1 – 1 g m^{-2} d^{-1}, followed by an asymptotic decrease of the rate by 3 – 4 orders of magnitude within a few weeks or months. Apparently, the rate reached a stable minimum value within 1 – 2 years, the so-called *residual rate*[3], which was used in the reference scenario of previous Nagra's safety assessments to define a "source term" for radionuclide release into the bentonite buffer.

The large number of experiments carried out during the JSS project allowed assessing the dependence of glass corrosion kinetics on key chemical/physical parameters (such as alpha-activity, temperature and pH) and studying the influence of engineered barrier materials (bentonite and iron corrosion products). Yet, these data are inconclusive for the evaluation of the long-term corrosion behaviour of borosilicate glass due to limited leaching times (two years or less) which is not sufficient to ascertain whether final steady state corrosion rates had been really attained. Moreover, the chosen technique of determining corrosion rates from several parallel experiments generally led to large uncertainties in the calculated corrosion rates.

In order to obtain more reliable and precise values of the *residual rate*, long-term glass corrosion experiments with a minimum foreseen duration of 5 years were started at PSI soon after completion of the JSS project (on December 19th 1990). A short description of the kinetic results is provided in Section 4.3.4 of this report. A detailed documentation of all scientific results in connection with these experiments can be found in Curti (2003), Curti et al. (2006, 2009, 2012) and Gin et al. (2013a).

In contrast to the JSS project, large solution volumes of distilled water and glass amounts were used, allowing a sequential aqueous solution sampling technique that improved the precision of the rate determination for each single experiment. Moreover, for each of the two glass types used (SON68 and MW) five identical experiments were carried out, making it possible to assess the reproducibility of the *residual rate*. After 10 years leaching at 90 °C, residual corrosion rates of 1.3 (± 0.2) x 10^{-4} g m^{-2} d^{-1} and 9.6 (± 5.3) × 10^{-4} were determined from the dissolution of boron for SON68 and MW glass, respectively (Curti 2003).

Besides the assessment of dissolution kinetics, another objective of the PSI long-term experiments was to determine the selective retention of radionuclides, i.e. to quantify the percentage of radionuclides that did not undergo dissolution and remained trapped in the glass alteration layer or in secondary corrosion products (Curti et al. 2006). A major result was that more than 95% of the inventories of all elements representing dose-relevant nuclides (including Cs) was retained in the degraded glass, i.e. less than 5% of the inventories in the reacted glass was effectively released to the solution and thus susceptible to become mobile. The retention of lanthanides, U, Th, Zr, and Sr was even higher (> 99%).

The secondary solids formed during the glass dissolution process were characterized via advanced techniques, with specific emphasis on the trapping of dose-relevant nuclides. Transmission electron microscopy coupled with X-ray fluorescence analyses (Curti et al. 2006) allowed determining the chemical composition of secondary clay-like minerals formed during the glass degradation. Whereas corrosion of the MW glass led to formation of abundant Mg-clay (saponite), only small amounts of poorly crystalline Ca-Zn clay was formed during corrosion of the SON68 glass. This reflects the minor, but critical differences in the composition of the two glasses (see Tab. 1-1).

---

[3] The term residual rate is used in this report in a purely empirical way, i.e. it is not associated to a model. For instance, a residual rate can be calculated with the help of the "affinity law" model (Section 6.2) once specific parameters such as the "silica saturation" concentration are known. Here, it is defined as asymptotic value of NL(B) or NL(Li) derived from a specific experiment of sufficient duration.

X-ray absorption spectroscopy and micro-diffraction investigations were conducted at a spatial resolution of few µm. These studies (Curti et al. 2009, 2012) aimed at identifying trapping mechanisms of selected elements representing dose-relevant radionuclides (Ni, Cs) or their analogues. This type of study was possible only on MW glass samples. Due to the much slower corrosion rate, the amount and size of secondary solids formed during leaching of the SON68 glass was not sufficient for application of this technique. We could assess that cerium (chemical analogue for Pu) is efficiently trapped via reductive coprecipitation in the secondary Mg-clays. Moreover, Ni was found to partition preferentially in micro-particles of trevorite ($NiFeO_4$) formed during the glass synthesis. This means that the release of the dose-relevant nuclides ^{63}Ni and ^{59}Ni from the vitrified waste will not be controlled by the rate of glass matrix dissolution, but by the stability of trevorite in the aqueous solution in contact with the waste.

Tab. 1-1: Composition of SON68 (ORANO) and MW (Sellafield, Ltd.) glasses

After Zwicky et al. (1992)

Components with largely different contents in the two glasses are highlighted in bold.

	SON68	**MW**		**SON68**	**MW**
Al_2O_3	4.91	5.33	Na_2O	9.86	8.10
B_2O_3	14.02	16.65	Nd_2O_3	1.59	1.61
BaO	0.60	0.57	NiO	0.74	0.27
CaO	**4.04**	**0.03**	P_2O_5	0.28	0.18
CeO_2	0.98	1.02	$Pr_6\ O_{11}$	0.44	1.02
Cr_2O_3	0.51	0.41	SO_4	0.00	0.07
Cs_2O	1.42	1.13	SiO_2	45.48	46.20
Fe_2O_3	2.91	2.69	Sm_2O_3	0.00	0.32
K_2O	0.00	0.00	SrO	0.33	0.36
La_2O_3	0.90	0.52	ThO_2	0.33	0.00
Li_2O	1.98	3.79	UO_2	0.52	0.00
MgO	**0.00**	**5.85**	Y_2O_3	0.20	0.21
MnO_2	0.72	0.00	**ZnO**	**2.50**	**0.00**
MoO_3	1.70	1.76	ZrO_2	2.65	1.71

1.3 International research on glass corrosion

In the past years, active research on vitrified waste corrosion has not been prioritised in Switzerland as well as in other countries that foresee direct disposal of spent fuel disposal (e.g. Sweden, Finland). On the contrary, research activities on this topic are continuously conducted in countries where all or the majority of the HLW will disposed of in vitrified form (e.g. France, Belgium) or where a final decision has to be taken (U.S., U.K., Germany).

In contrast to the mostly empirical and generic experimental studies conducted in the past century, aiming at quantifying the kinetics of borosilicate glass dissolution as a function of chemical-physical and environmental parameters, present-day research focuses on mechanistic studies and integrated setups. Specifically, the majority of modern studies aim at: (i) identifying and quantifying the fundamental mechanisms driving the glass corrosion process, (ii) studying the long-term corrosion process under faithful repository conditions, (iii) characterizing archaeological or natural analogues to unravel the behaviour of vitrified waste on a time scale not accessible in the laboratory. These new studies benefit from the advances in modern analytical techniques, which now allow chemical and physical analyses with resolution at the nanometre or even atomic scales.

Item (ii) implies a clear shift from the simple, standardized leach tests towards complex setups aiming at reproducing the repository environment as closely as possible. However, it must be understood that even when optimized and at full scale (e.g. in an underground laboratory), integrated mock-up experiments will never reliably mimic the actual behaviour of a nuclear glass canister under geological repository conditions, as too many coupled processes are at play over an experimentally inaccessible timescale. Archaeological and natural analogues (item iii) are certainly useful in extending the observation timescale to geological times; however they reproduce only partially the geometry and material characteristics of a repository. In conclusion, it can be stated that a precise prediction of vitrified waste dissolution and alteration in a repository environment is not possible. Nevertheless, integration of all the available knowledge from the different experimental methods will help to build reliable estimates on long-term dissolution rates.

International research on glass corrosion is maintained at a high scientific level by a network of well-interconnected researchers (Gin et al. 2013b). There are two leading groups, namely the "Service d'études de vitrification et procédés hautes températures (DE2D/SEVT)" at the Commissariat à l'Energie Atomique (CEA) in Marcoule, France and a dedicated group at the Pacific Northwest National Laboratory (PNNL), U.S. Because the research conducted at CEA is focussed to the ORANO-type glass compositions, many results are directly applicable to the Swiss program. Moreover, U.K. has recently resumed its research on Magnox-type (MW) glasses after two decades-long break, which is also applicable to the Swiss program. In this report, we review the recent data provided by the aforementioned groups and assess its relevance for the Swiss performance assessment.

1.4 Goals and structure of this report

The main goal of this report is to provide an *overview* of the progress made in nuclear glass corrosion research during the past two decades, i.e. starting from about the year 2000, and to recommend glass corrosion rates for Nagra's safety assessment. This is achieved through a *selective* review of published studies, i.e. only studies judged by the author to have either seminal character for the development of the field or to be directly relevant for the Swiss safety assessment will be discussed in detail. The review is embedded in the thematic framework set by the following chapters:

Chapter 2: General purpose section on the atomic structure, composition and general physical-chemical properties of nuclear waste glasses, putting the compositions of the Swiss glasses in a broad perspective

Chapter 3: Description of mechanistic atomic-scale models of glass dissolution

Chapter 4: A section devoted to a review of experimental data on glass corrosion kinetics (from laboratory, field and archaeological analogues) and its dependence on physical/ chemical parameters

Chapter 5: A Section devoted to experiments quantifying the selective release of radionuclides (or analogues thereof) during aqueous glass alteration

Chapter 6: A Section devoted to models predicting the dependency of borosilicate glass dissolution kinetics on chemical and other environmental factors, with emphasis on those applicable to integrated systems compatible with the Swiss disposal concept

Chapter 7: Description of Swiss repository concept and safety assessment model. Selection and justification of glass corrosion rates recommended for the upcoming Swiss safety assessment (SGT-3)

2 Structure, composition and properties of nuclear waste glasses

2.1 Physical properties of glasses

Despite the widespread occurrence of natural and artificial glass in everyday life, it is not easy to give a precise definition of this material. In the excellent monography of Gutzow & Schmelzer (2013) an entire Section (2.1) is dedicated to this topic, at the end of which the authors do not dare giving a final definition. The best approach to a definition is perhaps one based on the comparison of physical properties of glasses (vitreous materials) and crystalline solids. A key (though not sufficient) difference is that glasses are, contrary to crystals, XRD-amorphous due to the lack of long-range order in their structure. SiO_2 can exist both as glass and as several crystalline polymorphs, whereby the latter can be readily identified in an XRD analysis by the presence of well-defined reflections following Bragg's law.

The following conditions favour vitreous instead of crystalline solidification (Vogel 1979, p. 37): (a) the large increase in viscosity during cooling due to polymerisation of "molecular units" e.g. interlinking of SiO_4-tetrahedra in the case of silicate glasses; (b) fast cooling (quenching) which inhibits the mobility and thus ordering of the tetrahedral units.

The thermodynamic properties of glasses differ from those of compositionally equivalent crystalline solids. For instance, the heat capacity curve of a glass does not exhibit the typical discontinuity observed for crystalline solids at their well-defined melting temperature. Instead, a continuous sigmoidal decrease of the heat capacity with simultaneous strong (but not discontinuous) increase in viscosity is observed as the melt solidifies as glass (Fig. 2.3 in Vogel 1979). The inflection point in the sigmoidal portion of the heat capacity curve is defined as glass transition temperature (T_g) which can be regarded as analogous (but not identical) to the crystallization (melting) temperature (T_m) defining the change from liquid to solid state of a crystal. Contrary to the melting temperature in crystalline materials, T_g is not a fixed material property of the glass, as it varies with the cooling rate. Not only temperature, also other key physical properties, e.g. the expansion coefficient, may lack in glasses the typical discontinuities of liquid to solid transitions observed for crystalline materials.

From the previous description, one may tentatively define glass as *a supercooled, metastable solid characterized by the absence of a well-defined melting temperature and long-range order*.

2.2 Crystal-chemical properties of glass

The existence of complex molecular units with the capability to form polymeric structures is a necessary condition for the formation of glasses. This puts restrictions to the chemical boundaries allowing formation of homogeneous vitreous materials. Much effort has been devoted to the prediction of compositional spaces suitable to synthesize glasses with the desired properties. Already Goldschmidt (1926) set up a simple crystal chemical rule to predict whether any binary ionic compound would be able to form a glass. He stated that only compounds with cation radius to anion radius ratio between about 0.2 and 0.4 are likely to produce glass at normal cooling rates. For oxides, this rule successfully predicts that SiO_2, P_2O_5 and B_2O_3 are glass formers, while e.g. NaO, CaO, K_2O are not. This rule has however notable failures, as it is impossible to make Al_2O_3 glasses under normal quenching conditions (Rosenflanz et al. 2004) although the Al/O ratio obeys it.

Zachariasen (1932) and Warren (1933) later defined more precise and reliable criteria. Most importantly, they found that glass formation is favoured when cations form with the anions three-fold or tetrahedrally coordinated corner-shared polyhedra. In the latter case 3D-networks can form, leading to highly viscous melts that hinder nucleation and growth of crystals.

A multicomponent silica glass can be rationalised by the generic formula A_mX_nO (Zachariasen, 1932) where both *m* and *n* are less than 1. In this generic formula, X represents the so-called *network formers*, i.e. the small cations (B^{3+}, P^{5+}, Si^{4+}, Ge^{4+}) at the center of the polymerizing X_nO polyhedra, whereas A represents *network modifiers*, i.e. larger low-charge cations (e.g. Na^+, K^+, Ca^{2+}, Ba^{2+}, Sr^{2+}, Pb^{2+}) that are unable to enter the network-formers polyhedra due to the higher coordination numbers required. They thus fill the "interstitial holes" in the structure, at the same time compensating the excess negative charge generated by non-bonded oxygen ions (NBO). Some elements form cations that may be either tetrahedrally or octahedrally coordinated and therefore can assume both the role of network formers or modifiers (e.g. Al^{3+}, Zn^{2+}, Fe^{3+}).

Dietzel (1942) refined Zachariasen's classification by introducing the concept of field strength *F*. This is expressed by the formula $F = Z/a^2$, where *Z* is the cation charge and *a* is the cation-oxygen interatomic distance. With the help of this parameter, network modifiers are identified by the range $F = 0.1 – 0.4$, while network formers fall in the range $F = 1.3 – 2.0$ and the "ambivalent" cations are characterized by intermediate *F*-values. Moreover, the difference $\Delta F = |F(\text{oxide1}) - F(\text{oxide 2})|$ is a useful criterion to decide whether a mixture of two network-former oxides will result in a homogeneous glass or in distinct unmixed phases. Homogeneous glasses are obtained if $\Delta F < 0.3$, as in the case of B_2O_3-SiO_2. In contrast, the solidification of SiO_2-P_2O_5 or B_2O_3-P_2O_5 melts results in unmixing since $\Delta F \approx 0.5$.

Recent advances in experimental methods and molecular modelling nowadays allow a precise determination of the structure of silicate glasses. Advanced techniques such X-ray photoelectron spectroscopy (XPS), small angle X-ray scattering (SAXS), infrared spectroscopy (IR) and Nuclear magnetic resonance (NMR) are currently used to reveal the influence of composition on bond distances and network polyhedra linkages (Reiser et al. 2021, Lu et al. 2021).

2.3 Optimization of nuclear waste glass composition

Because SiO_2 and B_2O_3 are miscible in all proportions, while SiO_2 and P_2O_5 are not (Vogel 1979) two distinct groups of glasses suitable for immobilization of radioactive waste have been developed so far: borosilicate and phosphate glasses (Tab. 2-1). The extensive miscibility of silica and borate explains the wide use of borosilicate in glass technology and ultimately their selection as favourite matrix for vitrified nuclear waste. Borosilicate glass proved to have a number of advantageous properties with respect to alternative formulations, not only as a matrix for radioactive waste: by varying appropriately the SiO_2-B_2O_3 ratio, a lower thermal expansion coefficient is obtained compared to Ca oxide glasses, which had been previously used for electric lamps and other glassware. Minimization of thermal expansion is important also for nuclear waste glasses, in order to reduce cooling-induced fragmentation (thus minimizing the surface area exposed to intruding water). Moreover, the chemical resistance of borosilicate glasses to aqueous leaching, though weaker than that of pure SiO_2 glass, is good and their flexible structure can accommodate for a large amount and a variety of network modifiers, including most of the dose-relevant actinides and fission products. Finally, production of borosilicate glasses takes advantage of an advanced production technology, as it is the most widespread glass type for optical and other technical purposes, including well-known types such as Pyrex or Duran glasses.

It is therefore logical that borosilicate glass became the most widespread matrix for reprocessed nuclear waste, however with a much lower Si/B ratio compared to usual borosilicate glasses, due to the need of incorporating a large amount of radionuclides (up to 10 – 15 wt.-%). Low Si/B ratios have the beneficial side effect to reduce the transition (i.e. "solidification") temperature and

thus limit the undesired vaporization of volatile and semi-volatile radionuclides (e.g. ^{135}Cs, ^{99}Tc). Borosilicate glasses are melted between 1'000 °C and 1'200 °C (Gin et al. 2017) compared to 1'600 °C for pure SiO_2 glass. The cost for these favourable properties, on the other hand, is a reduction of the chemical resistance against aqueous attack with increasing boron content.

Tab. 2-1 shows the (simplified) composition of several nuclear waste glasses worldwide, compared to the composition of selected commercial glasses. It illustrates the preference of borosilicate glasses over phosphate glasses as matrix of nuclear waste. Tab. 2-1 also shows that nuclear waste glasses have much lower silica contents than commercial borosilicate glasses.

Tab. 2-1: Simplified composition of SON68 and MW glasses, compared to the compositions of other nuclear waste glasses and commercial non-active borosilicate glasses

Empty cells indicate contents of less than 0.1 wt.-%.

Oxides [wt.-%]	**Nuclear waste glasses**					**Commercial borosilicate glasses**		
	SON68[1] [F]	**MW**[1] [UK]	**DFPW**[2] [USA]	**GP WAK1**[3] [D]	**Mayak**[4] [Ru.]	**Duran**[5]	**Pyrex**[5]	**Supremax**[5] [Thermometers]
Al_2O_3	4.9	5.3	4.0	2.6	19.0	3.5	2.2	21.0
B_2O_3	14.0	16.7	8.0	14.8		14.0	12.0	10.0
BaO	0.6	0.6	0.2			3.0		
CaO	4.0		1.0	4.5				5.0
Fe_2O_3	2.9	2.7	10.3					
K_2O			3.8					
Li_2O	2.0	3.8	4.4	2.9				
MgO		5.9	1.3	1.8				10.0
MoO_2	1.7	1.8						
Na_2O	9.9	8.1	8.7	10.3	21.2	4.5	4.3	
P_2O_5	0.3	0.2			52.0			
SiO_2	45.5	46.2	49.8	50.4		74.0	80.8	53.0
TiO_2				1.0				
ZnO	2.5		0.1					
Others*	11.7	8.8	8.6	11.7	7.8	1.0	0.7	1.0

1 Zwicky et al. (1992)
2 Tab. 2 in Plodinec (2000)
3 Lukscheiter & Nesovic. (1996)
4 Ojovan et al. (2019)
5 Vogel (1979), p. 37
* Other minor oxides, mainly representing radionuclides

2.4 Solubility of radionuclides in borosilicate glass

The presence of trivalent boron in silicate glasses partially disrupts the polymeric structure of the glass and introduces a charge deficit that must be compensated by cationic network modifiers (Ojovan et al. 2019). It is this effect that allows for incorporation of a large amount and variety of radionuclides in the borosilicate glass matrix (up to about 35 wt.-%, see Mendel 1986 and Tab. 19.2 in Ojovan et al. 2019). Borosilicate nuclear glass formulations are optimized via addition of a number of minor oxides, such that the highest possible radionuclide loading is obtained by keeping the chemical resistance to aqueous corrosion sufficiently high and $T_g \approx$ 1'100 – 1'250 °C (Ojovan et al. 2019).

Due to the widely different ionic radii and chemical properties of actinides and fission products, distinct solubilities and modes of incorporation are expected. Glass-soluble ions are incorporated at well-defined structural positions, either as network former in A_nO polyhedra (network formers) or in interstitial X position (network modifiers). According to Tab. 19.4 in Ojovan et al. (2019), most dose-relevant radionuclides have sufficiently high solubilities in silicate glasses to guarantee homogeneous distribution as truly dissolved ions. Such ions will then be released congruently (i.e. in proportion to the rate of dissolution of the A_nO network) during aqueous corrosion, as long as their solubility limit in the leaching aqueous solution is not reached.

However, not all radionuclides will be incorporated in A or X positions. The solubility of an element in silicate glasses strongly depends on its oxidation state. Noble metals (e.g. Ru, Rh, Pd, Ag), molybdate, sulphate, and chloride are immiscible and thus segregate as separate phases (Gin et al. 2017, Ojovan et al. 2019). Moreover, microchemical analyses have shown that in the MW glass Ni concentrates in separate immiscible Fe-Ni oxide spinels (Curti et al. 2009). These observations indicate that the low solubility of specific chemical components can severely limit the homogeneous distribution of quite a number of radionuclides in the glass matrix.

The release of radionuclides segregated in exsolved phases will be controlled by the chemical stability of the latter. The noble metal and spinel inclusions frequently formed during the vitrification of radioactive waste are sparingly soluble in aqueous solutions, so that a preferential release of dose-relevant nuclides such as ^{99}Tc, ^{107}Pd, and ^{59,63}Ni is unlikely. In contrast, ^{93}Mo will presumably partition in the so-called "yellow phase" inclusions, heterogeneous multiphase exsolutions also detected in Magnox-type glasses (Ojovan et al. 2019). They consist of an assemblage of chromate, sulphate and the molybdate $CaMo(VI)O_4$, which is fairly soluble in water (Spytsin 1952, Khodokovskiy & Mishin 1971). Thus, a preferential release of ^{93}Mo cannot be excluded a priori. ^{79}Se, which occurs as selenate in the MW glass (Curti et al. 2013), may also be partitioned in the yellow phase and undergo preferential dissolution. Nevertheless, as long as the inclusions are microparticles in a large homogeneous borosilicate matrix, the average release of soluble radionuclides from the yellow phase should remain congruent, since the exposure rate of microparticles is controlled by the dissolution rate of the borosilicate matrix.

While caesium volatility is intentionally suppressed by addition of acid oxides during the melting process (Ojovan et al. 2019) no such measures are normally taken to limit the evaporation of iodine. However, being more volatile than caesium, iodine evaporates nearly quantitatively already during the spent fuel PUREX dissolution process. According to NEA (2010), about 97% of the iodine initially present in the spent fuel evaporates as I_2(g) in this way. During the glass melting process, some of the iodine left evaporates further and is trapped in special filters, leaving only small residual inventories of ^{129}I in the glass.

3 Mechanisms of glass dissolution

3.1 Preliminary remarks

This chapter addresses the fundamental chemical-physical mechanisms that control the borosilicate glass dissolution kinetics at the reacting water-glass interface. Knowledge of such molecular to nanoscale mechanisms is essential in order to understand changes in dissolution kinetics regimes and quantify the rates of glass matrix dissolution and radionuclide release. Thanks to the advent of instrumental techniques with unprecedented spatial resolution, the understanding of the processes taking place in the thin reactive layer at the glass/water interface has dramatically improved in the past few decades, yet a complete understanding and consent on the key processes has still to be reached. This is partly a consequence of the compositional complexity of nuclear waste glasses, and of the diversity of chemical and environmental conditions (e.g. different engineered barrier materials and solution compositions) in leach experiments that have to be taken into account for the various national programmes. Moreover, it is still challenging to obtain unequivocal experimental evidence over sufficiently extended leaching times at such small spatial scales. As shown below, a debate persists on the very nature of the reactions occurring at the glass-water interface.

3.2 The classical model – short-term interactions

The nature of microscopic processes occurring in the *short-term* (hours to few days) at the water-(boro)silicate glass interface was established in the eighties of the past century. The essential findings were summarised in the excellent publication of Bunker (1994). Experimental evidence allowed identifying three distinct stages in the glass dissolution process, which are now generally accepted:

(1) *Hydration* – Non-reactive penetration of water molecules into the glass structure, occurring by molecular diffusion preferentially through small openings defined by closed rings of polymerized $(Si,B)O_4$ tetrahedra. In the compositionally complex nuclear waste glasses, hydration is slow and negligible, because the presence of network modifiers (e.g. Na^+, Zr^{4+}) tends to "close" such openings.

(2) *Ion exchange of alkalis with protons* – This is a cation exchange reaction according to following schemes:

$$\equiv Si - ONa + H_3O^+ \rightleftarrows \equiv Si - OH + Na^+ + H_2O$$
$$\equiv Si - ONa + H_2O \rightleftarrows \equiv Si - OH + Na^+ + OH^-$$

In most publications, only the former of the two reactions is mentioned. However, since the reaction of alkali borosilicate glasses with water is basic under normal circumstances (pH 9 – 10), the second reaction is usually more relevant one. Under alkaline conditions, the concentration of H_3O^+ is negligibly small, so the first reaction does not play a role.

This process is also known as *selective leaching* or *interdiffusion*, but the definition given by Bunker (1994) (ion exchange) is more precise because it refers directly to the chemical exchange reaction effectively taking place. The interdiffusion of the exchanged cations is then simply a consequence of the penetration below the original glass surface due to processes (1) or (3). The term "selective leaching" implies that alkalis (mainly Na^+) are dissolved preferentially to other glass components. Usually, ion exchange is the first observable glass leaching phenomenon but only in the very short-term, before being masked by reaction (3) due to the decrease in concentration gradients as the interdiffusion zone progressively widens.

(3) *Network dissolution (hydrolysis)* - Network dissolution is the breaking of the polymerized ≡Si-O-Si≡, ≡Si-O-B= or ≡Si-O[-B≡]$^-$ bonds[4] through hydrolysis, according to reactions of the following type (Bunker et al. 1987, Gin et al. 2016):

$$\equiv Si - O[-B \equiv]^- + H_3O^+ \rightleftarrows \equiv Si - OH + B \equiv + H_2O$$
$$\equiv Si - O - Si \equiv + H_2O \rightleftarrows \equiv Si - OH + HO - Si \equiv$$
$$\equiv Si - O - Si \equiv + OH^- \rightleftarrows \equiv Si - OH + {}^-O - Si \equiv$$

The first reaction represents the electrophilic attack of hydronium ions on the bridging oxygen and dominates under strongly acidic conditions (Bunker et al. 1987). A free water molecule is produced in this process. The other two reactions take over at neutral and alkaline pH. Both water molecules and hydroxyl ions have a lone electron pair and thus act as nucleophiles towards the electropositive Si^{4+} cation, replacing one of four bridging oxygen ions. As a result of the hydroxyl attack, a single ≡Si-O-Si≡ bond is broken, leaving a formally neutral ≡Si-OH (silanol group) and a negatively charged ≡Si-O$^-$ group. The negative charge of the latter is compensated by a network-modifier cation (not indicated in the reaction scheme). After this first bond is broken, three further ≡Si-O-Si≡ bonds must be destroyed by the same mechanism before the group is completely depolymerized and dissolved, producing orthosilicic acid. This multistage mechanism is illustrated by the following reaction scheme, which shows the progressive hydrolysis of the (initially fully polymerized) SiO_4^{4-} tetrahedron at the left side (in blue):

$$O_3 \quad \equiv Si - O - Si \equiv O_3 + OH^- \rightleftarrows O_3 \quad \equiv Si - OH + {}^-O - Si \equiv O_3$$
$$OH\ O_2 \equiv Si - O - Si \equiv O_3 + OH^- \rightleftarrows OH\ O_2 \equiv Si - OH + {}^-O - Si \equiv O_3$$
$$OH_2\ O \equiv Si - O - Si \equiv O_3 + OH^- \rightleftarrows OH_2\ O \equiv Si - OH + {}^-O - Si \equiv O_3$$
$$OH_3 \quad \equiv Si - O - Si \equiv O_3 + OH^- \rightleftarrows Si(OH)_4(aq) + {}^-O - Si \equiv O_3$$

Network dissolution is very slow in pure silica glass because it is fully polymerized. It is faster in complex alkali-borosilicate glasses because many non-bridging oxygens (NBOs) are already present from the start.

The three mechanisms described above have been identified many decades ago based on experimental evidence using the (at that time) available advanced techniques, e.g. Nuclear Magnetic Resonance (NMR) and Raman spectroscopy. Modern molecular dynamics and ab initio methods now allow studying these processes computationally at an unprecedented level of detail. It is beyond the scope of this report to address specifically this topic. The interested reader may access the related literature with the help of the recent overview by Gin et al. (2021).

3.3 The classical model – long-term interactions

Among the three processes occurring at the glass/water interface discussed in the previous section, network dissolution appears to be the rate-limiting step controlling glass dissolution. Yet, the experimental observations addressed in the pioneering work of Bunker et al. (1987) all referred to simple sodium silicate glass and were limited to few days leaching time. Long-term and compositional effects specific of the much more complex nuclear waste glasses and their impact on glass corrosion kinetics, which is the major interest for radioactive waste disposal, were not covered. Starting from the mid of the eighties, a large number of experiments with durations

[4] Note: [-B≡]$^-$ represents 4-fold coordinated boron, which has a formal negative charge, contrary to formally uncharged 3-fold coordinated B≡.

ranging from several months to decades were carried out mostly with simulated nuclear waste glass[5] under the physical/chemical conditions relevant for a geological repository. In order to overcome the limited time scale of laboratory experiments, the alteration process was frequently artificially "accelerated" by using glass powders and so produce high glass surface area to water volume ratios (S/V).

In a recent publication, Gin et al. (2016) has summarized, based on the vast body of experimental observations, the interfacial interactions occurring between multicomponent borosilicate glasses and aqueous solutions and their impact on glass dissolution rates. As the nature of these phenomena typically depends on temperature, pH and composition (both of glass and aqueous phase) they are not unique. In this section, we focus on dissolution of nuclear waste borosilicate glasses with compositions equal or similar to those specified for Swiss vitrified waste at mild temperatures (40 °C – 110 °C) and moderate pH (≈ 5 – 10), reflecting the conditions expected in the Swiss HLW repository near field.

In contrast to boron, which is highly soluble in water at all pHs, the release of silica into solution is limited by the relatively low solubility of amorphous or crystalline forms of SiO_2 in the sub-alkaline pH region (Alexander et al. 1954). After sufficient leaching time under closed system conditions, the solubility of SiO_2 is approached and condensation reactions (i.e. re-polymerisation) soon start to counteract the dissolution of the $(Si,B)O_4$ network in the glass (Bunker et al. 1987):

$$\equiv Si - OH \ + OH \ - Si \equiv \ \rightleftarrows \ \equiv Si - O - Si \equiv \ + \ H_2O$$

In pure sodium borosilicate glass, the interplay of network dissolution and condensation reactions leads to formation of a porous surface layer a few micrometres thick consisting of almost pure hydrated silica (Bunker et al. 1987), because the highly soluble B and Na are leached out quantitatively. In the case of chemically complex borosilicate glasses, similar surface layers also form, but their composition is more complex due to the retention of sparingly soluble elements (e.g. Al, Fe, Zr, lanthanides, actinides). More importantly, their porosity is smaller, so that diffusion of solutes into the bulk glass is considerably slower than in simple alkali glass. Such transition zones are denoted as "gel layer" in the French literature (Vernaz & Dussossoy 1992). Alternative denominations exist, such as "surface layer", "leached layer" (Bunker 1994) or "glass reaction zone" (Wicks et al. 1993). Dedicated studies indicate that they are nanoporous, hydrated, and generally sharply bounded towards the pristine glass surface (Gin et al. 2001a, Curti et al. 2006, Perea et al. 2020).

In pure alkali borosilicate glass, the gel layer does not hinder the exchange of soluble components between dissolving glass and solution. In the case of chemically complex glasses, it may act as a powerful diffusion barrier. Much effort has been (and is still being) devoted to the study of chemical and solute transport properties of gel layers, with the aim of determining their impact on the long-term glass corrosion rates. The nanostructural properties of gel layers are now regarded to be the main corrosion rate-limiting factor in the long-term, as they control the rate of exchange of chemical components between aqueous solution and corroding glass. In general, a densification of the gel via polymerisation of silanol groups (recondensation) will hinder the transport of hydrolysed species and thus reduce the residual dissolution rate. The gel layer may be more or less passivating, depending on leaching conditions, pH and glass composition. Cailleteau et al. (2008) demonstrated that a high percentage of insoluble network modifiers in the glass, such as Zr, may inhibit silica recondensation reactions thereby preventing passivation effects. Typically, passivation appears to be suppressed in silica-poor environments, either under

[5] In a simulated nuclear waste glass, fission products are replaced by stable isotopes of the same elements and actinides are replaced by analogue elements (e.g. trivalent lanthanides for Cm, Am)

continuous exchange of Si-poor solutions (Soxhlet tests, flow-through experiments with Si-poor solutions) or when dissolved silica is efficiently removed via sorption on engineered barrier materials (e.g. bentonite, Fe-corrosion products) or precipitation of secondary silicates. This critical issue will be repeatedly addressed in more detail in Chapter 4.

In the initial stages of the glass corrosion process, the gel can be regarded as a residual layer of the pristine glass, mostly consisting of hydrolysed silica with nano-channels through which soluble species can migrate. Recent investigations on the International Simple Glass (ISG)[6] have shown however that the gel layer is not simply a relic structure. It constantly re-organizes through continuous hydrolysis-recondensation reactions, as shown by combined ^{29}Si-^{28}Si and ^{18}O-^{16}O isotopic exchange experiments (Gin et al. 2018). These reactions dynamically modify the gel morphology and transport properties of the solutes and have thus an impact of passivation.

At advanced stages of glass alteration, a micrometre-thick sheet of secondary phases may accumulate on top of the gel layer via direct precipitation from the leaching solution. The nature and amount of such precipitates strongly depend on glass and/or solution composition, pH, temperature, as well as on precipitation kinetics (Feng et al. 1993, Curti et al. 2006, Thien et al. 2010, Ferrand et al. 2014, Hopf et al. 2018). At circum-neutral pH for the glass compositions of interest, mostly clay-like minerals form in the precipitated layer (Curti et al. 2006, Thien et al. 2010, Thien et al. 2012).

Fig. 3-1 shows an idealized cross-section through an altered borosilicate glass - water interface, showing the different zones discussed above, based on the classification of Gin et al. (2016). Approximate concentration profiles of water, boron and silicon have been superposed to illustrate how the various regions can be defined based e.g. on nano-SIMS[7] analyses. The composition, properties and evolution of the glass-water interface may strongly vary as a function of pH and environmental parameters even for the same glass composition. For instance, Gin et al. (2020a) recently showed that at low pH boron accumulates in the interdiffusion zone, possibly affecting the rate of hydrolysis.

The gel layer, with its more or less passivating properties, plays a major role in determining the residual rate, but is not the only factor. Gin et al. (2021) have recently summarized the current understanding of the glass corrosion process in aqueous media in a mechanistic model. Accordingly, two driving forces are responsible *simultaneously* for the drop by several orders of magnitude of the glass dissolution rate:

(i) the reduction in the *affinity* of the Si-O-M hydrolysis reactions (M = Si, B, Fe^{III}) as the aqueous silica concentration approaches a steady state "saturation" activity (thermodynamic effect);

(ii) the dynamically changing passivation properties of the gel layer, which limit the *inter-diffusion* of hydrolised species from the glass and of water and solutes from the bulk solution

This model is therefore named here "Inter-Diffusion / Affinity model", shortly IDA. The affinity is a thermodynamic quantity equal to the difference between total free energy of products and educts for a given reaction at a given reaction progress (Anderson 2005, p. 564). The affinity is zero only at true thermodynamic equilibrium, which is never reached in a glass dissolution reaction because glass is thermodynamically unstable in aqueous solutions and thus dissolves irreversibly. This implies that the affinity of a glass dissolution reaction has always a finite value, which is large in the initial stages of dissolution and decreases to a minimum (but not zero) as the residual rate is reached in the absence of passivating gel layer.

---

[6] The International Simple Glass (Gin et al. 2013b) is a borosilicate glass containing the essential oxide components found in most nuclear waste glasses, serving as standard for inter-laboratory studies. It has the following composition (in mol%): 60.2 SiO_2, 16.0 B_2O_3, 12.6 Na_2O, 3.8 Al_2O_3, 5.7 CaO, 1.7 ZrO_2.

[7] nano-SIMS: Secondary Ions Mass Spectrometry at nanometric resolution

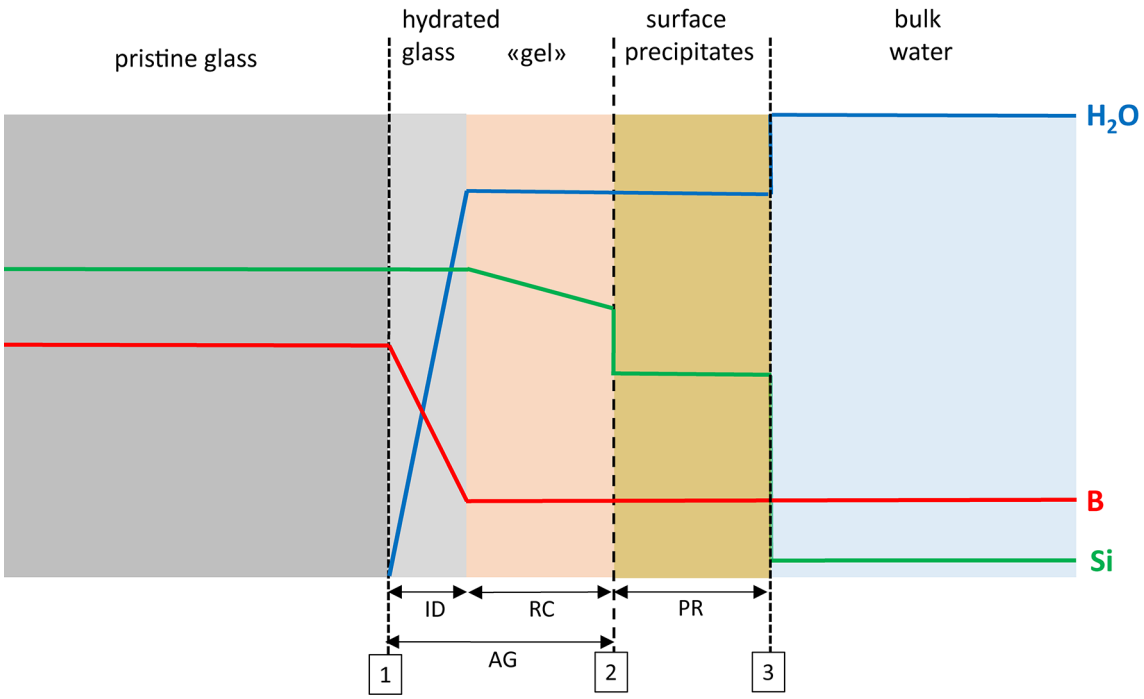

Fig. 3-1: Schematic cross section through altered borosilicate glass in contact with the leaching aqueous solution, showing idealized profiles of Si, B and water concentrations

Freely redrawn from Gin et al. (2016)

ID = Interdiffusion zone. RC = Recondensation zone. PR = Precipitation zone. AG = amorphous gel layer. Numbers denote the positions of [1] hydration front, [2] pre-leaching (pristine) glass-water interface and [3] current solid-water interface. Coloured lines indicate schematically the concentration profiles of the indicated components (H_2O, B, Si).

3.4 Alternative models

Recently, the classical picture of the mechanistic evolution of the water/glass interface discussed in the preceding section has been challenged by observations that question the idea that the dissolution of silicate glass is controlled by diffusion through a nanoporous gel layer. Indeed, three studies (Geisler et al. 2010, Hellmann et al. 2015, Geisler et al. 2015) provided data apparently contradicting the IDA model. Based on advanced microscopic techniques coupled with elemental and isotopic analyses down to atomic-scale resolution (Atom Probe Tomography, Transmission Electron Microscopy, Tof-SIMS, LA-ICPMS) these authors showed that the contact between pristine and altered glass is sharp in their experiments, with only a thin film of free water separating altered and pristine glass. The altered layer was interpreted to be solely the product of direct precipitation of dissolved silica from the solution, without any relic structure of the glass. In other words, they claimed that a gel layer does not exist; the entire altered zone is seen as a layer of precipitates directly on top of the receding pristine glass surface. Evidence for such a mechanism was provided, besides the abrupt boundary between altered and pristine glass, from stable isotope data obtained from the dissolution of pure sodium borosilicate glass doped with ^{30}Si in water spiked with ^{18}O. The isotopic data indicate that the silica in the gel layer is largely derived from the external solution and not from the glass itself. This new model is named here Interfacial Dissolution/Precipitation (IDP) model to distinguish it from the previously described Inter-Diffusion/ Affinity Model (IDA).

3.5 Evaluation of the IDP and IDA models

In the opinion of the present author, the evidence provided by Geisler et al. (2015) is equivocal. Careful inspection of their results indicates widely different morphological and isotopic patterns. Even in the same experiment, portions of the alteration layer are porous (hence more accessible to external water), while other are dense. The authors selectively focus on observations made in the high-porosity regions to provide evidence in favour of the proposed dissolution/precipitation mechanism, disregarding the more dense regions.

The IDP model is actually analogous to the isovolumetric mineral replacement model proposed by Putnis & Putnis (2007) to explain pseudomorphic replacement of a primary mineral by a secondary phase. A necessary condition for the isovolumetric replacement to proceed is that the replacing solid (in this case the alteration layer of the glass) must have a high porosity in order to guarantee continuous access of the aqueous solution to the reaction interface. This condition is probably met in some of the glass corrosion experiments of Geisler et al. (2015), particularly the one illustrated in their Fig. 3d, j and 3b,h. In these experiments, the high $^{28}Si/^{30}Si$ ratios indeed indicate that most of the silica in the alteration layer was derived from the bulk solution, not from the pristine glass. In other experiments, however, (Fig. 3a,g and Fig. 3c,i in Geisler et al. 2015) the isotopic profiles show signatures identical to that of the pristine (uncorroded) glass, coupled with Na and hydration profiles typical of diffusion control. The silica in such samples is thus inherited from the glass undergoing corrosion, in agreement with the IDA model. In summary, the data of Geisler et al. (2015) and Hellman et al. (2015) provide evidence that both glass alteration mechanisms may be operating in parallel, depending on the local porosity and other factors (e.g. cracking of the alteration layer) affecting the accessibility of water to the reactive interface.

Moreover, Geisler's experiments were carried out either under strongly acidic conditions (initial pH = 0) and at high temperatures (150 °C), i.e. far away from the the usual leaching conditions of nuclear waste glass experiments (pH 9 – 10 and 90 °C) (Geisler et al. 2010), or with pure sodium borosilicate glass, a much simpler composition than nuclear waste glasses (Geisler et al. 2015). Bunker (1994) explicitly state that "*The ultimate result of silanol polymerization* [of pure sodium borosilicate glasses] *is the total restructuring of glass from the initial random network into a material which resembles an aggregation of colloidal silica particles*" and "*The other major implication of surface restructuring is that the leached layer is transformed from a diffusion barrier into a material containing 'large' (> 3 nm) interconnected voids through which water and other species can rapidly diffuse*". Bunker's observations thus perfectly explain the results of Geisler et al (2015) on pure sodium silicate glass, which lack insoluble components (Al_2O_3, CaO, MgO, Fe_2O_3, ZrO_2) known to affect the transport properties of the gel.

Gin et al. (2016), in the attempt to reconcile the two mechanistic models, concluded that there are still open questions. More recently, Gin et al. (2020b) studied the aqueous alteration of a ternary sodium borosilicate glass at 90 °C and pH 9 and showed that both mechanisms were active in the same experiment. O and Si isotopic data showed that after an initial phase during which the $(Si,B)O_4$-tetrahedra were completely hydrolysed and released to solution (IDP), with progressing alteration the gel layer densified and the hydrolysed silica was retained, thus producing the "relic structure" predicted by the IDA model. In conclusion, it appears that the two models are not mutually exclusive but rather complementary: the IDA model is appropriate for complex nuclear waste glass compositions corroding under conditions typical in repository environments (T < 100 °C, pH 5 – 10, low to moderate ionic strength). In acidic or hyperalkaline or saline solutions, the increased reactivity of the glass may induce sharp alteration fronts that can be better explained by the IDP model, see e.g. the banded alteration structures observed by Ferrand et al. (2018) and Mann et al. (2019).

4 Kinetics of nuclear waste glass dissolution: experimental evidence

4.1 Experimental techniques and evaluation of glass corrosion experiments

Glass corrosion experiments have a long tradition. Since it became clear that vitrified waste would become the standard matrix for reprocessed spent fuel waste, aqueous leaching experiments have been conducted with many different glass compositions and a large variety of physical-chemical conditions, reflecting the needs of the different radioactive waste disposal programs. This included the expected repository temperatures, leaching solution composition, pH and the use of additives representing the foreseen engineered barrier materials. In the beginning, however, most glass leaching experiments were carried out under simplified standardized conditions and without additives in order to allow for the comparability of results obtained in different laboratories with different types of glass. Such efforts are best illustrated by the definition of standard experimental procedures at the Materials Characterization Center (MCC) of the Pacific Northwest National Laboratory (PNNL) on behalf of the U.S. Department of Energy (Strachan et al. 1982). Test protocols were defined for five standard leach tests (MCC-1, 2, 3, 4, 5). Although this standardisation has not been followed strictly in Europe, some elements have been tacitly adopted, resulting in the following typical types of experiments and conditions:

- *A set of standard temperatures at which leaching experiments are carried out*: 40, 70, 90 °C. Although higher than expected in most repository sites, 90 °C is by far the preferred temperature in glass leaching experiments as it allows obtaining significant alteration within short experimental times (< 1 year). Alteration is much weaker at 70 °C and 40 °C.
- *Soxhlet-type tests*: in these tests, monolithic polished glass specimens with 1cm^2 per face are leached in a Soxhlet device, an extraction apparatus that operates via boiling-recondensation. The condensate (distilled water) flows back and continuously flushes the glass sample at constant temperature and pH[8]. This test is carried out to determine the so-called *forward glass corrosion rate*, i.e. the initial corrosion rate. This is usually the maximum corrosion rate measured in the course of a static leach experiment (see below) started in initially pure water.
- *Static tests*: in these tests, monolithic or powdered glass samples are leached in a closed vessel made preferably of chemically inert material. The soluble species released from the glass remain in contact with the glass, which causes a rapid and strong reduction of the glass corrosion rate. In most cases, the *forward corrosion rate* is reduced by several orders of magnitude and reaches an asymptotic minimum, termed *residual corrosion rate*. Understanding and modelling the mechanisms leading to such reductions of the corrosion rate, in the short and particularly in the long-term, is the main task in radioactive-waste related glass corrosion science.

In the course of the years, other types of (more complex) experiments have been devised to account for more repository-relevant setups, including field experiments in underground research laboratories (Valcke 2007). These will be described later in Section 4.4. The MCC standardisation also includes universally adopted guidelines for the evaluation of results of glass corrosion experiments. For instance, the results of glass leaching experiments should be expressed as *elemental mass loss*, NL_i [g m^{-2}]. This quantity is calculated by combining the solution concen-

[8] Because the leachant is distilled water, the pH will be determined by the pCO_2 in the air or glove box in which the experiments are carried out. In general, the pH will be close to neutral or slightly acidic.

trations of any element *i* released from the glass, the water-exposed glass surface area, *S* [m^2], the element weight fraction in the fresh glass, f_i [-], and the solution volume, *V* [L]:

$$NL_i = \frac{[i]}{f_i(S/V)} \tag{1}$$

For congruently dissolving elements that are not retained in the alteration layer and are so soluble that any precipitation can be ruled out (typically B or Li) *NL(i)* [g m^{-2}] yields the mass of glass dissolved per unit exposed surface area. Ideally, all elements that dissolve congruently should yield the same *NL(i)*-values and rates. The comparison of *NL(B)* and *NL(Li)*-values is thus an important consistency test. The corrosion rate is then determined from the slopes in *NL(B,Li)* vs. time plots. For any element '*i*' that dissolves incongruently due to retention in the alteration layer or precipitation, the ratio *NL(i) / NL(B, Li)* readily yields the fraction of element *i* released to solution during the corrosion process.

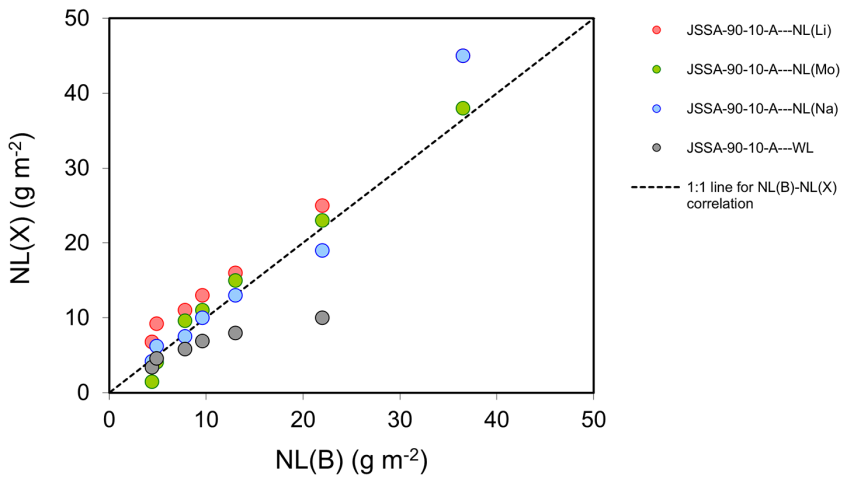

Fig. 4-1: Congruency plot showing for the same experiment NL(Li), NL(Mo), NL(Na) and gravimetric weight losses (WL in the legend) against NL(B)

If all data were perfect tracers of the glass corrosion, they would plot exactly on the 1:1 line. The fact that NL(Mo) and NL(Li) plot above the 1:1 line suggests that Mo and Li may trace glass dissolution better than B (i.e., that more B than Mo or Li is retained in the gel layer. Data are from the JSS project.

It is important to realize that this evaluation technique only works when no external element source is present. For instance, in experiments with additives such as clay minerals, *NL(Si), NL(Al), NL(Mg)* cannot be determined since the clay also supplies these elements to the leaching solution. The same applies for experiments started in complex multi-element solutions rather than pure water. In general, it is however still possible to use *NL(B)* and *NL(Li)* as a tracer of the glass corrosion process since most additives and solutions used in nuclear waste glass leach tests are boron and lithium-free. Finally, it must be noted that in experiments mimicking repository conditions, it is normally impossible to retrieve aqueous solutions, particularly when compacted clay is involved. In such cases, other techniques must be applied to determine the extent of glass corrosion. Typically, the mass loss of the leached glass specimen is then determined gravimetrically or from microscope images showing the thickness of the gel layer. This technique may lead to underestimated glass dissolution, as evident from Fig. 4-1, where *NL(B)* values are plotted against measured mass losses and other *NL(i)* values from the same experiment.

The data in Fig. Fig. 4-1 were taken from JSS project (JSS 1984a,b,c, JSS 1985, JSS 1986, JSS 1987a,b, JSS 1988a,b) and refer to an experiment with a radioactive borosilicate glass of omposition equivalent to SON68.

4.2 Aqueous solution effects

This Section deals with the effects of solutes on glass corrosion kinetics, with emphasis on empirical results arising from a large body of experiments. Interpretational aspects are mentioned, but not discussed in depth. For the details, the reader is referred to the cited literature. We address particularly kinetic effects caused by specific dissolved elements (particularly Si). These elements either may be already present in the leachant or released by the dissolving glass or by additives simulating engineered barrier materials. The effects of pH and salinity are also discussed. Not included in this section are effects arising from differences in glass composition (e.g. presence/absence of Mg in the glass), which are treated in Section 4.3.4.

4.2.1 Effect of Si (in conjunction with gel properties)

A large number of experiments indicate that the dissolution rate of borosilicate glasses is inversely proportional to the silica concentration in the leaching solution, at least in the initial stages of the alteration process. An empirical equation, known as *affinity law* or *first order law,* was soon formulated to describe this correlation quantitatively (Grambow 1985). This equation regards the difference between the silicic acid activity in the aqueous solution and an empirically determined *glass* "*solubility constant*" as the main driving force controlling the glass dissolution process. From the mid-eighties to the early nineties of the past century this model of glass corrosion was the most widely accepted. Later, work by the French CEA group in Marcoule (Vernaz & Dussossoy 1992) revealed inconsistencies in the *affinity law*.

One such inconsistency was the dependence of the *glass* "*solubility constant*" (and thus of the residual corrosion rate) on the glass surface area to solution volume ratio (S/V) in otherwise identical experiments (see Tab. 2 in Vernaz & Dussossoy 1992). At high S/V the aqueous silica concentration approaches more rapidly the so-called "*silica saturation*"[9] conditions at which the minimum *residual rate* is attained. The data indicated a progressively slower *residual rate* as S/V increased to very large values (up to 20'000 m^2/m^3), suggesting that the kinetics at high reaction progress is no longer controlled by silicic acid activity, but rather by diffusion phenomena arising from the increased thickness and porosity reduction of the gel layer. As discussed in Chapter 3, according to the IDA model the gel layer acts in most cases as a diffusion barrier, slowing down the exchange of chemical species between pristine glass and aqueous solution and thus reducing the *residual rate* (Vernaz et al. 2001).

The current view is that dissolved silica controls glass alteration kinetics only in the initial stages of the dissolution process and in those cases where low silica concentrations (far from "saturation") are maintained. Such conditions are typically achieved in Soxhlet or flow-through tests, where the silica concentration is essentially zero or kept to low fixed values. Recondensation of silica then does not occur and a porous non-protective layer of hydrated glass forms, from which the soluble components (LiO, B_2O_3, NaO_2) are easily leached out. In a deep geological repository, however, conditions similar to those in high S/V static experiments are established, as water availability will be limited in a HLW repository, so that the factor controlling the *residual rate* will be diffusion through the altered layer, not aqueous silica concentration. There are

[9] The concepts of "glass saturation" and "glass solubility constants" are placed in quotation because they have not a strictly thermodynamic meaning in glass corrosion science. There cannot be equilibrium in the thermodynamic sense since the corroding glass is a metastable compound that is transformed irreversibly into more stable alteration products. A thermodynamic "glass solubility constant" would imply that an amorphous glass with the same composition and structure as the pristine glass would reprecipitate once the solubility constant is exceeded.

nevertheless notable exceptions to this rule where even at high S/V conditions and long leaching times, the alteration layer is not passivating (see Section 4.4.3, 4.4.4). In such cases, the aqueous Si concentration still plays a major role.

4.2.2 Effect of pH

Borosilicate glasses of the type used to immobilize the residues from reprocessed spent fuel in Switzerland (SON68 and MW, see Tab. 1-1) contain about 15 wt.-% boron oxide and 8-10% sodium oxide. In the absence of external pH buffers, these two components will largely determine the pH of the leaching solution in contact with the glass. Accordingly, the pH should stabilize in the mildly alkaline region (pH 9-10) (Advocat 1991, Advocat et al. 1991, Curti 2003) due to dissolution of alkali oxides (Na_2O, K_2O) and buffering by the $H_3BO_3/H_2BO_3^-$ acid-base pair, which has a pKa value of 9.2 at 25 °C.

It is nevertheless possible to study the dissolution kinetics of borosilicate glasses at any fixed pH by adding an appropriate buffer and in flow-through tests, or with static tests at very low S/V ratio. Experiments with pH-buffered solutions reveal an U-shaped form of the *forward corrosion rates* (Wicks 1986) across the pH-range 3-11, with minima in the slightly acidic region (pH 5-7, see Advocat et al. 1991). Owing to the well-known pH-dependence of SiO_2 solubility (Eikenberg 1990 and references therein), borosilicate glasses are expected to be highly soluble at pH > 11. This expectation is fully confirmed by glass corrosion tests in cement pore waters (see Section 4.4.4).

Systematic studies led to empirical equations predicting the *forward* glass corrosion rates as a function of pH, often in conjunction with other parameters such as temperature (Advocat et al. 1991, Strachan 2017, Vienna et al. 2018, Backhouse et al. 2018). These studies are of limited relevance for the long-term behaviour of nuclear waste glass under repository conditions, where close to "saturation" conditions will prevail. Unfortunately, it is not possible to define analogous pH-dependent equations for the *residual rate*, since at advanced stages of alteration the effect of pH cannot be separated from that of other continuously evolving parameters that also influence the *residual rate*, e.g. the retention of chemical species in the gel layer may dynamically modify the diffusivity of solutes through the gel.

In the current Swiss HLW reference repository setup, the vitrified waste forms encapsulated in cylindrical stainless-steel containers ("coquilles") will be loaded into dm-thick carbon steel canisters. After corrosion and breaching of canister and "coquille", neutral to mildly alkaline pore water pre-equilibrated with the bentonite buffer (pH 7-8, see App. C in Bradbury et al. 2014 and Curti 2021) will come in contact with the glass. Due to the unavoidable cooling-induced stress, the glass form will not be monolithic but fragmented, allowing the aqueous phase to permeate the entire glass body. Most of the glass surface exposed to water will be therefore inside the glass cylinder. In such environment, the glass itself will presumably control the local pH via boric acid/borate buffer, i.e. a range between pH 9-10 is expected. A gradient of up to 3 pH-units may thus exist from the centre of the glass body toward the external surface, which could in principle lead to a gradient in corrosion rates.

The effect of pH on *residual rates* is in general hardly predictable in the circum-neutral pH region, but there is a clear increase in dissolution rate at pH > 11. Recent studies allow a comparison of the *residual rate* for SON68 and MW glasses across the pH range 7 – 13 (see Section 4.4.4 and reference therein). In hyperalkaline KOH solutions, the corrosion rates measured after > 1 year leach time are orders of magnitude larger than at circum-neutral pH, owing to the increased SiO_2 solubility. In contrast, analogous experiments in $Ca(OH)_2$ dominated solutions indicate residual rates comparable or even slower than at circum-neutral pH. This contrasting behaviour is apparently due to the preferred incorporation of Ca and Si into the gel layer, which then becomes

passivating, and to the pH decrease associated to zeolite formation, see e.g. Ferrand et al. (2021). This example shows exemplarily the intrinsic difficulty in separating the pH effect on the residual rate from other superimposed chemical-physical effects.

4.2.3 Effect of salinity

The influence of dissolved aqueous species on borosilicate glass dissolution kinetics can be manifold due to the large variety of elements involved. Each dissolved element interacts in a specific way with the gel layer and may affect its passivating properties (e.g. Thien et al. 2012, Utton et al. 2012, Gin et al. 2015). Therefore, the effect of salinity cannot be disentangled from the effect of specific dissolved elements that may be present from the start in the leaching solution, or are released from the glass during the glass dissolution process.

Here, however, we focus on the effect of high concentrations of the dominating soluble salts NaCl, KCl and $MgCl_2$. High ionic strengths up to 5 – 6 m caused by the dissolution of the mentioned salts are typical of waters associated to repositories in salt rocks, which are not considered as potential repository host-rocks in Switzerland. NaCl dominated pore waters with salinities up to ≈ 1 M have been identified in the Opalinus Clay formation (Mäder 2009), so that this issue bears some relevance also for the Swiss repository. However, the highest chloride content measured in borehole samples from the deep drilling campaign have been observed in samples from the Bülach borehole and amounts to 410 mmol/kg_w (Mazurek et al. 2021). However, the Bülach borehole lies at the southern margin outside of the NL perimeter and lower Cl^- contents in the order of 240 mmol/kg_w, are expected for the repository perimeter according to results from the Stadel boreholes (Aschwanden et al. 2022).

Only few systematic studies address the influence of salinity on glass corrosion kinetics. Lutze et al. (1988) measured the alteration of the French R7T7 glass (equivalent to SON68) in 5 – 6 M NaCl/$MgCl_2$ brines (with and without $CaCl_2$) at temperatures between 110 and 190 °C. The leach experiments had a duration of 11 to 556 days and S/V ratios were varied from 10 to 1'000 m^{-1}. From the comparison with reference experiments started in pure water (unfortunately not reported in the publication), these authors concluded that there is no detectable effect of salinity on glass dissolution kinetics.

Gin et al. (1992) studied the corrosion of the same R7T7 glass at 90 °C and 150 °C in (Ca, Na, K, Mg)Cl_2 brines during 180 days at S/V = 70 m^{-1}. In contrast to the study of Lutze et al. (1988) the brines were Ca-dominated with variable Mg concentrations. Apart from the temperature effect, no differences in the extent of glass dissolution could be detected due to the different Mg concentrations in the brines, although saponitic clay was formed at the glass-water interface in the presence of high Mg concentrations. No reference experiment in pure water is reported, so that the effect of the high salinity cannot be really identified. Nevertheless, the aqueous B concentrations show no measurable increase in glass dissolution after 56 days, i.e. essentially a corrosion rate of zero, however with a large uncertainty due to considerable scatter in the data, probably due to the "parallel experiment technique" probably adopted in that study.

Strachan et al. (1985) carried out a study on salinity effects, including reference experiments in pure water, with the SRL-131 glass, an U.S. glass formulation mainly differing from SON68 and MW by a higher Fe_2O_3 content (9 – 14% by weight). Fig. 4-2 shows the data of dissolution tests carried out at 90 °C in deionized water, in a 1.5 M NaCl – 1.3 M $MgCl_2$ – 0.7 M KCl brine, and in two synthetic (Mg-free) ground waters of low ionic strength (I = 0.03/0.1 m). The results show that glass dissolution was about ten times smaller in the brine compared to the reference experiment in pure water. However, the *residual rate* regime was not yet attained after 1 year leaching time and the scatter of the data in the experiments proceeding for two years does not allow extraction of a *residual rate*. Therefore, also in this case no conclusive results can be derived.

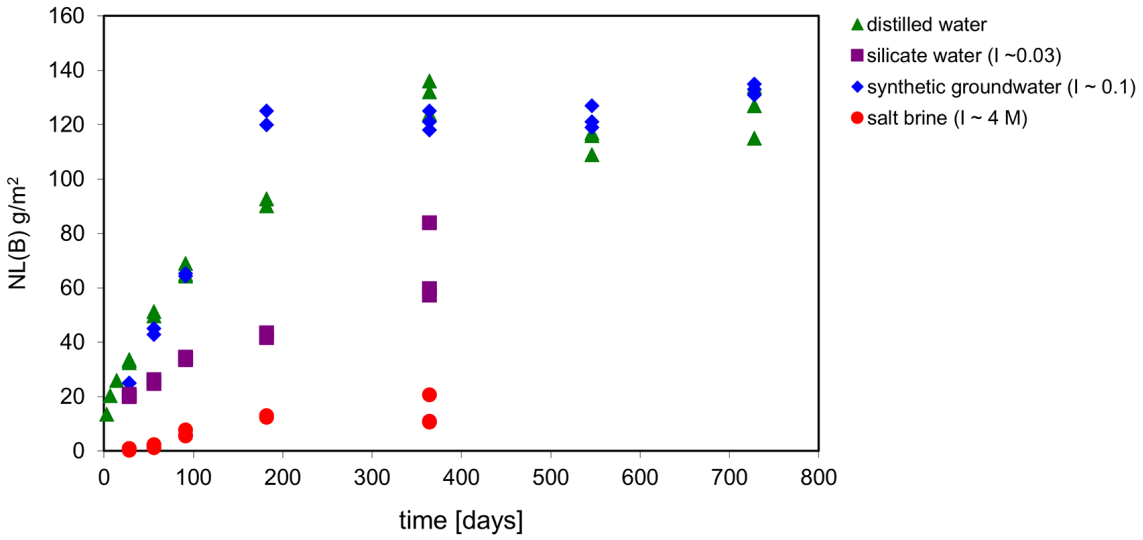

Fig. 4-2: Normalized mass loss of boron from selected leach experiments carried out with the SRL-131 glass at 90 °C under static conditions

Data taken from Strachan et al. (1985).

The study of Jollivet et al. (2012) described in detail in Section 4.2.4 also yields some insight on the effect of salinity, however limited to the forward rate regime. These authors found a strong increase in measured r_0-values when the NaCl or $NaClO_4$ concentration was increased from 0.02 M to 0.7 M (see for more details). These results are opposite to those of Strachan et al. (1985) illustrated in Fig. 4-2, but since they were obtained with a different glass and far from silica "saturation" they are not comparable with those of the aforementioned study.

4.2.4 Dependence of forward rate on aqueous solution composition

Jollivet et al. (2012) systematically studied the influence of leaching solution composition on the initial (forward) dissolution rate for the SON68 glass. The experiments were conducted with glass powder flushed with the solutions of interest at high flow rates, mostly at 90 °C but also at lower temperatures (30, 50, 70 °C). The effects of ionic strength, single alkali and earth-alkali cations (Li^+, Na^+, K^+, Rb^+, Cs^+, Mg^{2+}, Ca^{2+}, Sr^{2+}, Ba^{2+}) and single anions (Cl^-, SO_4^{2-}) were investigated separately.

The forward rate of SON68 was also measured in a water pre-equilibrated with Callovo-Oxfordien clay, bearing some similarities with the Swiss Opalinus Clay and bentonite pore waters[10]. At all temperatures the forward rates measured in clay water were about 5 times larger than in distilled water, in spite of the presence of dissolved silica (Tab. 4-1). The pH (25 °C) was always in a restricted range close to neutrality (5.8-7.8) so that superposed pH effects can be excluded (see Section 4.2.2).

[10] It has almost the same pH and equilibrium pCO_2 as Swiss reference bentonite pore waters, but a considerably lower ionic strength (100 mM vs. 350-0.78 mM, Curti et al., 2022).

This result is noteworthy for two reasons. First, it represents a failure of the "affinity law", which requires the rate of glass dissolution at a fixed temperature to *decrease* with silicic acid activity (Section 6.2). The opposite is observed, implying that the "affinity law" model is evidently too simplistic; other dissolved components must play a role in determining the glass dissolution kinetics. Second, because the ratio of the forward rates measured in distilled and clay water is more or less constant through the 30 – 90 °C, the forward rate in clay water can be extrapolated to equilibrium repository temperatures (~ 40 – 50 °C). The specific effect of temperature on forward rates is treated in Section 4.3.2.

Tab. 4-1: Forward rates of SON68 glass in g m^{-2} d^{-1} measured by Jollivet et al. (2012) in pure water and clay water at different temperatures

	30 °C	**50 °C**	**70 °C**	**90 °C**
Pure water	0.002	0.017	0.084	0.33
Clay water	0.011	0.093	0.47	1.7
Ratio (pw/cw)	5.5	5.5	5.6	5.2

Measurements in pure NaCl or $NaClO_4$ solutions at 90 °C showed for both electrolytes a nearly linear increase in r_0 by up to a factor 4 as the ionic strength was raised to 0.7 M. There is no possible superposed effect in these measurements, since no other dissolved component was present and the pH remained always near neutrality. Based on these data, for SON68 leached in the NaCl dominated bentonite pore water 450 mM ionic strength one may thus extrapolate a forward rate increased by a factor of 3 compared to leaching in pure water (i.e. 3 g m^{-2} d^{-1} instead of 1 g m^{-2} d^{-1} at 90 °C).

Replacing NaCl or $NaClO_4$ with Na_2SO_4 at 0.1 M ionic strength (i.e. replacement of the anion) did not have a significant effect on r_0. In contrast, replacing single dissolved cations as chloride salts at IS = 0.1 M had in some cases a considerable effect. The results (all obtained at 90 °C) reveal no or little dependence of r_0 if Na^+ is replaced by Li^+, K^+, Cs^+ or Mg^2, but replacing Na^+ with Rb^+, Ca^{2+}, Sr^{2+} or Ba^{2+} increased r_0 by a factor of 2-3. There is therefore a tendency for earth alkali cations with large radii to enhance the initial dissolution rates.

Jollivet et al. (2012) explained this effect by the different surface complexation of the various cations. Their calculations indicate that Ba^{2+}, Ca^{2+} and Sr^{2+} form stronger =Si-O-Me complexes at the reacting glass surface than K^+, Cs^+, Na+, Li^+ and Mg^{2+}, leading to an increased rate of network bond breaking (Fig. 9, op. cit.). According to this model, the increase in dissolution rate observed in the clay water was attributed to the presence of dissolved Ca. Because the Ca concentration in Swiss bentonite pore water is about twice that in the clay water used in Jollivet et al.'s experiments, one has to assume that the enhancement of the initial glass dissolution rate could be even stronger in the Swiss repository.

4.3 Effect of temperature and "intrinsic" parameters

4.3.1 Preliminary remarks

This Section deals with the influence of temperature and "intrinsic" parameters on glass dissolution kinetics. Parameters defined here as "intrinsic" are those related to the specific glass used in the experiments, such as its chemical composition, but also atomic-scale structural damage arising from long-term self-irradiation. The effects of variations in such parameters on glass corrosion kinetics are highlighted and discussed based on the published literature.

4.3.2 Effect of temperature

A large number of leach experiments on various types of borosilicate glasses show that the *forward corrosion rate* depends exponentially on temperature, following an Arrhenius type law (JSS 1988b, Mc Grail et al. 1997, Pierce et al. 2008). Depending on glass composition, activation energies (E_a) ranging from ≈ 50 to ≈ 80 kJ mol^{-1} were determined in the temperature range 20 – 110 °C at circum-neutral to mildly alkaline pH.

The magnitude of the activation energy yields clues on the molecular-scale mechanisms responsible for the glass dissolution process. The aforementioned range of $E_a \approx 50 – 80$ kJ mol^{-1} is typical for the breaking of (Si,B)-O bonds, implying that the rate-limiting mechanism far from "silica saturation" is network dissolution and not interdiffusion, in which case much lower activation energies are expected (Abraitis et al. 2000). Moreover, the ranking in E_a is a measure of the intrinsic chemical resistances of the glasses to aqueous corrosion: the higher E_a, the more resistant is the glass.

From boron release measurements, Pierce et al. (2008) calculated $E_a = 52 – 56$ kJ mol^{-1} for the studied aluminoborosilicate glasses, while for a Magnox waste glass with composition very close to the MW-glass, Abraitis et al. (2000) determined 64 kJ mol^{-1}. For SON68, Godon (2004) quote 76 kJ mol^{-1}, implying that of the three types, SON68 should be the most corrosion-resistant. Using the aforementioned activation energies and values of the *forward rates* at 90 °C given in the literature (2.1 g m^{-2} d^{-1} for SON68 at 100 °C from Godon 2004, p.87, and 1.2 g m^{-2} d^{-1} for MW from Zwicky et al. 1989) we constructed the *Arrhenius plot* shown in Fig. 4-3 for the two Swiss reference glass compositions. It is based on the equation:

$$r_0 = A \exp[-E_a/(RT)]$$

where r_0 [g m^{-2} d^{-1}] is the *forward* glass corrosion rate, A [g m^{-2} d^{-1}] is a pre-exponential factor, E_a [kJ mol^{-1}] the activation energy, T [K] the absolute temperature and R [kJ mol^{-1}] the universal gas constant. Such plots are obtained from experimental determinations of the *forward rates* for at least three different temperatures. If the experimental r_0 data define a linear trend at sufficient level of confidence, then an activation energy can be determined and the *forward rate* of the specific glass can be extrapolated at any temperature within the range defined by the experiments.

From Fig. 4-3 *forward rates* of 4.7×10^{-2} g m^{-2} d^{-1} for SON68 and 8.7×10^{-2} g m^{-2} d^{-1} for MW are extrapolated at the temperatures expected under repository conditions at canister failure time (i.e. about 50 °C at 10'000 years after repository closure, see Fig. 6-1 in Bradbury et al. 2014).

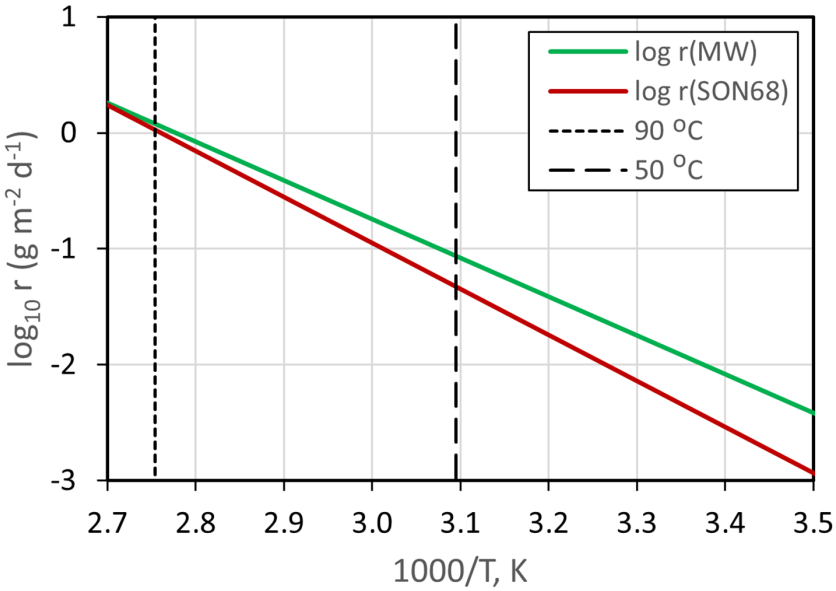

Fig. 4-3: Arrhenius plot showing the decimal logarithm of the *forward* corrosion rates for the Swiss reference glasses MW and SON68

It should be noted that forward rates as defined above refer to experiments conducted in pure water under dynamic conditions, i.e. with a flux of leachant sufficient to remove all solutes dissolved from the glass. Therefore, the r_0 temperature dependencies shown in Fig. 4-3 are valid for solutions devoid of silica or other solutes and pH close to neutrality. As shown earlier (Section 4.2.4), different (even higher) *forward rates* are measured as a function of pH and leachant composition. Forward rates in silica-free solutions can be measured at the desired pH by using appropriate buffers. As already discussed (Section 4.2.2) such experiments were conducted e.g. by Advocat et al. (1991) for the R7T7 glass (equivalent to SON68) in the range pH 7 – 10 at 90 °C. They found that the forward rate remained constant from pH 4 to pH 7 and then increased by one order of magnitude from pH 7 to pH 10. It would however be misleading to extrapolate this finding to the results discussed in Curti et al. (2006), since the pHs in the range ~ 9 – 10 they observed are reached after dissolution of alkalis and silica from the glass, i.e. close to "silica saturation" and thus far off *forward rate* conditions.

Because the large majority of glass dissolution experiments are conducted at 90 °C, i.e. 40 – 50 °C above the expected repository temperatures at canister failure times, the question of temperature extrapolation of glass dissolution rates is central for the Swiss radioactive waste disposal. Whereas extrapolations based on Arrhenius equations are demonstrably quite reliable for *forward rates*, this is unfortunately not the case of *residual rates,* which are more relevant for realistic safety assessment calculations. The comparison of long-term experiments conducted on six different borosilicate glasses, including SON68 and MW, shows no direct correlation between *forward* and *residual rates* (Gin et al. 2013a). Contrary to *forward rates, residual rates* are very sensitive to the transport properties of the gel layer, which are a complex function of many chemical-physical parameters. This makes temperatures extrapolations of *residual rates* practically impossible. More importantly, glass corrosion data of good quality and sufficient leach time duration (several years), that could be used directly to determine *residual rates* at 40 – 50 °C with confidence, are scarce.

To illustrate the problem, Fig. 4-4 shows selected data from the JSS project obtained at different temperatures (JSS 1984a,b,c, JSS 1985, JSS 1986, JSS 1987a,b, JSS 1988a,b). The data were obtained from powders (S/V = 1'100 m^{-1}) of the ABS118 glass (an alpha-doped version of SON68) leached in initially pure water. After 1 year, the results indicate the expected "ranking" of *forward rates*, with the highest boron release at 90 °C and the lowest at 50 °C. The *residual rates* are determined by the slope defined by data between 3 months and 1 year. Also in this case, the temperature "ranking" is as one expects. Between the last two sampling times, the 50 °C data indicate no further release of boron, implying a corrosion rate approaching zero; at 70 °C a weak positive slope indicates very slow glass dissolution. Finally, at 90 °C the release of boron can be converted into a rate of about 0.001 g m^{-2} d^{-1}. However, the 90 °C data clearly show that a *residual rate* regime is not attained after 1 year and a large scatter, likely due to the unreliable "parallel experiments" technique. Moreover, the *residual rates* at 50 °C and 70 °C are based on just one time increment. We know presently that 1 year leach time is not sufficient to obtain well assessed *residual rates*. Even if appealing, it would be quite speculative to affirm that at 50 °C the corrosion of the glass has stopped completely.

Recent results (Gin et al. 2020a) obtained from dedicated experiments with a simple borosilicate glass (International Simple Glass, ISG) aiming at clarifying the factors governing the *residual rate*, apparently indicate that pH-dependent diffusion properties controlled by the linkage of Si-O-B bonds play a much more important role than temperature in determining long-term corrosion rates. If confirmed these results would imply that *residual rates* are relatively insensitive to temperature and that the results obtained at 90 °C could be even taken as representative also for repository conditions.

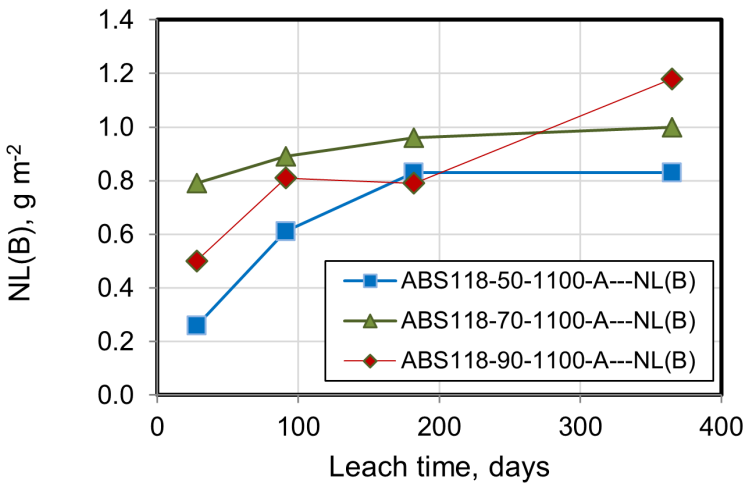

Fig. 4-4: Normalized boron mass losses for leach experiments carried out with powders (S/V = 1100 m^{-1}) of glass ABS118 at three different temperatures

50 °C (blue), 70 °C (green) and 90 °C (red)

4.3.3 Effect of self-irradiation

4.3.3.1 Preliminary remarks

As already noted, most glass corrosion experiments are carried out with simulants of the actual vitrified radioactive waste. In such analogue materials, dose-relevant fission products such as ^{135}Cs, ^{89}Sr, ^{107}Pd ^{126}Sn, ^{93}Mo, ^{93}Zr are replaced by stable isotopes of the same elements, while ^{99}Tc and actinides are replaced by surrogate elements (Mn and REEs, respectively). Fast decaying U and Th isotopes are replaced by natural U and Th. The use of simulants greatly simplifies technical issues and makes the use of advanced analytical tools for the characterization of solutions and altered glass possible. This explains the overwhelming dominance of glass dissolution data from inactive glasses.

Therefore, knowledge on the effect of α,β,γ-irradiation on glass corrosion kinetics is scarce. Particularly α-radiation gives rise to reversible or irreversible damage in the glass network structure, which potentially has an impact on the dissolution kinetics. One must also take into account that carrying out a corrosion experiments with present-day radioactive vitrified waste is not sufficient, because the effects of damage accumulated over thousands of years, until canister failure occurs, are not yet present in the glass. Fortunately, there are however techniques for simulating cumulative doses representative of such failure times, e.g. doping with appropriate amounts of fast decaying actinides.

The issue of the transferability of the results from corrosion experiments with simulants to vitrified radioactive waste at the relevant time is of course a central one for the safety assessment and has to be considered carefully. In this Section, we first review published data on structural damage caused by external and internal irradiation of the (non-leached) glass. This is followed by a review and interpretation of the limited data available on aqueous corrosion of radioactive borosilicate glass and some concluding remarks on the status of this topic.

4.3.3.2 Effects of irradiation on molecular borosilicate glass structure

In vitrified radioactive waste, a number of self-irradiation processes take place (Matzke 1988, Weber et al. 1997). The processes are similar to those taking place in spent fuel, although doses (particularly the α-dose) are in general lower due to the almost quantitative extraction of U and Pu during reprocessing. Tab. 4-2 gives a summary of the relevant self-irradiation processes for the R7T7 (SON68) glass, including their length ranges, the number of atomic displacements per single event, and the cumulative number of displacements after 1'000 years ageing time. Tab. 4-2 readily reveals that the effect of neutrons and fission fragments on structural changes in the glass is negligible compared to the effect of α, β and γ radiation. Moreover, it is evident that atomic displacements in the glass structure are mainly caused by alpha particles and the related recoil nuclei.

In order to simulate the effect of radiation on the glass structure over thousands of years, either bombardment of the glass sample with heavy ions/ electrons/ gamma radiation, or doping with fast-decaying isotopes (^{244}Cm, ^{238}Pu, ^{241}Am, ^{137}Cs) is used. The former method is easier and popular but has several shortcomings, e.g. a very limited penetration depth (particularly for heavy ions) undesired thermal effects on the sample and the impossibility to simulate the effect of alpha particles. The preferred method is clearly doping, which however requires complex synthesis techniques and generates highly radioactive materials.

Macroscopic changes observed due to self-irradiation are: (i) volume changes, either densification or expansion (depending on type of irradiation and dose) and (ii) formation of fissures and cracks (Weber et al. 1997). For R7T7 (SON68) glass doped with ^{244}Cm, a progressive densification by up to 0.6% was observed when the cumulative dose was increased to 3×10^{18} decays/g. At higher

doses, no further volume change took place, i.e. a saturation effect was observed (Godon 2004). In addition, similarly to spent fuel, helium bubbles are formed due to accumulation of alpha particles. The saturation effect of the volume change suggests that a steady-state equilibrium is reached between the production of radiation-induced structural defects and the recovery of such defects (healing).

Another issue is the increase in solid-state diffusivity of sodium observed under the effect of external beam irradiation. Matzke & Vernaz (1993) report that the diffusivity of sodium is increased by several orders of magnitude after bombardment of the glass with electrons and heavy ions (suggesting that enhanced diffusivity could apply also to radionuclides). This effect (see e.g. Boizot et al. 2000) was however identified by Matzke & Vernaz (1993) to be an artefact induced by the accumulation of charges during the external bombardment. It is not observed in actinide-doped glasses.

More recently, radiation damage research on glasses has focused on atomic-scale effects that are potentially relevant to dissolution kinetics. Mendoza et al. (2014) studied the structural evolution of the network structure in simplified SiO_2-B_2O_3-Na_2O-(CaO-Al_2O_3-ZrO) glasses under irradiation with Kr and Xe ions, using Raman spectroscopy and NMR (^{11}B, ^{23}Na, ^{27}Al and ^{29}Si). The results indicate a significant depolymerisation of the network structure. The mean boron coordination number was reduced and overall structural disorder increased. These authors concluded that "*the glass structure after irradiation resembles a vitreous state frozen from a very high-temperature liquid*". Moreover, the identification of 5-fold and 6-fold coordinated aluminium and high concentrations of three-membered rings of [SiO_4]-tetrahedra was interpreted as evidence of structural disequilibrium.

Tab. 4-2: Summary of nuclear reactions taking place in vitrified radioactive waste

Simplfied after Godon (2004)

Irradiation type	**Length range**	**Displacements per decay**	**Displacements/g** [10^3 y]
α	20 µm	100 – 200	$(1.7 – 3.4) \times 10^{20}$
Recoil nuclei	30 µm	1'000 – 2'000	$(1.7 – 3.4) \times 10^{21}$
β	1 mm	≈ 1	4×10^{19}
γ	cm	<< 1	$<< 2 \times 10^{19}$
Neutrons (α,n)	1 m	200 – 2'000	$(0.6 – 6) \times 10^{15}$
Fissions	10 µm (fragments)	10^5	$(0.1 – 6) \times 10^{17}$
	1 m (neutrons)	200 – 2'000	$(0.02 – 1) \times 10^{15}$

In a later study, Peuget et al. (2018) compared the effects of external heavy ion irradiation (Au) with those of self-irradiation induced by ^{244}Cm doping with the same methods used by Mendoza et al. (2014) and XANES. Overall, the results, obtained on the ISG glass, confirmed the findings of Mendoza et al. (2014). However, the external irradiation experiments were found to overestimate the structural damage actually observed in the self-irradiated glass. The overestimation resulted from the lack of recovery effects in the externally irradiated (non-doped) glass, which are instead efficient in self-irradiated glass.

Peuget et al. (2014) and Tribet et al. (2020) summarized the modifications of the glass structure induced by real α self-irradiation or external heavy ion bombardment. Accordingly, such modifications include: a decrease in density, Young's modulus and hardness, an increase in the number of non-bridging oxygens (i.e. depolymerisation of the (Si,B)-O network), the formation of molecular oxygen, changes in coordination of network formers such as boron and aluminium. The depolymerisation is expressed by an increase of three-fold coordinated boron at the expense of four-fold coordinated units. NMR studies show that the number of non-bridging oxygen ions increase up to a limiting cumulative dose, beyond which no further increase is observed (saturation). These changes reduce the number of interlinked (Si,B)-O bonds, implying that less of such bonds must be broken for the glass to dissolve. This suggests a potentially faster glass dissolution kinetics compared to simulated vitrified waste.

4.3.3.3 Effect of irradiation on glass corrosion kinetics

Prolonged α, β and γ self-irradiation may influence the aqueous corrosion of vitrified borosilicate waste due to the induced atomic-scale structural damage (cf. Section 4.3.3.3). Secondary effects could play a role as well. For instance, radiation may alter the passivating properties of the gel. Water radiolysis may affect glass corrosion via (i) production of oxidizing radicals that may increase the local Eh or (ii) production of nitric acid, potentially reducing the pH in corrosion experiments carried out in contact with air or nitrogen gas (Godon 2004). It is seldom possible to separate these multiple effects when evaluating the scarce published experimental data available. In this section, an overview of the results so far obtained from corrosion of active glasses is given in chronological order, with emphasis on recent results that apparently resolve long-standing issues on the role of self-irradiation.

One of the first studies including leach experiments with radioactive borosilicate glass was the JSS project (Werme et al. 1990, Curti 2018). Corrosion experiments were conducted with a radioactive version of the French glass (denoted JSS-A) as well as with non-active glasses (denoted ABS-118 and R7T7) under the same conditions. All three glasses have compositions almost identical to SON68, except that JSS-A was doped with 2.2 wt.-% of PuO_2 and other radionuclides, simulating the specific α,β activity of 100-year aged vitrified waste (8.5×10^9 Bq/g). Fig. 4-5a and Fig. 4-5b show the normalized mass losses of B and Li after corrosion in deionized water during about 1.5 years for the JSS-A and ABS-118 glasses, compared with the results obtained later on SON68 (Curti 2003, Curti et al. 2006) under comparable conditions (static tests with initially pure water). The data indicate a larger extent of corrosion for the radioactive glass during at least the first 3 months. Later, the difference in cumulative B and Li releases between active and inactive glasses decreased, suggesting that the initially enhanced corrosion of the active glass is a transient phenomenon. Unfortunately, the short time ranges and poor statistical quality of the data make it impossible to derive usable *residual rates* from the JSS-A and ABS-118 data. The only provisional conclusion that can be drawn is that, despite the short-term enhancement, the corrosion rate of the JSS-A glass decreases to values comparable to that of the inactive SON68 and ABS118 glasses after three months and up to 1 year leach time.

Fig. 4-6 shows boron normalized mass loss data for experiments under the same conditions as shown in Fig. 4-5, but in the presence of bentonite and magnetite powder (simulating the buffer material and canister corrosion products). In this case, the extent of corrosion can be considered, within experimental uncertainties, to be equal for the radioactive and non-active glass, indicating no influence at all of self-irradiation during 1 year leaching. Based on these data, Werme et al. (1990) concluded that "*the dissolution behavior of the radioactive glass JSS-A was similar to that of the simulated waste glasses [...] for the short-term, transient period*". Note that the amount of glass corroded in the presence of bentonite and magnetite was in all cases much larger than in the experiments with no additives. Such effects are described in detail in Section 4.4.

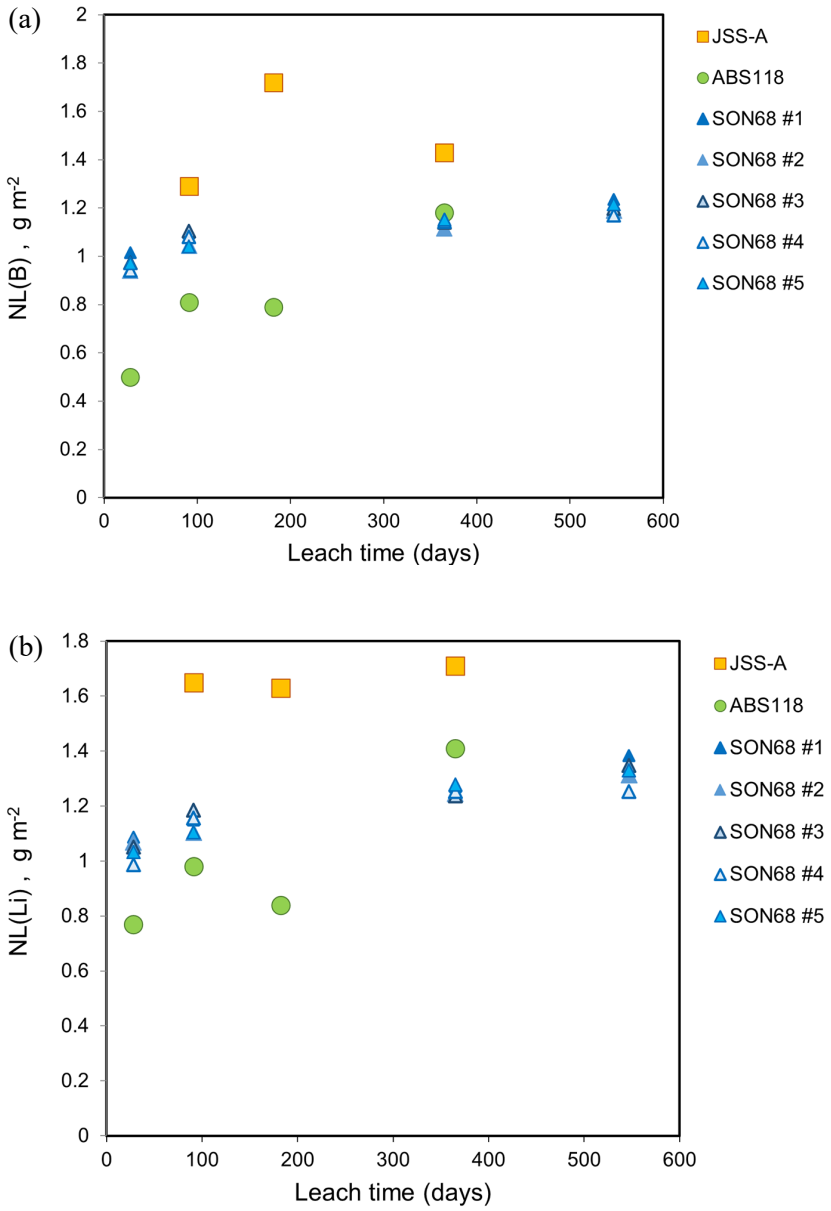

Fig. 4-5: Normalized mass losses of B and Li for the radioactive glass JSS-A and two equivalent simulants (ABS-118, SON68) from static experiments in deionized water at 90 °C and S/V = 1'100 – 1'200 m^{-1}

A good summary of data on radioactive glasses obtained up to the early 2000's is given in Godon (2004), pp.135 – 139. Based on the CEA-internal data and other published studies (McVay & Pederson 1981, Werme et al. 1990, Feng et al. 1993) the following conclusions were reached:

- The *forward rates* of inactive borosilicate glasses and their counterparts doped with activities comparable to industrial vitrified waste are identical.
- A comparable decrease by several orders of magnitude in corrosion rate is observed both for inactive and radioactive glasses.
- β, γ-radiolysis retards the attainment of the *residual rate* regime via pH decrease or modification of the gel layer properties. This effect is not observed for alpha radiolysis.

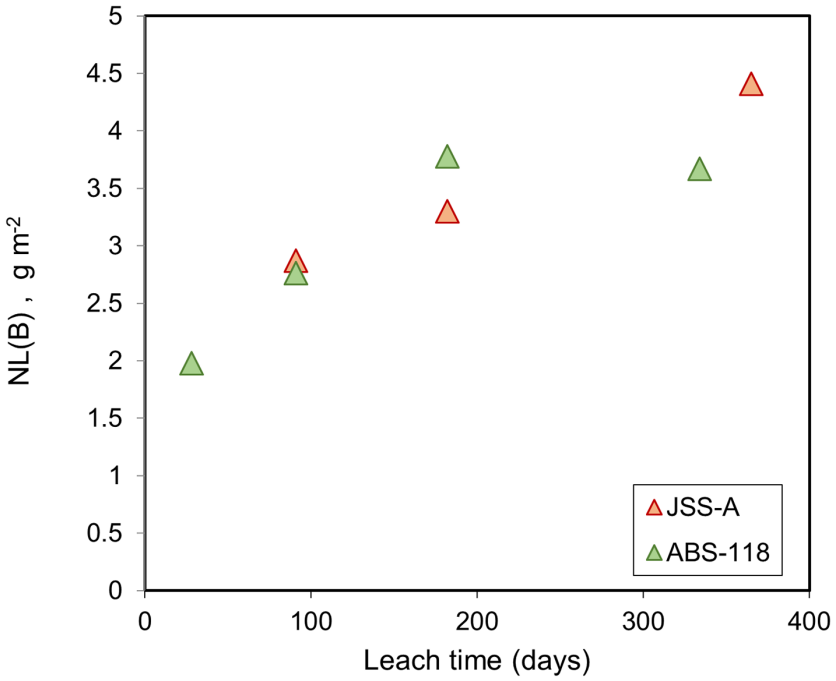

Fig. 4-6: Normalized mass losses of B for the radioactive glass JSS-A and the equivalent simulant ABS-118 from static experiments in deionized water at 90 °C and S/V = 1'100 m^{-1}, in the presence of magnetite powder and bentonite

Accordingly, Advocat et al. (2001) state that "*experimental results obtained with high-level radioactive glass [...] confirm the behaviour on simulated non-radioactive glass*" and further, rather optimistically, that "*no difference was found between the initial alteration rates measured on active glass specimens, nor in the long-term alteration rates*".

After this study, practically no further data on radioactive glass corrosion appeared until 2013, when a renewed interest emerged and new glass corrosion experiments with α.β-doped glass were carried out under strictly controlled conditions, higher S/V ratios and longer leach time. These new studies mainly focused on the *residual rate* regime and conditions relevant to geological disposal.

In order to separate the effects of α and β radiation, Rolland et al. (2013) studied two SON68 glasses, one doped with 0.85% $^{239}PuO_2$ (α emitter), the other with 0.24% $^{99}TcO_2$ (β emitter). No glass combining the two types of radioactivity was studied. The α-activity is representative of vitrified waste aged about 1'500 years. Leach experiments were carried out statically with a duration of almost 3 years in initially pure water at 90 °C and compared with those of the inactive SON68 glass. High S/V ratios (2600 m^{-1}) were selected in order to attain rapidly the *residual rate* regime. Furthermore, a sequential sampling technique similar to that used by Curti et al. (2006) was employed, with considerable amounts of glass (10 g) and water (300 mL) in a stainless-steel vessel under Ar flushing, allowing achieving a better precision of the calculated rates.

The results indicate that in the *residual rate* regime both active glasses corrode at very low rates comparable to that determined for the non-active reference ($\leq 1 \times 10^{-4}$ g m^{-2} d^{-1}). Actually, the uncertainties in the *residual rate* determination did not allow defining minimum rates above zero. The data in Fig. 2 of Rolland et al. (2013) confirm for the Pu-doped glass the initial preferential dissolution observed in older experiments with alpha-doped glasses. However, after 1 year leaching time the total amount of corroded inactive SON68 glass was larger than for both

radioactive glasses. This might be explained by the lower pH in the "active" experiments (pH 8.2 – 8.5) compared to the "inactive" experiment (pH 9.3), possibly arising from radiolysis of air contaminating the Ar stream. Electron microscopy images show a type of alteration similar to that described in Curti et al. (2006) with no substantial differences among active and inactive glass.

In two subsequent studies (Mougnaud et al. 2016, Mougnaud et al. 2018), corrosion experiments in initially pure water were carried out with two borosilicate glasses at 90 °C, a REE-doped glass (Z4C4) and ISG. Before leaching, the glass samples were subject to external irradiation with 10 MeV electrons (in order to mimic the effects of β-irradiation) or with Au ions (0.3 – 3.5 MeV) with a cumulative dose of 214 MGy (simulating long-term α-irradiation). In both cases, the glasses were leached at very high S/V (20'000 m^{-1}) in order to establish quickly a *residual rate* regime. In the experiments simulating β-irradiation, the NL(B) values determined over a leaching time of two months proved to be identical (within analytical uncertainties) to those measured in the reference experiment, indicating that the external irradiation with electrons had no effect on the corrosion kinetics. The electron irradiation apparently had no or only minor effects on the structure of the glass and of the altered layer. In contrast, the bombardment with Au ions had a significant impact on the corrosion kinetics of the glass. From microscopic observations of monolithic glass samples added to the glass powders (see Fig. 2 in Mougnaud et al. 2018) it could be established that the thickness of the altered layer progressively increases with cumulative dose, reaching a plateau (saturation) at about 1/10th of the maximum deposited energy (op. cit., Fig. 5). The irradiated glasses were 4 – 5 times more altered than the reference non-irradiated materials after 2 – 3 months leaching. Nonetheless, a very low *residual rate,* comparable to that of the non-irradiated material appeared to be established after 2 months, suggesting that the increased corrosion rate of the irradiated glasses was a transient phenomenon.

Tribet et al. (2020) examined the properties and evolution of the alteration layers formed in the ISG glass during the experiments of Mougnaud et al. (2018), using advanced TEM microscopy on FIB samples. They found that, despite the similar evolution of the altered layer in irradiated and non-irradiated glass, after 13 days of leaching the alteration layer thickness of the irradiated glass was 6 times larger than for the non-irradiated glass. From this observation, the authors concluded that up to this time the faster corrosion of the irradiated glass was due to the Au-ions induced damage of the primary glass structure, not by different properties of the alteration layer. Afterwards, the evolution of the gel layer differed in that nanoporosity evolved faster in the irradiated glass. According to the authors, this could have increased the diffusivity of water and solutes through the alteration layer of the irradiated glass between 13 days and 58 days (end of leaching). The latter conclusion was supported by the observation that ^{18}O (added to the leaching solution as stable isotope tracer) diffused faster into the alteration layer of the irradiated glass compared to the non-irradiated counterpart. Thus, in conclusion the faster dissolution of the irradiated ISG glass observed during 58 days leaching can be ascribed to a dual effect of the irradiation pre-treatment: (a) a "weakening" of the glass network structure (formation of dangling bonds, depolymerisation) and (b) a faster maturation of a nanoporous gel compared to the non-irradiated glass.

New important data on the long-term effects of irradiation on borosilicate glass alteration are provided by the Ph.D. thesis of Mougnaud (2017), who conducted a corrosion experiment with SON68 glass doped with 0.43 wt.-% $^{244}CmO_2$. The objective was to determine the influence of a realistic long-term accumulation of α decays (i.e. a cumulative α-dose representative of canister failure times) on the corrosion rate of the glass. ^{244}Cm has a short half-life (18.11 a), allowing to accumulate a dose comparable to that experienced by vitrified waste at canister failure times within laboratory timescales, however at much higher dose rates than in real vitrified waste. The total cumulative dose at the start of the experiment was calculated to be 3.3×10^9 Gy, which corresponds to an age of the waste of about 1'000 y (the standard assumed failure time in France).

The results of this experiment were compared with those of a reference test carried out with non-radioactive SON68 and of an earlier experiment carried out with ^{239}Pu-doped glass by Rolland et al. (2013). Owing to its long half-life (24'110 a), ^{239}Pu provides dose rates typical of aged vitrified waste at canister failure time, but the total dose that can be accumulated during a laboratory experiment is much lower. To summarize, none of the two glasses simulates simultaneously the cumulative dose and the alpha dose rate that real vitrified waste would have at canister failure times.

Tab. 4-3: Cumulative doses and dose rates of α-doped SON68 glasses used in experiments to determine the effect of alpha-decay on glass corrosion, compared to corresponding values for real vitrified waste of 10'000 years age

	^{239}Pu-doped glass [1]	**$^{238/239}$Pu-doped glass** [3]	**^{244}Cm-doped glass** [2]	**^{244}Cm-doped glass** [3]	**Vitrified waste**[a] [at 10^4 y]
Dose rate (Gy/h)	150	3'500	21'050	23'500	<100
Cumulative dose (Gy)	≈3 E+05 [b]	1.4 E+07 (< 1 E +05)[c]	3.3 E+09	3.5 E+07	1 E+10

[1] Rolland et al. (2013). [2] Mougnaud (2017). [3] Tribet et al. (2021)
[a] Numbers taken from Fig. 35 in Mougnaud (2017)
[b] Estimated from cumulative dose data given in Table 1 of in Tribet et al. (2021)
[c] After annealing

The results of the leach experiments carried out with the two aforementioned α-doped glasses and with non-active SON68 are shown in Fig. 4-7. While the final extent of corrosion of the ^{239}Pu-doped glass is, as noted earlier in this Section, by 20 – 30% lower than in the reference experiment with non-active glass, the boron release from the ^{244}Cm-doped glass considerably exceeds the release from both ^{239}Pu-doped and non-active reference glass. More importantly, after two years the ^{244}Cm-doped glass had apparently not yet reached a *residual rate* regime. From the last three data points (between 400 and 700 days leaching time), a constant rate of 6×10^{-4} g m^{-2} d^{-1} was extracted by Mougnaud (2017), compared to final rates of about 1×10^{-4} g m^{-2} d^{-1} for the other two glasses.

Because, as already noted, neither the ^{244}Cm-doped glass nor the ^{239}Pu-doped glass simulate simultaneously the cumulative dose and the alpha dose rate of real vitrified waste, the effects of the two parameters cannot be disentangled. In particular, it is not possible to determine unequivocally which of the two mechanisms is responsible for the enhanced corrosion rate of the ^{244}Cm doped glass. Mougnaud (2017) suggests (but cannot prove) that the high corrosion rate it is mainly due to irreversible damage in the glass structure arising from ballistic effects induced via α-decay (recoil nuclei).

Very recently, new leach tests with radioactive SON68 glass doped with ^{244}Cm or ^{238,239}Pu were carried out with the aim of disentangle the effects of cumulative α-dose and dose rate (Tribet et al. 2021). The cumulative dose and alpha dose rates of these two additional glasses are also reported in Tab. 4-3. The glasses were leached under static conditions at 90 °C and high S/V ratios (from 2'300 to 7'600 m^{-1}) in initially pure water during 2.2 to > 5 years. Due to the high S/V ratios, silica concentrations raised within few months to characteristic "saturation" values (~ 1 – 2 mM Si), so that virtually all tests then proceeded in the *residual rate* regime.

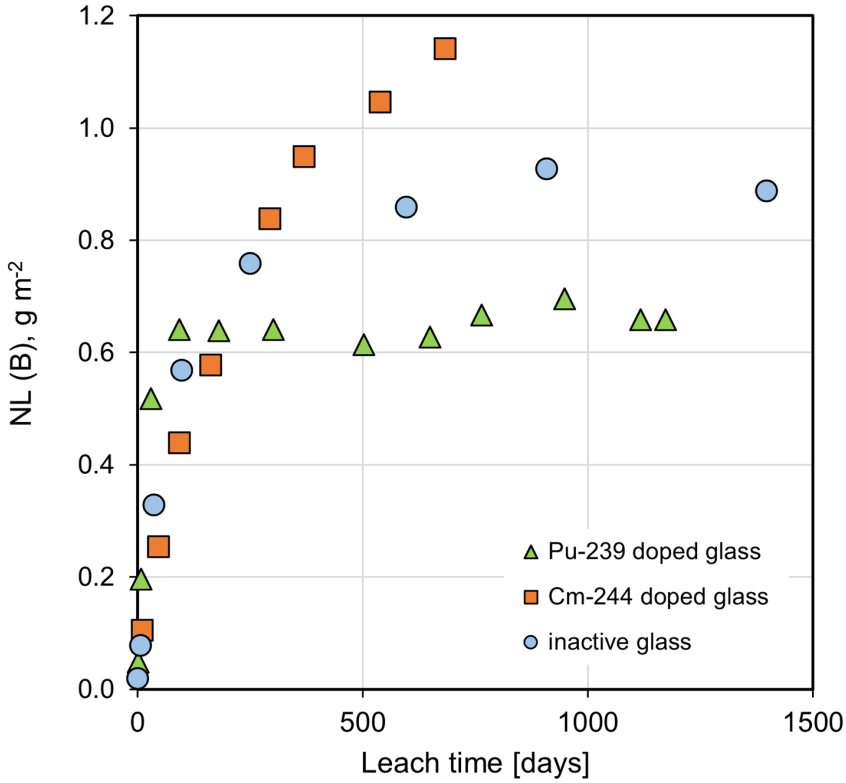

Fig. 4-7: NL(B) data for the corrosion of ^{239}Pu-doped, ^{244}Cm-doped and inactive SON68 glass in pure water at 90 °C and S/V = 20'000-27'000 m^{-1}

Redrawn after graph digitation from Mougnaud (2017)

The effect of dose rate alone was evaluated by comparing the results of the leach test with the annealed ^{238,239}Pu-doped sample (high dose rate, negligible cumulative dose) to the results of the previously discussed test with ^{239}Pu-doped glass of Mougnaud (2017) (intermediate dose rate, negligible cumulative dose) and of reference tests with inactive SON68 (negligible dose rate, negligible cumulative dose). The data (not shown, see Fig. 2 in Tribet et al. 2021) indicate that the dose rate has no effect, since in all experiments (including those with inactive reference glass) residual rates in the range 1 – 3 × 10^{-4} g m^{-2} d^{-1} were obtained.

The effect of cumulative dose was evaluated with the help of the ^{238,239}Pu-doped SON68 glass sample, aged ~ 30 years and therefore having accumulated a substantial total dose at comparatively low dose rate. Half of the sample was separated and thermally annealed[11], drastically reducing the cumulative dose. The annealing led to almost complete recovery of the structural defects induced by alpha radiation, leaving a residual cumulative dose more than two orders of magnitude lower than in the non-annealed sample. Then, leach experiments with annealed and non-annealed glass were carried out under identical conditions. By comparing the results of the two experiments, it is then possible to isolate the effect of cumulative dose.

[11] The glass was heated for 3 hours at 545 °C, i.e. 35 °C above the glass transition temperature of the specific glass.

The results, summarized in Fig. 4-8, are conclusive as they show that differences in cumulative doses *at equal dose rate* have a strong effect on the glass dissolution kinetics. From the normalized boron losses, residual rates of $(1.14 \pm 0.03) \times 10^{-3}$ g m^{-2} d^{-1} are obtained for the alpha-damaged

(non-annealed) glass, while the recovered (annealed) glass corrodes at $(2.3 \pm 0.2) \times 10^{-4}$ g m^{-2} d^{-1}, which is close to the long-term rate determined for non-active SON68 glass over 12 years, $(1.3 \pm 0.2) \times 10^{-4}$ g m^{-2} d^{-1}. Therefore, it can be concluded that the effect of the high cumulative dose alone was to increase the residual corrosion rate by about 5 times.

We conclude this section by briefly mentioning the results obtained in the framework of a Ph.D. by De Echave (2018), focusing on the corrosion behaviour of SON68 under repository-like conditions. All experiments were carried out at 70 °C, reflecting the early failure scenario in the Callovian-Oxfordian (COx) repository in France. According to the results obtained from boron releases, the dissolution of a SON68 glass doped with 0.85% $^{238}PuO_2$ (α dose rate = 3400 Gy h^{-1}, cumulative α-dose =1.1×10^9 Gy) in simulated clay (COx) water was found to be identical to that measured for the non-active reference glass. After 34 days of leaching, in both cases the average thickness of the weathered glass was about 1.2 µm while after 104 days it was approximately 2.5 µm. Thus, contrary to the experiments in pure water no short-term effect of alpha radiation on glass corrosion kinetics could be found in clay-dominated environments. The limited leaching times in these experiments however do not allow any conclusion on the long-term behaviour.

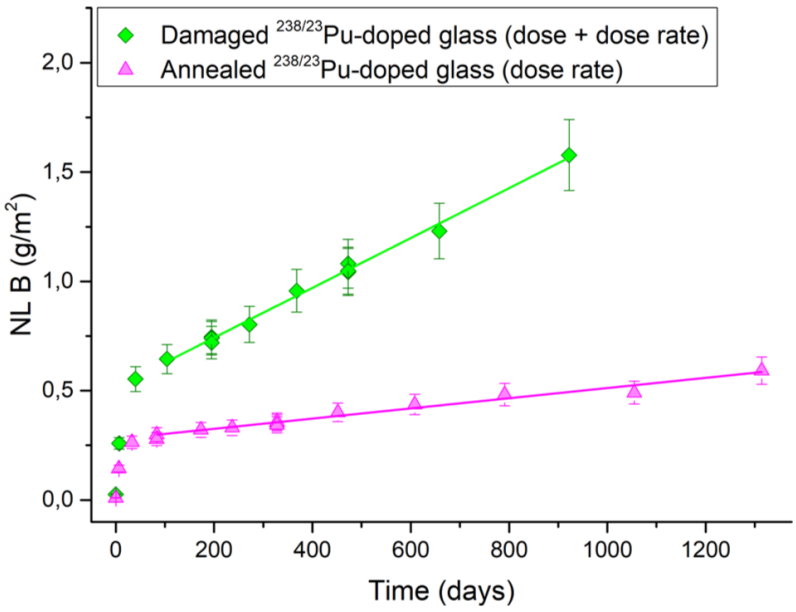

Fig. 4-8: NL (B) data from static leach experiments carried out with alpha-damaged (green diamonds) and annealed $^{238/239}$Pu-doped SON68 glass (pink triangles)

Reproduced from Tribet et al. (2021)

4.3.4 Effect of glass composition (Mg only)

Intrinsic effects on aqueous corrosion arising from the composition of the glass are manifold and complex due to the wide compositional range of silicate glasses. It is not the purpose of this review to treat this topic in detail, since the compositional range of vitrified waste arising from Swiss nuclear reactors is quite restricted by the specifications of the two reprocessing plants in La Hague (France) and Sellafield (U.K.) in charge to reprocess the Swiss spent fuel. These are reflected in the "limiting" compositions of the SON68 and MW simulants, which differ significantly only in the contents of Ca, Zn and Mg oxides. Whereas SON68 is Mg-free and contains a few wt.-% of CaO and ZnO, these two components are absent in the MW glass and are "replaced" by about 6 wt.-% MgO (Tab. 1-1). In spite of the minor compositional differences, the *residual rate* of the MW glass in pure water at 90 °C ($9.6 \pm 5.3 \times 10^{-4}$ g m^{-2} d^{-1}) is 5-7 times larger than for SON68 ($1.3 \pm 0.2 \times 10^{-4}$ g m^{-2} d^{-1}) (Tab. 4-4, Fig. 4-9) (Curti 2003, Curti et al. 2006).

This large difference in kinetic rates in spite of relatively small compositional differences is quite surprising and calls for an explanation. After a series of dedicated studies, it is now clear that the presence of Mg in the glass formulation is responsible for the enhanced dissolution of the MW glass. Frugier et al. (2005) found that, in spite of comparable *forward rates* in pure water, the 1-year rates of the French Mg-bearing AVM[12] glasses at 50 °C were on average higher than for the Mg-free R7T7 glasses ($1.8 \pm 1.9 \times 10^{-3}$ g m^{-2} d^{-1} and $1.8 \pm 0.8 \times 10^{-4}$, respectively, see Fig. 4-10). This was attributed to the formation of Mg-rich "phyllosilicates" precipitated on top of the AVM-glass alteration layers, which sequestrates silica released from the dissolving glass, thereby reducing the steady state aqueous silica concentration and thus limiting the silica recondensation reactions responsible for the passivation of the gel layer. Curti et al. (2006) come to similar conclusions, emphasizing the role of magnesium as a known catalyst for clay mineral formation. They identified the Mg-rich reaction products in the MW glass as trioctahedral smectites with composition intermediate between montmorillonite and saponites.

Later studies elucidated more precisely the role of Mg in the evolution of borosilicate glass alteration. Thien et al. (2010) identified the Mg-rich products in the AVM glass as saponitic clay close to the composition of hectorite (a Li-Mg clay mineral) which is also compatible with the presence of lithium in the glass formulation. In a subsequent study, Thien et al. (2012) found that magnesium, depending on pH and Mg concentration in the glass or in the external solution, may also have the opposite effect. In such cases, it improves the passivation properties via exchange of Mg^{2+} for Na^{+} in the gel. This is possibly the reason for the lack of a clear correlation between glass corrosion rate and MgO content in the glass (Fig. 4-10, see also Fig. 2 in Thien et al. 2012).

In the repository environment, effects related to glass composition cannot be decoupled from the influence of other solutes present in the pore water corroding the glass after canister failure. Major dissolved components can interfere and compete with such primary "intrinsic" effects. This is exemplarily shown in the experimental work of Aréna et al. (2017, 2018) who studied the influence of dissolved Mg^{2+}, Fe^{2+} and Ca^{2+} on the kinetics of the ISG glass dissolution and their interplay with the gel properties. It was shown that these cations, when added to the leachant in substantial concentrations, trigger the precipitation of secondary silicates, thereby preventing the formation of a passivating (polymerized) Si-rich gel. The result is an increase in corrosion rate compared to leaching in water or dilute solutions. As soon as the silicate precipitation ceases (due to attainment of saturation equilibria) Mg^{2+}, Fe^{2+} and Ca^{2+} tend to be incorporated into the gel, making it denser and more protective. Such effects from the solution may overprint those induced by the elements released from the glass.

---

[12] AVM is a specific (minor) category of nuclear waste glass arising from reprocessing of French graphite-gas reactors operated with natural uranium, in contrast to the dominating R7T7-type (to which SON68 belongs) arising from reprocessing of the LWR spent fuels.

Tab. 4-4: Long-term glass dissolution rates for the MW and SON68 glasses calculated from B and Li normalised mass losses at reaction times ranging from 548 to 3'650 days

The data of all ten experiments were considered in the regression calculations.

Rates [g m^{-2} d^{-1}]	**Rates from *NL(B)***	**Rates from *NL(Li)***
MW	9.6 (± 5.3) × 10^{-4}	6.8 (± 4.3) × 10^{-4}
SON68	1.3 (± 0.2) × 10^{-4}	1.3 (± 0.3) × 10^{-4}

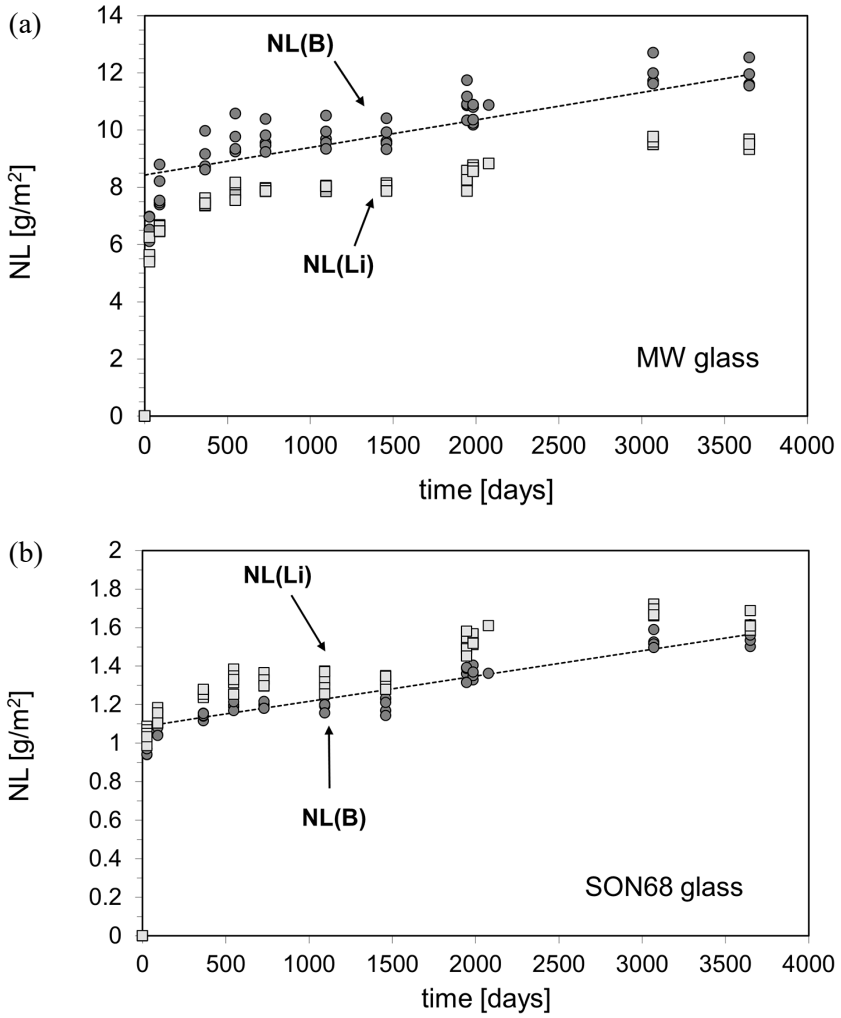

Fig. 4-9: Normalised mass losses for the MW (a) and SON68 (b) glass determined from the PSI long-term experiments in initially pure water at S/V = 1'320 m^{-1}, at 90 °C and free pH-drift

The dotted line show the linear regressions through *NL(B)* data.

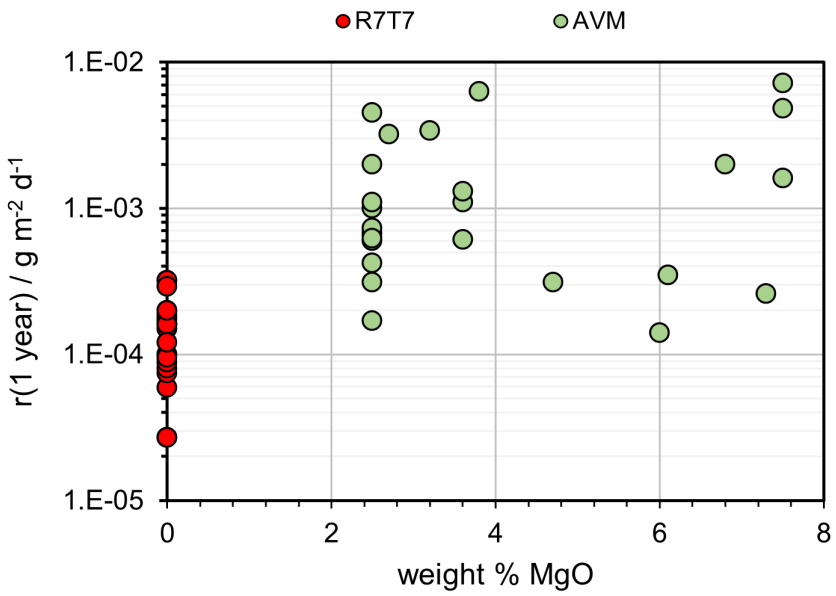

Fig. 4-10: Corrosion rates of R7T7 and AVM glasses compared after 1 year leaching time

Data were taken from Frugier et al. (2005)

4.4 Effects of near-field repository environment

4.4.1 Preliminary remarks

Most of the preceding discussion in this chapter was focused on the alteration of the waste glass under simplified laboratory conditions, in which external effects due to the repository environment were intentionally excluded. The main purpose of the experiments described in Sections 4.2 and 4.3 was to identify the main chemical-physical parameters affecting the corrosion kinetics. In the present section, the focus is on indirect effects arising from the materials surrounding the vitrified waste in the repository. The materials to be considered in the near-field of the reference HLW repository are compacted clays (specifically bentonite), iron and iron corrosion products formed via anaerobic corrosion of the carbon steel canister (with or without copper coating). The vitrified waste itself is emplaced in a thin container made of stainless steel alloy ("coquille"), which is more resistant to aqueous corrosion than the carbon steel canister.

Also included in this Section are the effects of cementitious materials. Cementitious backfill materials instead of bentonite, similar to those envisaged in the Belgian concept, were considered in the framework of a potential alternative repository design (Cloet et al. 2019). This setup has been analysed by Nagra only for comparison purposes and is not considered as realistic alternative emplacement concept.

4.4.2 Effect of clay

The influence of clay-based host-rock and engineered barrier materials on glass corrosion kinetics has been studied thoroughly during decades. Godon (1988) showed for the first time that R7T7 glasses degrades faster when smectitic or other types of clay are added to pure water in standard leach experiments. The phenomenon was attributed to silica sequestration via sorption on the clay surface which would decrease the silica concentration in solution and thus, according to the *affinity law*, increase the corrosion rate. In the subsequent years, a collaboration on this topic was established between PSI and CEA Marcoule to test this assumption. A model (GLADIS) was developed at PSI to interpret and explain the results of dedicated experiments conducted by CEA.

The experiments (Godon & Vernaz 1989) consisted of monolithic glass samples placed in the middle of dry smectite clay within cylindrical stainless-steel vessels. After sealing, the clay was saturated with water thermostated at 90 °C. A series of such experiments was started and interrupted at the desired time. At the end of each experiment, the glass was retrieved and the mass loss was determined gravimetrically up to a leaching time of two years.

In the model (Curti & Smith 1991), which assumes a cylindrical geometry, the *affinity law* (Grambow 1985, Vernaz & Dussossoy 1992) was fully coupled to solute diffusion and instantaneous reversible sorption of silica on the water-saturated clay. The sorption of Si was quantified via distribution coefficient (K_d [m^3/kg]), treated as adjustable parameter to be fitted to the data. All other parameters were known or measured independently. In spite of the large spread (0.005 to 0.5 m^3/kg), the results of the modelling (Fig. 4-11) indicated optimised K_d-values lying within the range of Si distribution coefficients measured in batch experiments with dilute clay slurries (published literature). The most important finding of the modelling was however that it was not possible to predict the observed mass losses without assuming significant silica sorption on the clay (cf. curve "no Si sorption" in Fig. 4-11).

The comparison of the curves for 0.005/0.01 m^3/kg with the results labelled "no sorption" in Fig. 4-11 clearly shows an increase in the extent of corrosion by a factor of 10-20 with respect to the reference calculation with no Si sorption on the clay. This is indeed a strong effect, which has been repeatedly confirmed (see below). From today's perspective, the successful modelling of these experiments with GLADIS appears quite surprising, given that the *affinity law* does not consider the now well-established passivating effects of the gel layer.

This apparently contradictory result may be explained by the relatively low S/V ratio and high clay/glass ratio involved in the modelled experiments, which probably caused effective sequestration of silica and prevented the formation of a passivating gel.

The role of clay/glass ratio has been confirmed by experiments conducted both in the underground and in the laboratory. In the framework of the Belgian program, polished wafers of α-doped SON68 glass were corroded in the underground laboratory at Mol (B) in direct contact with the host rock (Boom Clay) or with compacted moist Ca bentonite, at 16 °C – 170 °C and pHs from 6 to 9 (Kursten et al. 1997). At the end of the experiments (duration 1.3 – 7.5 years) the normalized mass losses were determined, showing up to a 1'000 times larger extent of corrosion compared to the reference test in pure water (see Fig. 4-12). Similar results were obtained later in the framework of the CORALUS II project (Valcke 2007).

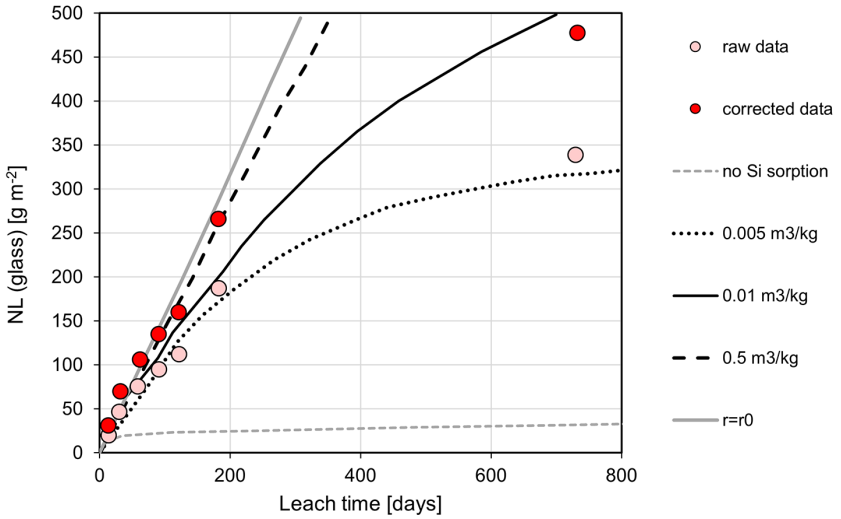

Fig. 4-11: GLADIS model calculations (lines) compared with results of R7T7 glass corrosion tests in saturated smectitic clay

Pink circles represent raw data (gravimetric mass losses), red circles are corresponding data corrected for the estimated weight of adhering surface alteration products. Redrawn from Curti et al. (1993)

Lemmens (2001) summarized the results on the effect of Boom Clay on the corrosion of SON68 and showed that the corrosion extent of the glass at 90 °C is very sensitive to the amount of clay in close contact with the glass. At high clay/water ratios, much more glass was corroded than at low clay/water ratios, after about two years leaching time. He also pointed out that Si sequestration may occur by two distinct mechanisms with contrasting consequences for the long-term behaviour: (i) sorption on available sites on the clay, or (ii) precipitation of newly formed precipitates. In the former case, the increase in corrosion rate is limited by the sorption capacity of the clay; as soon as the available Si sites are saturated, a slow *residual rate* comparable to that measured in experiments in pure water should be established. In the case of silicate precipitation, there is no such limiting factor and high glass corrosion rates could persist until complete corrosion of the glass. Lemmens (2001) concluded that the results available to date were still conflictual and that more research would be required to resolve this issue, as expressed by a list of questions posed at the end of the paper.

Although later laboratory experiments carried out with SON68 in contact with Boom clay at 30 °C showed a continuous decrease in corrosion rate (Lemmens et al. 2007), after more than 5 years leaching the rate was still one order of magnitude faster than in reference experiments with pure water at 90 °C (Fig. 4-13). The experiments were carried out in percolation cells, in which a small amount of glass in close contact with large amounts of clay was flushed across a pressure gradient with clay water. Glass and clay were in direct contact except for separation by a thin permeable filter providing a clear confinement between the two materials. The initial rate of 0.014 g m^{-2} d^{-1} obtained from the derivative of the fit was, decreased to 0.0042 g m^{-2} d^{-1} by the end of the experiment, thus there was a reduction of only a factor of 3.3 during 5 years. In the case of a temperature effect on the residual rate analogous to that observed for the forward rate, the required reduction factor would be 1 – 2 orders of magnitude higher, as residual rates of 10^{-5} – 10^{-6} g m^{-2} d^{-1} would be expected at 30 °C. These considerations clearly indicate that even after 5 years leach time the SON68 glass dissolution in a setup simulating the (former) Belgian repository setup is still far away from the residual rate regime observed in experiments without engineered barrier materials.

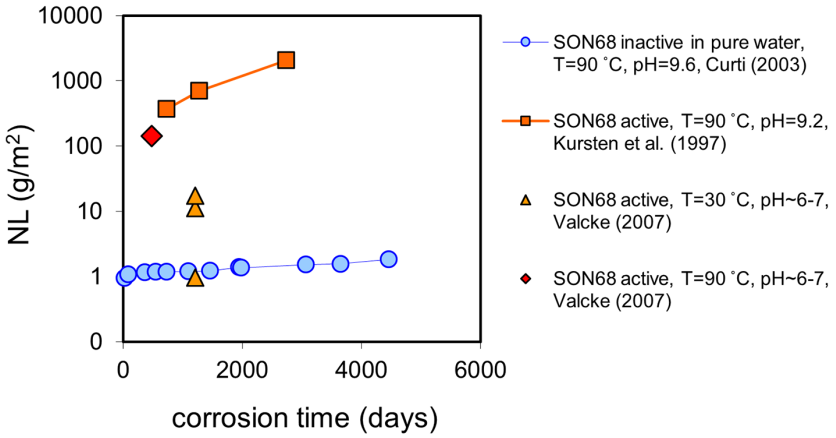

Fig. 4-12: Normalized mass losses from in-situ corrosion experiments on SON68 glass in contact with Boom Clay, compared to the reference corrosion test in pure water

In all the experiments discussed so far in this section, the glass was in close contact with the clay. An important parameter to consider is the effect of the distance separating clay and the glass, ideally in a setup closely reproducing the repository geometry. Such studies are reviewed in Section 4.4.5. Direct contact between glass and bentonite is unlikely in the Swiss reference repository scenario, as the vitrified waste will be physically separated from the clay materials through a thick canister, steel corrosion products and the mostly intact stainless steel "coquille". Therefore, the effect of Fe and Fe corrosion products on the dissolution of vitrified waste is a much more important issue for the Swiss HLW repository.

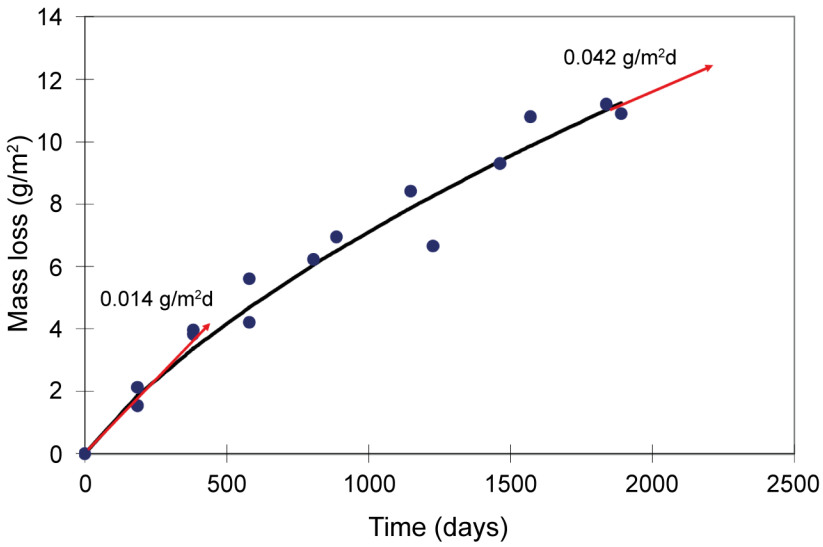

Fig. 4-13: Normalized mass losses from a long-term leach experiment with SON68 glass in close contact with a large amount of Boom clay, carried out at 30 °C in a percolation cell flushed with clay water

Reproduced with permission from Lemmens et al. (2007).

Gin et al. (2001b) studied the corrosion of SON68 glass in a series of static experiments at 90 °C in the presence of FoCa7 clay, a natural Ca-dominated bentonite with beidellite/montmorillonite as the main smectitic components and minor amounts of kaolinite, goethite, quartz, gypsum and calcite. This paper is discussed in more detail, as four different types of experiments were carried out specifically to identify the role of the clay and other competing factors in controlling the kinetics of glass corrosion. In the experiment type #1, a polished coupon of SON68 glass was corroded in pure water together with a loose mixture of clay and sand during 760 days at S/V = 100 m^{-1}. During the first 100 days, a very fast corrosion rate of 0.75 g m^{-2} d^{-1} (close to the *forward rate* in Soxhlet tests) was measured. Later, a decrease was observed but the corrosion rate after 760 days (5.7×10^{-2} g m^{-2} d^{-1}) was still more than two orders of magnitude faster than the *residual rate* in the absence of any material. This confirms the detrimental effect of smectitic clays on glass dissolution kinetics. This experiment was repeated under the same conditions but now with FoCa7 clay doped with amorphous silica. Under these conditions, much lower corrosion rates were observed (initially 2.6×10^{-2}, then 4×10^{-3} g m^{-2} d^{-1} after 182 days) indicating that an excess of soluble silica (either by saturating the Si sorption sites on the clay or directly favouring recondensation reactions in the gel layer) significantly slows down the corrosion kinetics of the glass. In experiment type #2, a solution previously "equilibrated" with SON68 glass was percolated through raw FoCa7 clay. From this test Gin et al. (2001b) determined the Si retention capacity of the clay and calculated K_d value of 0.034 m^3 kg^{-1}, in good agreement with the fitted values (0.005 – 0.05 m^3 kg^{-1}) of Curti et al. (1993). Experiment type #3 involved static leaching of SON68 without addition of any clay, either in a solution pre-equilibrated with FoCa7 clay, or with pure water. Although initially a much higher rate was measured in the experiment with clay water compared to the experiment with pure water, after about 40 days comparable low rates were measured in the two experiments (1-2 $\times$ 10^{-3} g m^{-2} d^{-1}) until the end of the test (unfortunately stopped after only 76 days). The results of the experiment in clay water, when compared to those of experiment #1, clearly show that the physical presence of the clay near the glass is a necessary condition to sustain high corrosion rates for a long time. This finding demonstrates that the clay actively supports the accelerated corrosion kinetics. Therefore, a sufficient physical separation between glass and clay should be sufficient to prevent persistent fast corrosion rates. In the final experiment type #4, Gin et al. (2001b) placed fresh glass coupons into the moist clay (without silica doping) recovered at the end of experiment #1, i.e. after 760 days leaching. In addition, they carried out a reference experiment under the same temperature and S/V conditions in clay-free pure water. The results showed that the "aged" clay was still reactive towards the glass, since the fresh glass was altered more rapidly in the "aged" clay compared to the reference experiment in pure water. At the same time, the glass corrosion rate of the fresh glass in the "aged" clay was higher than the final rate measured in experiment #1 in the same clay, indicating that also the glass corrosion progress plays a role. The authors interpreted this finding as evidence for the increasingly passivating properties of the gel as it evolves with time. In summary, these data show unequivocally that the glass corrosion kinetics in the residual rate regime is governed by multiple effects. These include the Si concentration in the aqueous solution, Si sequestration by the clay and increasing passivation of the alteration layer. The presence of (silica-free) clay in direct contact with the glass sequestrates the Si dissolving from the glass, thus preventing the formation of a passivating gel.

Neeway et al. (2015) carried out flow-through experiments to study the influence of Callovian-Oxfordian (Cox) clay[13] on the dissolution kinetics of SON68 at 90 °C and high S/V ratio. To this aim, glass powder and a glass coupon were placed in the middle of a stainless-steel percolation cell filled with Cox claystone (ρ_{dry} = 1.2 kg/L), through which a synthetic clay water solution was percolated via pressure gradient. Reference experiments carried out under similar conditions, but without claystone were also carried out. Glass dissolution was evaluated from the B concentrations in the outlet solution. The results showed that glass corrosion rates of the glass embedded in the clay ($1 – 3 \times 10^{-2}$ g m^{-2} d^{-1}) were persistently fast and about one order of magnitude higher compared to the reference experiment without claystone (leaching time: 200 days).

To conclude, all the experimental data reviewed so far point to a strong penalizing effect of clay materials on the dissolution kinetics of glass via silica sequestration, which is normally interpreted as reversible sorption. However, dedicated studies on the Si uptake mechanisms are practically inexistent. A notable exception is the study of De Cannière et al. (1998), who attempted to measure diffusion and sorption of dissolved Si at pH 8.5 with through-diffusion experiments using ^{32}Si tagged solutions. At mildly alkaline pH the dominant dissolved species is the neutral $Si(OH)_4(aq)$, with a minor contribution by $SiO(OH)_3^-$. From four separate experiments, bulk distribution coefficients of Si on the clay between 0.005 and 0.011 m^3 kg^{-1} could be determined, which also agrees well with the determinations of Gin et al. (2001b) and Curti et al. (1993). However, after 90 days diffusion time all four experiments showed consistently Si profiles through the clay far off steady state conditions, most Si being immobilized in the two first cm on the upstream side (total length of the cell: 40 cm). Even after 2.5 years diffusion time, no Si had reached the downstream reservoir. These results indicate that the sorption of Si on the clay was not reversible, which suggests the silica either precipitated within the clay or was incorporated in the pristine clay mineral via recrystallization. These results are thus in contradiction with the common hypothesis of reversible sorption.

4.4.3 Effect of iron and iron corrosion products

As noted in the previous Section, the corroding glass would most probably not be in direct contact with the clay. According to the current Swiss HLW repository setup and that of other countries (e.g. Sweden, France), the glass be physically separated from the bentonite backfill by the thin stainless steel flask containing the waste form and, more importantly, by a thick carbon steel canister[14]. Most of the glass will corrode in close contact with the metal and its corrosion products (magnetite or other Fe-oxides/silicates in case of steel).

Considering this premise, it is somehow surprising that studies on the effects of iron and iron corrosion products on glass corrosion have received attention only in recent years, particularly because it was known quite early that iron is very reactive towards silica. Experiments in the context of the JSS-project had clearly shown that the addition of Fe-oxides to the R7T7-type ABS-118 glass has a detrimental effect similar to that of clay. Fig. 4-14 shows that both the amount of glass corroded and the corrosion rates are increased in the presence of magnetite (Fe_3O_4) and goethite (FeOOH), and that the effect depends on the type, specific surface and quantities of the added Fe-oxides.

---

[13] The host rock foreseen for the French HLW repository.

[14] Coating the canister surface with copper could be evaluated in the optimisation phase in a later stage of the Swiss disposal program.

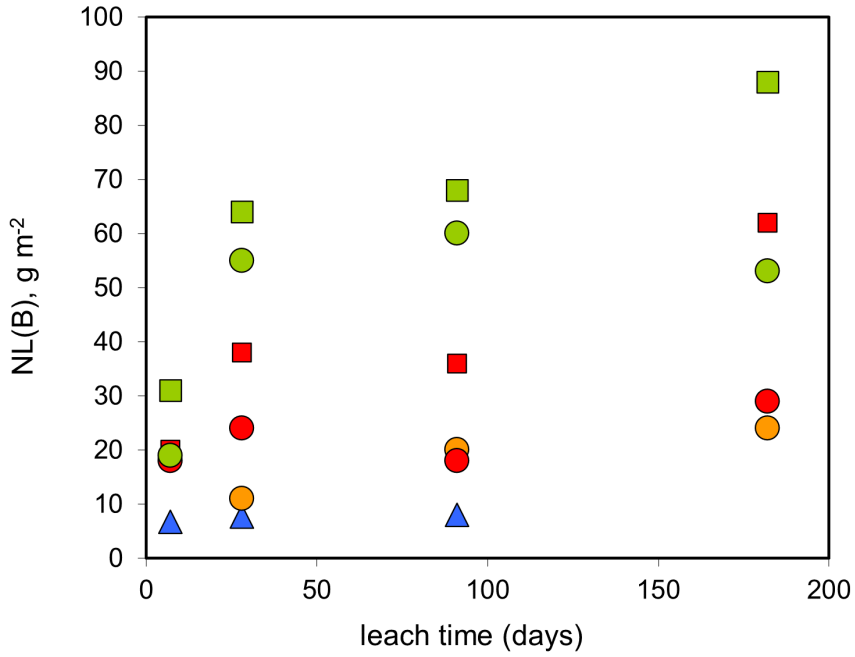

Fig. 4-14: Results of glass leaching experiments with ABS118 (R7T7) glass at 90 °C and S/V = 10 m^{-1} in pure water (blue triangles) and in the presence of different amounts of Fe corrosion products

40 g/L commercial magnetite (orange circles). 4 and 40 g/L synthetic magnetite (red circles and squares, respectively). 4 and 40 g/L FeOOH (green circles and squares, respectively)

Godon et al. (2013) carried out similar experiments with SON68 glass. The glass powder (6 g) was leached at 50°C in synthetic clay-water during 800 days, in contact with commercial magnetite or without magnetite (reference experiment). The results were analogous to those obtained in the JSS experiments, showing greatly increased amounts of glass dissolved and much higher, persistent *residual rates* in the experiments with magnetite compared to the reference additive-free experiment. The dependence on the mass of added Fe oxide was also confirmed: the glass dissolution rate doubled when the amount of magnetite added was increased from 10 g to 20 g. In the experiment with 20 g magnetite, no sign of decrease in glass corrosion rate was observed after 600 days leaching time (op. cit., Fig. 3). A notable result from this investigation is that the presence of magnetite lowered the dissolved Si concentration by about 20%-30% and caused an almost quantitative removal of dissolved Mg from the leaching solution. This is a strong indication that precipitation of Fe-Mg silicates, rather than sorption, was the cause of the enhanced glass corrosion kinetics. Although no mineralogical analyses were carried out, thermodynamic modelling indicated saturation equilibrium with Fe-silicates such as nontronite (an iron(III) rich member of the smectite group of clay minerals).

More recently, studies mimicking the repository near-field setup (including natural and archaeological analogues) were carried out, in which the combined effect of a steel canister and clay on the kinetics of glass dissolution was investigated. These studies are discussed later in Section 4.4.5.

4.4.4 Effect of cementitious materials

4.4.4.1 Preliminary remarks

During Stage 2 of the Sectoral Plan for Deep Geological Repositories (SGT-2), Nagra evaluated alternative repository concepts (Nagra 2016), including one foreseeing the use of cementitious materials as backfill of the HLW emplacement tunnels instead of compacted bentonite (cf. Cloet et al. 2019, Wyrzykowski et al. 2019). The concept is similar to the current Belgian disposal concept. Nagra is no longer considering this alternative scenario. However, for the sake of completeness, the consequences of this scenario on the corrosion of vitrified waste is briefly discussed, based on the available literature.

Starting in the early nineties of the past century, a number of experimental studies dealing on the corrosion of borosilicate glasses in cement waters (with or without the addition of solid cement material) have been carried out in Belgium, France, and the United Kingdom. For details, the reader is referred to Andrianbololona et al. (1992), Ferrand et al. (2013), Ferrand et al. (2014), Fournier et al. (2014), Gin et al. (2015), Liu et al. (2015), Ribet & Gin (2004), Utton et al. (2012), Utton et al. (2013). In most cited studies, SON68, MW or compositionally similar borosilicate glasses were used. The vast majority of these investigations showed that in the short-term glass corrosion rates under hyperalkaline conditions (pH > 11) are 1 – 2 orders of magnitude faster than under normal conditions (pH 9 – 10) in the time frame of the laboratory experiments. This is not surprising, considering the well-known exponential increase in silica solubility at pH > 10 (Alexander et al. 1954, Greenberg et al. 1955).

4.4.4.2 Literature review

Fig. 4-15 shows data from the experiments of Liu et al. (2015), carried out with SON68 glass at 70 °C and pH 13.5 in young cement pore water (YCPW), corresponding to the initial stage of cement degradation. The composition of this water is dominated by KOH (331 mM) and NaOH (143.5 mM), with minor $Ca(OH)_2$ (0.4 mM). These results are compared to data from a reference experiment conducted with the ABS-118 glass (p. 38 in JSS 1988b) at the same temperature and similar S/V ratio, but under usual pH free-drift conditions (pH < 10). The ABS-118 glass is compositionally almost identical to SON68. Fig. 4-15a shows the normalised boron losses as a function of corrosion time, while in Fig. 4-15b the corresponding calculated corrosion rates are displayed. The graphs reveal that the glass corrosion rate in cement water was still very high and close to the initial rates even after one year of leaching (~ 0.1 g m^{-2} d^{-1}). Similar results have been reported in other studies for the MW glass (Utton et al. 2012, 2013). Although a later decrease due to passivation effects cannot be ruled out, the data so far discussed give no indications of a reduction in corrosion rate.

Ferrand et al. (2014) carried out comparative static leach tests at 30 °C with SON68 and with the high-alumina SM539 glass under inert atmosphere (Ar) at S/V = 2'250 m^{-1}. The glass powder was leached in 100 mL of young cement pore water (YCPW, pH 13.5) in the presence of ordinary Portland cement (OPC) powder. The addition of OPC was the only difference with respect to the protocol of Liu et al. (2015), who worked with buffered solutions without addition of cement. Glass dissolution was determined from the mass loss of monolithic glass samples mounted above the glass-cement powder in such a way to avoid any direct contact with the cement paste. The experiments lasted for 2 years and were conducted in quadruplicate.

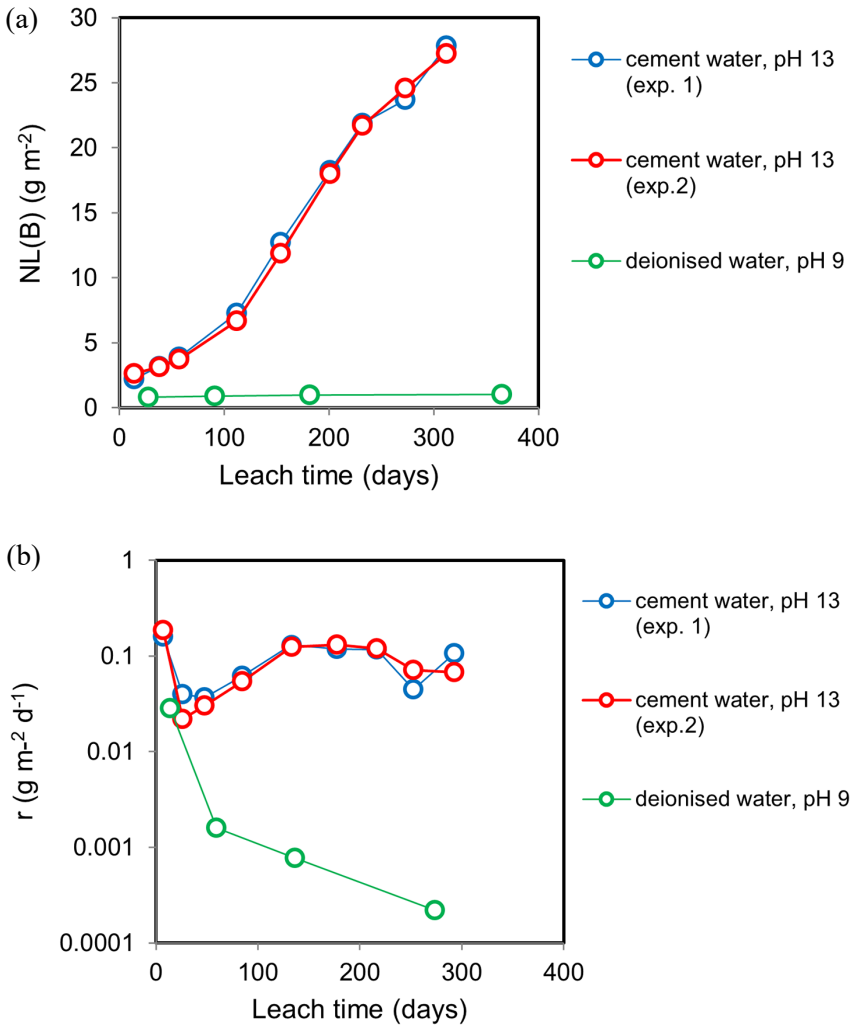

Fig. 4-15: Dissolution of SON68 glass powder in young cement water (pH ~ 13) and in pure water (pH ~ 9) at 70 °C

(a) normalized boron loss, NL (B). (b) glass corrosion rates calculated from the NL(B) values

The results indicate roughly constant dissolution rates for the SON68 glass, i.e. no decrease towards a *residual rate* regime was observed even after 2 years leaching time. The final rate was however highly dependent on the amount of added OPC. With 2.4 g added OPC, the rate (0.005 g m^{-2} d^{-1}) was about the same as in YCPW without added cement (0.0062 g m^{-2} d^{-1}). With 7.5 g OPC added, it increased by a factor of 8 to 0.040 g m^{-2} d^{-1}. With 22.5 g OPC, however, the rate unexpectedly decreased to 0.012 g m^{-2} d^{-1}, which the authors ascribe to a "*conglomeration effect limiting the access to reactive sites*". The authors probably mean here a reduction of the exposed surface area due to precipitation of C-S-H phases on the glass surface (see below). A similar phenomenon was also observed by Utton et al. (2013).

Ferrand et al. (2014) also observed a reciprocal relation between Ca and Si concentrations in solution, which they interpret as due to the conversion of portlandite to C-S-H. Dissolution of portlandite releases Ca whereas precipitation of C-S-H phases reduces the Si concentration. This explanation is supported by XRD analyses showing the disappearance of portlandite peaks and the appearance of peaks assigned to tobermorite and C-A-S-H phase in the Al-rich SM539 glass.

HRTEM images and EDS-analyses on SON68 show a Ca,K-enriched gel layer with interconnected porosity and C-S-H precipitates on top. The high porosity and low Si retention factor (40%) of the gel layer (compared to 80-90% for protective layers) imply that the gel was non-protective, explaining the high and constant measured glass corrosion rates. Probably, the formation of C-S-H-phases on top of the gel layer removes sufficient silica to maintain low Si concentrations and avoid formation of a passivating layer. Accordingly, the authors conclude that "*two main reactions are proposed to explain why the glass dissolution remains close to the initial rate for 2 years in tests with 7.5 g of cement: the reaction of Si released by the glass with portlandite, leading to the formation of C-S-H phases [...] and the conversion of C-S-H into C-A-S-H phases*". As long as portlandite is present, its conversion to C-S-H ensures that Si is removed from solution and thus avoids formation of a passivating gel.

Utton et al. (2012) measured the alteration of a Magnox (MW-type) glass at 40 °C in alkaline Na(OH) and $Ca(OH)_2$ solutions at pH 12. While the results in Na(OH) yielded corrosion rates approaching 0.1 g m^{-2} d^{-1}, comparable to those obtained from the Belgian and French studies discussed above, the analogous test in $Ca(OH)_2$ resulted in much lower rates. No interpretation was given by these authors to explain the different behaviour in the presence of $Ca(OH)_2$. Corkhill et al. (2013) carried out analogous experiments on a U.K. glass produced by blending 25% of Magnox waste and 75% UO_2-oxide waste. The experiments were carried out at 90 °C in portlandite-saturated $Ca(OH)_2$ water at high S/V ratio (10'000 m^{-1}) and produced results analogous to those obtained by Utton et al. (2012) in $Ca(OH)_2$ solutions. After an initial rate of about 6×10^{-5} g m^{-2} d^{-1} during the first 30 days, a parabolic drop to 1.4×10^{-5} was observed from 30 days until the final leach time (168 days) based on NL(B) data. More importantly, the comparison with the reference experiment in pure water showed that the total extent of glass dissolution was even lower than in the reference experiment in pure water, and that the initial pH of 12.4 progressively decreased to 10.5 during the experiment. Based on geochemical modelling and microanalyses, this was attributed to the formation of C-S-H phases with progressively decreasing Ca/Si ratio and incorporation of Ca into a passivating gel layer.

The contrasting results of the previously discussed studies deserve a short parenthesis on the evolution of cement pore water during cement hydration/degradation (Berner 1992, Jacques & Mallants 2011). While the KOH-NaOH dominated YCPW cement pore waters at pH > 13 are representative of early stages of OPC hydration (stage I), $Ca(OH)_2$-rich waters are typical of a more advanced stages in the hydration and degradation of OPC characterized by equilibrium with dissolving portlandite at pH 12.5 and high Ca/Si ratios in the pore water (stage II). Stage III starts after complete dissolution of portlandite and is characterized by solution equilibria with C-S-H phases, with progressively decreasing Ca/Si and pH until C-S-H phases are consumed (final stage IV).

More recently, corrosion studies in hyperalkaline media have been extended to the International Simple Glass (ISG). Mann et al. (2019) carried out leach experiments on ISG at S/V = 8'280 m^{-1} in YCPW with addition of 0.4 mM $Ca(OH)_2$ (about the same solution as in Ferrand et al. 2014). At 30 °C, an almost constant corrosion rate was measured (4×10^{-3} g m^{-2} d^{-1}) and the pH remained above 13 until the end of the experiment (two years leaching time). Considering the low temperature of this experiment, the measured rate was fast. At 70 °C, high corrosion rates were measured only in the first three months (4.4×10^{-2} g m^{-2} d^{-1}), then the rate rapidly decreased by almost two orders of magnitude (9×10^{-4} g m^{-2} d^{-1}) in concomitance with a decrease and stabilisation of Si concentrations. Moreover, the pH decreased to about 12. This contrasting behaviour suggests that in the two experiments different corrosion regimes were operating, an anticipation confirmed by the microscopic data collected in that study. The fast corrosion kinetics was found to correlate (at both temperatures) with the formation of a porous, non-protective, Zr-bearing alkali-alumosilicate gel, the formation of which is favoured at pH > 13. At such pH dissolved silica nanoparticles are negatively charged, hindering the polymerisation process and thus leaving a porous gel through which diffusion of solutes from and to the glass reactive surface is facilitated.

This regime corresponds to stage I of cement degradation. As the pH decreases and Ca concentrations increase due to equilibrium with portlandite and other phases (C-S-H, zeolites and phyllosilicates), more Ca^{2+} is incorporated into the gel layer, improving its protective properties. This regime corresponds to stages II/III in the cement degradation evolution and was observed only at 70 °C. These results show quite impressively how sensitive glass corrosion kinetics can react on changes in the alteration layer properties induced by solution composition and temperature effects.

The experiments at 70 °C were repeated by Ferrand et al. (2021) with finer ISG glass powder (20 – 25 µm, S/V = 264'000 m^{-1}) and leaching times extended to 952 days, in order to achieve a higher reaction progress and thus simulate longer corrosion times. The initial pH of 12.5 (at 70 °C), dropped quickly to less alkaline values 9.4, suggesting that conditions close to stage III were achieved by the end of the experiments. NL(B) values showed initially a steep rise followed by a stabilization after two months of leach time. From these data, the authors derived fast initial rates (6×10^{-3} g m^{-2} d^{-1}) and a very low *residual rate* (6×10^{-6} g m^{-2} d^{-1}). The latter rate must however be taken with some caution due to the large uncertainties deriving from the limited number of samplings and the "parallel experiments" technique (see Fig. 2b in Ferrand et al. 2021). An additional uncertainty arises from the calculation of NL(B) values assuming that the reactive surface area of the glass remains constant at the initial value. At such high S/V and after leaching time of almost 3 years significant fractions of the initial glass volume will be corroded[15], implying that the reactive surface area of the glass will have significantly decreased from its initial value. Thus, the quoted *residual rate* might be an underestimation.

The major value of the study of Ferrand et al. (2021) lies in the advanced characterization techniques, including SEM, TEM-EDX/HAADF on FIB lamellae and XRD. Crystals of Na-philippsite and K-zeolite formed on the surface of the corroded glass particles could be identified. After removal of the surface precipitates, the altered glass surface of many grains appeared to be covered with nanopores. The cross section through the FIB lamella showed homogeneous pristine glass, followed by a tiny (80 – 250 nm thick) K,Si-enriched and Na,Ca-depleted gel-like layer (defined by the authors as "porous altered layer") and a 1 – 1.5 µm thick sheet of amorphous precipitates with a fibrous morphology typical of C-S-H-phases and a low Ca/Si ratio (0.3 – 0.4). The gel-like layer had a "foam-like" structure similar to that observed in altered synthetic basaltic glass by Parruzot et al. (2015). This terminology is somehow confusing, as it suggests that the layer is permeable. The boron data however indicate that this layer is passivating, implying that either the small pores observed in the TEM images are not interconnected (closed porosity) or the passivating layer is thinner and not identified (as suggested by Parruzot et al. 2015).

Gin et al. (2015) also carried out a study with ISG glass (90 °C, S/V = 60 m^{-1}), with the objective of deciphering the glass alteration mechanisms as a function of increasing pH. The results indicate a fundamental "switch" of the glass alteration mechanisms between mildly-alkaline and alkaline conditions. At pH 9, an approximately 200 nm-thick dense gel layer of amorphous aluminium and silicon oxide formed within a few months. This layer is passivating, as it consists of a dense polymerised three-dimensional Si-O-Si/Si-O-Al network that hinders the penetration of water to the fresh glass surface and severely restricts the diffusion of the dissolved components out of the glass to the free water. As a result, the glass corrosion rate decreased by two orders of magnitude (from initially 0.1 to 0.001 g m^{-2} d^{-1} at 90 °C). After intentionally raising the pH to 11.5 by addition of KOH, the corrosion rate increased abruptly to values of more than 1 g m^{-2} d^{-1}. This rate was maintained until the end of the leaching experiment (100 days). Ion beam analyses and electron micrographs showed that, after the pH increase, the original passivating gel layer was dissolved and replaced by a new permeable layer formed via dissolution/precipitation processes.

---

[15] This anticipation is confirmed by the authors' description of SEM/BSE images of glass particles < 5 µm.

On the glass surface, typical secondary cement phases (C-S-H phases, zeolites) formed, which are apparently also permeable. This change in corrosion mechanism, combined with the increased solubility of SiO_2 at high pH, explains the very faster glass corrosion kinetics in alkali dominated cement pore waters. Note that no calcium was added to the leaching solution; this is probably the reason why no passivation was observed at high pH.

Mercado-Depierre et al. (2013) have highlighted the role of calcium during glass dissolution under alkaline conditions. An antagonistic behaviour of Ca on glass dissolution was proposed, based on four distinct pH- and S/V-dependent mechanisms. Two cases are distinguished: (a) low S/V, i.e. no or poor development of the alteration layer and (b) high S/V, i.e. well-developed alteration layer at high reaction progress. In case (a) (low S/V) at circum-neutral pH, Ca^{2+} forms surface complexes that favour Si,B-O network hydrolysis and thus increase the *forward rate*, while at pH > 11, Ca penetrates into the nascent alteration layer, making it passivating. Conversely, in case (b) (high S/V) at circum-neutral pH, Ca has a passivating effect which is however cancelled at pH>11 due to Ca and Si removal via precipitation of C-S-H phases, explaining the increase in corrosion rate observed by Gin et al. (2015) when pH is raised to 11.5. However, in the light of the previously discussed, more recent results from the Belgian and British groups (showing that Ca most frequently acts as passivating element at high pH) the latter explanation cannot be generalized. Probably the suppression of passivation is a transient effect that also depends on the magnitude of dissolved Ca concentration and maturation of the alteration process.

4.4.4.3 Concluding remarks

Contrary to clay and iron, which actively react with the glass via Si sequestration, the enhancement of glass corrosion rate in cementitious environments is not necessarily related to the direct interaction with the added material. It is rather a solution effect related to the increase in solubility of the Si-O network induced by the dissolved alkali hydroxides. Therefore, cement may influence the glass corrosion rate even if there is no direct contact with the glass and the material is located at considerable distance ("remote action") provided its buffering capacity is sufficient. This will primarily depend on the relative material proportions, i.e. how much cement is present in the near-field compared to the other materials (glass, canister, bentonite).

An important conclusion from the literature review is however that dissolved KOH/NaOH and $Ca(OH)_2$ have contrasting effects on the dissolution kinetics. While dissolved K^+ and Na^+ in high concentrations tend to exchange into the gel layer and render it permeable, high concentrations of Ca^{2+} have the opposite effect; the gel can densify and become passivating. From this, one can conclude that the effect of cement pore water on glass dissolution will strongly depend on the progress of cement degradation at canister failure time. Moreover, one should also take into account that, in a typical repository environment, the effects of Fe and Fe corrosion products will be superposed to those of cementitious backfill materials, making the prediction of the passivating properties of the gel in such environments even more difficult.

In the framework of Nagra's evaluation of alternative repository concepts, a scenario in which cementitious materials replace compacted bentonite as buffer material of the HLW emplacement tunnels was also investigated (Cloet et al. 2019, Wyrzykowski et al. 2019). For this scenario, glass dissolution rates of 0.1 g m^{-2} d^{-1} (reference case) and 1 g m^{-2} d^{-1} (conservative case) were assumed in safety assessment calculations (cf. Tab. 7-4 in Cloet et al. 2019). This covers the expected enhanced dissolution of borosilicate glass during the initial stages of cement degradation.

4.4.5 Combined environmental effects and analogues

4.4.5.1 Preliminary remarks

This section is devoted to an overview of studies dedicated to synergistic environmental effects on the corrosion of borosilicate glass, with special focus on those relevant to the Swiss repository scenario. In such studies, the conditions encountered in the repository near-field after failure of the waste containment are simulated either in laboratory experiments or through natural, archaeological and industrial analogues. In the first case, the experimental conditions are well controlled, at the cost of limited interaction time. In contrast, analogue studies allow to access repository-relevant timescales, but knowledge of the actual "experimental conditions" is poor. Because most of the discussed investigations were conducted at CEA Marcoule, the studied materials and experimental configurations reflect the setup of the French HLW repository (Cigéo project, see IRSN 2014). In spite of considerable differences in the geometry and design of the waste form emplacement, the environmental materials involved (steel, bentonite, claystone) and physical conditions are quite similar to those relevant for the Swiss safety case, so that chemical interactions are expected to be comparable.

A drawback of such complex experimental configurations is that the extent of glass corrosion cannot always be measured with the usual methods (B, Li concentrations or mass loss). The evaluation is based mostly on advanced microscopic characterization combined with spectroscopic techniques. This approach reveals details of the corrosion mechanisms but does not allow for an exact quantification of the corrosion rates.

4.4.5.2 Literature review

Michelin et al. (2013) conducted laboratory experiments to reproduce as closely as possible repository conditions. In a cylindrical vessel, SON68 glass powder was placed in direct contact with iron powder and iron discs, the iron being in contact with a borehole core sample of COx claystone. Helium-saturated synthetic clay water at 50 °C was then pumped at 15 bar overpressure into the vessel to saturate the system and start the leaching experiment. The pH was near-neutral (6.7) and the Eh reducing (-190 mV). After 756 days of leaching, the reacted materials were characterized by means of microscopy and X-ray spectroscopy.

The main finding was that the extent of glass corrosion appeared to be highly dependent on the distance separating a given glass grain from the contact to the iron. Grains a few µm away from the glass-Fe interface showed thick alteration rims and abundant formation of Fe-silicates, while grains farther away from the contact (at few mm distance) had much thinner alteration rims and lacked Fe-silicate precipitates. Magnetite was identified to be the major alteration product of the Fe powder. TEM-EDX analyses of glass grains close to the Fe-glass interface showed formation of a 1 µm-thick Fe-enriched amorphous layer (probably the "gel layer") followed by a thicker discontinuous layer of secondary precipitates, mostly Fe-Si-O rich phases, but also small particles of a P-bearing, lanthanide enriched phase (similar phases were identified in Curti et al. 2006). The iron in the gel layer was identified to be a mixture of Fe(II) and Fe(III), with Fe(III) increasing towards the pristine glass (the pristine glass contains only Fe(III) due to the oxidizing conditions during glass synthesis).

The studies of Michelin et al. (2013, 2015) also included the investigation of an archaeological analogue, consisting of slag samples from the 16th century ironworks at the Glinet archaeological site (Normandy, France). The slag samples remained buried during about 450 years in a clay-rich soil saturated with Ca-rich and carbonate-rich pore solution. They consist of a glassy matrix with embedded mm to cm-large iron inclusions. The material is intersected by cooling cracks (in analogy to the cooling-induced fracturing of nuclear waste glass). Although the composition of

the glassy matrix is quite different from that of nuclear waste glasses like SON68 and MW (higher SiO_2, FeO and CaO contents, no B_2O_3 and phase separation phenomena) many similarities to the laboratory experiments with the aforementioned glasses were found, e.g. the dependence of alteration extent on the physical distance from the Fe-glass interface. Owing to the different compositions of glass and pore solutions, however, in addition to Fe-silicates, secondary carbonates formed, mainly siderite ($FeCO_3$) and chukanovite ($Fe(OH)_2CO_3$).

Rébiscoul et al. (2015) investigated the effect of magnetite (without metallic Fe and/or clay present) on glass corrosion, taking into account the influence of (a) the amount of magnetite added and (b) the physical separation between glass and magnetite through an artificial diffusion barrier. The experiments were carried out with glass powder at 50 °C in synthetic COx water and under $Ar/H_2/CO_2$ atmosphere, in order to maintain the pCO_2 and Eh conditions expected in the repository. Experiments with glass in direct contact with commercial magnetite (Alpha Aesar, 99.997% purity) confirmed that glass corrosion is enhanced with increasing magnetite/glass surface area ratio, as already observed by Godon et al. (2013) and in the JSS experiments. The post-mortem analysis of the materials, using advanced microscopic and spectroscopic methods, revealed that silica released from the glass was sequestered both via adsorption and precipitation of Fe-silicates or SiO_2. Moreover, it was found that, when the glass is separated from magnetite by an inert diffusion barrier, no Fe(II) is incorporated into the gel layer of the glass. Instead, the in-diffusing Fe(II) precipitates in externally precipitated Fe-silicates together with lanthanide-rich phases and phyllosilicates.

The experimental setup of Rébiscoul et al. (2015) allowed collecting solution data as a function of leaching time. Most useful are the data on boron concentrations, which allowed us to determine glass corrosion rates as a function of time. The data were digitized from the original paper and are reproduced here in Fig. 4-16a. The extracted corrosion rates (Fig. 4-16b) are *in all cases* considerably higher the presence of magnetite compared to the magnetite-free reference experiment over leaching times extending to 3.5 years, and the total amount of glass corroded increases with the amount of magnetite added. At the end of the test, the glass corrosion rates in the presence of magnetite are about *two orders of magnitude* higher than in its absence and still far from an asymptotical *residual rate* regime. The most intriguing result however arises from the comparison of the GM1 and GSM1 experiments, in which exactly the same amounts of glass and magnetite were used, but in the former case the two materials were in direct contact, while in the GSM1 experiment they were separated by a diffusion barrier. In spite of the physical separation, the extent of glass corrosion and final rates were higher in the latter experiment. This result is counter-intuitive and apparently contradicts the results of Michelin et al. (2013), who found exactly the opposite dependence. Rébiscoul et al. (2015) explained their results with the help of the detailed microanalyses, which show incorporation of Fe in the gel layer only in the GM1 experiment. The gel layer in the GSM1 experiment consists, according to the authors, of "a porous gel" that was probably less passivating than the Fe(II)-bearing gel in the GM1 experiment.

De Echave et al. (2019) studied the corrosion of SON68 glass in an environment simulating the conditions at the inner side of a failed canister. To this aim, (2.5 × 2.5 × 0.2) cm^3 glass coupons were leached together with pristine or pre-corroded iron foil in a cell filled with COx water, thermostated at 90 °C. With the help of spacers made of chemically inert material, physical contact between the glass coupon and the Fe foil was avoided (the separation distance was 80 µm). In this way, the glass coupon was exposed to two distinct environments: the upper face close to the foil was defined as "confined environment" simulating the periphery of the glass form, close (but not in contact) to the canister inner side, while the downward face was exposed to the bulk solution at a larger distance from the canister material. This was defined as "dilute environment" and is more representative of internal parts of the vitrified waste. A reference experiment in which the Fe-foil was replaced by a chemically inert PTFE foil was also carried out. Also in this case, the results always showed enhanced glass corrosion in the presence of the Fe foil. For the "confined environment" no significant differences in the thickness of the corroded glass layer was

detected, using either the metallic Fe foil or the pre-corroded foil. In the "dilute environment" (i.e. "far" away from the Fe source) the thickness of the alteration layer was up to 4 times larger than in the upper glass coupon face close to the foil. This observation is in agreement with the findings of Rébiscoul et al. (2015), see GM1 and GSM1 curves in Fig. 4-16, thus again indicating (contrary to the results of Michelin et al. 2013) that a larger separation between glass and Fe source may lead (counterintuitively) to more glass corrosion. Consistently, De Echave et al. (2019) also interpret this phenomenon as an indication that the gel layer of the distal glass face is less passivating due to the absence of incorporated Fe(II).

Verney-Carron et al. (2008) investigated the corrosion phenomena in glass blocks of Roman age that remained partially buried during 1'800 years in mud sediments saturated with seawater. The blocks weighed several kg and were severely fractured. In spite of the limited chemical analogies (no B_2O_3, very high SiO_2 and NaO contents in the Roman glass, no Fe/Fe corrosion products present, saline leachant composition), this study provides a means to investigate the aqueous corrosion process on a scale comparable to that of a real nuclear glass form over a repository-relevant times. A key finding from this study was that the extent of glass corrosion, as revealed by the thickness of altered rims, was much weaker in the internal parts of the glass block, compared to peripheral regions directly exposed to the seawater-saturated mud. Based on a detailed geometrical analysis of crack radii and crack density, it was estimated that about 12% of the bulk glass volume were altered; however, the contribution of the external zone was much higher (23%) compared to the internal zone (8%). This result was explained in terms of different local S/V ratios and the increasing solute transport resistance towards the interior of the block.

In the peripheral regions of the block an average corrosion rate of 0.1 µm/a was estimated (7.4×10^{-7} g m^{-2} d^{-1} assuming a glass density of 2'700 g m^{-3}), similar to *forward rates* determined on basaltic glass at comparable temperatures (Techer et al. 2000). This finding is not entirely surprising, since at least part of the block was exposed to free seawater providing constant renewal of the leachant. In the internal part, the average altered thickness was 29 µm, i.e. about 8 times less, yielding a much lower rate of about 9×10^{-8} g m^{-2} d^{-1}.

Basaltic glasses are usually considered the closest natural analogues of borosilicate nuclear waste glasses, due to the similar silica contents. Accordingly, several attempts have been undertaken to extrapolate the long-term behaviour of vitrified nuclear waste from naturally altered basalts, with the support of leach experiments conducted in the laboratory (see Crovisier et al. 2003, for a review). Techer et al. (2000) first demonstrated that the *forward rate* and *residual rate* of synthetic basaltic glasses are comparable to those measured under the same conditions on SON68 glass. In a follow-up paper (Techer et al. 2001) the alteration of basaltic dykes intruded 1.4 Ma ago into a Permian argillaceous formation (Lodève Basin, France) was studied, and the corrosion rate was estimated from the thickness of the alteration layer ("palagonite") assuming isovolumetric conditions and permanent contact with meteoric water permeating at the clay/basalt discontinuity. Taking into account the variability of the alteration layer thickness, the authors derived alteration rates in the range of 1.4×10^{-11} to 7.1×10^{-10} m a^{-1} (1×10^{-10} to 5×10^{-9} g m^{-2} d^{-1}). These values are orders of magnitude lower than those measured in the laboratory. As in other former attempts to derive glass corrosion rates from natural basaltic glasses, these numbers probably largely underestimate the true corrosion rates, because the assumption of permanent contact with an aqueous medium during geological time is unlikely and non-conservative.

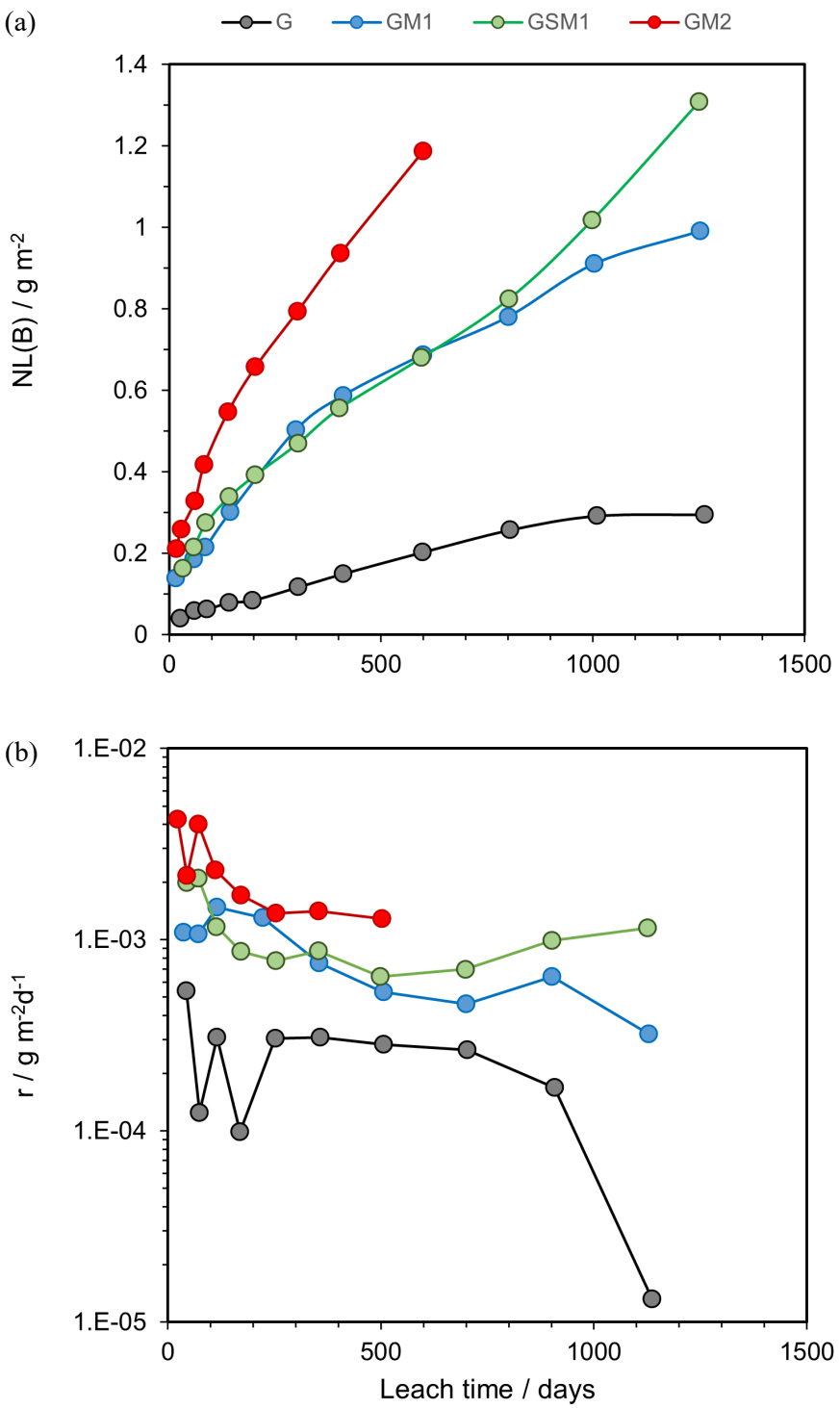

Fig. 4-16: (a) Normalized mass losses of boron reproduced from Fig. 2a in Rébiscoul et al. (2015) after digitazing the graphical data. (b) Corresponding average glass corrosion rates for each leaching time interval

The legend identifies the experiments following the terminology in the original paper: G = 6 g of SON68 glass powder without magnetite (reference experiment), GM1 = glass intermixed with 10 g magnetite, GM2 = glass intermixed with 20 g magnetite, GSM1 = glass with 10 g magnetite separated by a diffusion barrier.

Other sources of uncertainties are the poor knowledge of alteration temperatures. A notable exception are perhaps estimations based on young (< 1 Ma) Icelandic basaltic glasses altered under a permanent ice shield, since in this case probably a water film at temperatures close to the freezing point was always in contact with the basalt from eruption to sample collection. Based on such samples Crovisier et al. (2003) (op. cit., Fig. 16a) estimated corrosion rates of about 1– 3 × 10^{-10} m a^{-1} (7.4 × 10^{-10} – 2.2 × 10^{-9} g $m^{-2}d^{-1}$) for temperatures close to the ice melting point.

4.4.5.3 Concluding remarks

In summary, the data presented in this Section allow drawing the following conclusions, applied to the Swiss repository setup:

(i) Both clay materials and iron/iron corrosion products strongly enhance glass corrosion. However, in the repository setup clay materials (bentonite buffer, Opalinus Clay) will be physically separated from the glass at a distance of at least several cm from the corroding glass. Thus, the effect of Fe and Fe corrosion products will be much stronger and "overprint" any effect of clay materials, which will be limited to so far unidentified effects induced by solutes inherited from interactions with the Opalinus Clay and bentonite.

(ii) The presence of Fe and Fe corrosion products near the vitrified waste always increases the glass corrosion kinetics via Si sequestration *as long as secondary Fe-silicates precipitate.* When precipitation of silicates ceases due to attainment of thermodynamic equilibrium (usually at low pH and low Si concentration) and provided that sufficient Fe (or Mg, Ca) is incorporated into the gel, passivation occurs and the glass corrosion rate decreases. This interpretation follows the "organigram" shown in Fig. 13 of Aréna et al. (2018).

(iii) Due to transport resistance phenomena, corrosion of the vitrified glass form will probably not be homogeneous but differential, with the external (peripheral) regions corroding faster than the internal regions of the waste form.

(iv) In general, quantitative estimations of nuclear waste glass corrosion rates from natural, archaeological or industrial analogues are affected by large uncertainties due to the poor knowledge of boundary conditions in such "natural experiments" and unavoidable differences in leachant and glass compositions.

5 Radionuclide release during vitrified waste dissolution

5.1 Preliminary remarks

In contrast to glass corrosion kinetics, studies on the release and selective retention of radionuclides (or analogues thereof) during glass alteration are rare and far less systematic. This is a consequence of the conservative assumption made in the safety cases of many countries (including Switzerland) that all dose-relevant nuclides are released congruently from the dissolving glass. As discussed below, though conservative, this approach reduces the realism of such computations.

Nonetheless, a few studies on this topic, including quantitative measurements on radionuclide release, have appeared over the years. In this brief review, the focus will be as before on data relevant for the two types of glasses relevant for the Swiss disposal program, neglecting investigations carried out mainly in the U.S. on largely different glass compositions. Most of the available data stem from simple leach experiments in pure water and under conditions far different from those encountered in the repository near-field (with some notable exceptions). It cannot be excluded that some data may be biased by inappropriate pH-Eh conditions or by the lack of solutes that might influence the retention of specific nuclides (e.g. by modifying the retention properties of the gel, or by providing strong complexants that modify the charge and speciation of the main radionuclide species).

Finally, it must be emphasized that it is in general not possible to distinguish between radionuclide retention within the glass alteration layer, in secondary (co-)precipitates, since the majority of the available data are based on bulk solution analyses only. Advanced microscopic/spectroscopic studies revealing the distribution of the retained radionuclides at the nanoscale are very rare. The main objective of the present chapter is to show that the alteration layers of borosilicate glasses have a strong capacity to retain efficiently most radionuclides during aqueous corrosion. The following discussion is largely based on two reviews (Pirlet 2001, Gin et al. 2017) and a few dedicated studies (Vernaz & Godon 1991, Curti et al. 2006, 2009, 2012).

5.2 Literature review

5.2.1 Primary partitioning of radionuclides in the glass

Before discussing the data on radionuclide release during aqueous glass alteration, it is useful to recall briefly the available information on the partitioning of radionuclides during glass synthesis (see Section 2.4 for a more detailed discussion). Although the vitrification process is optimized to produce homogeneous borosilicate glass matrix, the low solubility of some elements in the glass melt causes formation of minor phases that can be detected as separated microscopic inclusions.

Gin et al. (2017) classify the elements present in R7T7 glasses, including actinides and fission products, as a function of their oxidation state and solubility in the glass melt (Fig. 3, op. cit.). Considering that most redox-sensitive elements will occur as oxidized species in the glass (as vitrification takes place in general at high oxygen partial pressures) this classification readily shows that elements such as S, Cl, I, Ag, Mo, Ru, Rh, Pd, Tc, Sn are insoluble or have very low solubilities (< 1 wt.-%) in the glass. The non-evaporated fraction of these elements will thus tend to partition outside the homogeneous borosilicate matrix as discrete micro/nanophases. Typically, dose-relevant radionuclides such as ^{106}Pd, ^{99}Tc, ^{93}Mo are found in melt-insoluble metallic fines inherited from the ε-particles present in the original spent UO_2 fuels. Molybdenum may form, together with sulphur, molybdate/chromate phases known as “yellow phases”. Such phases were detected e.g. in Magnox waste glasses (Ojovan et al. 2019). In addition, spinel-type metallic

oxides may form during cooling (Gin et al. 2017), such as trevorite ($NiFe_2O_4$) micro-inclusions, which may incorporate part of the dose-relevant ^{59}Ni. Such particles have been found and characterised in the MW glass (Curti et al. 2009). All other dose-relevant radionuclides should be homogeneously dissolved in the borosilicate matrix, since it is the goal of the nuclear waste vitrification process to produce glass compositions with sufficiently high solubility limits for as many elements as possible.

5.2.2 Release of radionuclides into aqueous phase

A few studies investigated the release of actinides and Tc during the alteration of radioactive (doped) borosilicate glasses. These investigations are important since they did not resort to inactive simulants; the release of key radionuclides, for which no stable isotope exist, could be measured directly.

Vernaz & Godon (1991) measured the release of Np, Pu, Am and Cm from a series of R7T7-type glasses doped with 0.85 – 2.8 wt.-% actinide oxides at room temperature. Although the authors do not specify the redox conditions, they must have been carried out under aerated conditions, as indicated by the relatively high measured aqueous concentrations of Np and U (see later). In a first series of tests, monolithic samples were leached in distilled water during 70 days, with daily water renewal. The retention of all four nuclides in the alteration layer was rather limited and their normalized release followed faithfully that of Cs. This indicates that at such early stage of dissolution, under oxidising conditions and far from "silica saturation" there is no passivating gel layer and that the solubility limits of the actinides were high. Such conditions are clearly not representative of the repository environment. However, the identity with the Cs release curve is a clear indication that these actinides are homogeneously dissolved in the borosilicate matrix and do not partition in metallic or oxide phases. Upon interruption of water renewal during 3 – 5 days (short-term static conditions), the release of the actinides decreased abruptly and departed from the Cs release, suggesting rapid formation of a gel layer capable to efficiently retain the actinides. The authors vaguely interpreted this phenomenon as evidence that the actinide release is controlled by the "*solubility of an actinide compound at the glass surface*".

Using the same glasses, Vernaz & Godon (1991) carried out additional experiments at 50/90 °C, but now in closed vessels and without water renewal. Due to the static conditions, higher temperatures and the longer leach time (1 year) these experiments are more representative of repository conditions, except for the oxidising conditions. The pH and elemental aqueous concentrations were also measured, partly also after ultrafiltration. The quite extensive data reported by Vernaz & Godon (1991) are re-evaluated here. The retention factors, defined as RF = NL(B)/NL(Actinide), and concentrations in mg/L were transformed to percentages of element retained in the alteration layer and molar concentrations, respectively.

The transformed data (Fig. 5-1) show that, after 1 year leaching, 70 – 99.9% of the leachable amount of all actinides remained trapped in the alteration layer, with retention factors systematically higher at 90 °C than at 50 °C. Probably, this is not an indication that the retention capacity is lower at 50 °C. The difference may be simply a consequence of the more advanced reaction progress at 90 °C. The corrosion process is much slower at 50 °C, implying that at equal leaching times a thinner, less passivating layer was formed at the lower temperature. At both temperatures, the retention follows the same ranking in retention capacity (Am > Pu > U > Np), which reflects the higher solubility of U and Np compared to Pu and Am under oxic conditions. The concentration curves (Fig. 5-1c, Fig. 5-1d) indicate that U and Np did not reach the solubility limit at 50 °C, as no plateau was reached yet at the end of the experiments. At 90 °C, it appears that the solubility limit was reached rapidly for all four radionuclides (the increase up to 100 days for Pu and Am is probably due to formation of colloids).

Pirlet (2001) reviewed experimental data available at that time on the release of Tc and actinides from various types of glasses. In general, the data indicate that, in glass leach experiments without additives, Tc and Np are released preferentially compared to Pu and trivalent actinides, regardless of redox conditions. Leach experiments with R7T7 glass in the presence of oxidized Boom clay also showed high concentrations of dissolved Tc and Np in the leachant, as under oxidizing conditions these elements form the non sorbing, soluble species $Tc(VII)O_4^-$ and $Np(V)O_2^-$. Analogous experiments were carried out with the same clay, however intermixed with magnetite, metallic iron and pyrite (providing reducing conditions as expected in the repository). In this case the final concentrations in solution were much smaller, indicating reduction of Np(V) and Tc(VII) to positively charged Np(IV) and Tc(IV) species sorbing on the clay or precipitated as sparingly soluble reduced compounds (e.g. TcO_2).

These results show that the presence of environmental materials under reducing conditions may limit the aqueous concentrations of redox sensitive nuclides. Nonetheless, the data by Vernaz & Godon (1991) indicate that the retention capacity of the glass was reduced under such conditions, probably due to Si sequestration by the clay. For instance, they determined that only 26% of the released Np was bound to the glass alteration layer in the presence of Boom Clay. This shows that environmental conditions (added materials, complexing agents in solution) may well affect the retention capacity of the glass for specific nuclides, either by modifying the protective properties of the alteration layer or the nuclide speciation. Including radionuclide retention in the glass alteration layer in safety assessment calculations would therefore require the quantitative determination of retention factors under the environmental conditions of the specific repository, which is not feasible with the current state of knowledge. This justifies the conservative choice of congruent radionuclide release from the vitrified waste with solubility limitation made in the Swiss safety case.

Curti et al. (2006) determined the intrinsic retention of many elements in SON68 and MW glass, after corrosion in deionised water during 5.8 and 12.2 years at 90 °C and high S/V (cf. Section 4.2.4). Because the two glasses are inactive simulants, actinides are replaced by chemically analogue elements (e.g. trivalent lanthanides for trivalent actinides and cerium for tri- and tetravalent Pu) or weakly radioactive isotopes (natural Th, U). The data shown in Tab. 5-1 indicate that all listed elements but Mo and Cs have very high retention factors (> 97%) for both glasses after 12.2 years leaching. The weak retention Mo may be attributed to the high solubility and poor sorption capacities of the negatively-charged molybdate species, $Mo(VII)O_4^-$, released from the glass. Cs is retained only slightly less efficiently than other elements (RF = 88 – 96%). Considering the importance of ^{135}Cs as dose-relevant nuclide, this result calls for a detailed explanation. To this aim, a detailed characterisation study was carried out (see next section).

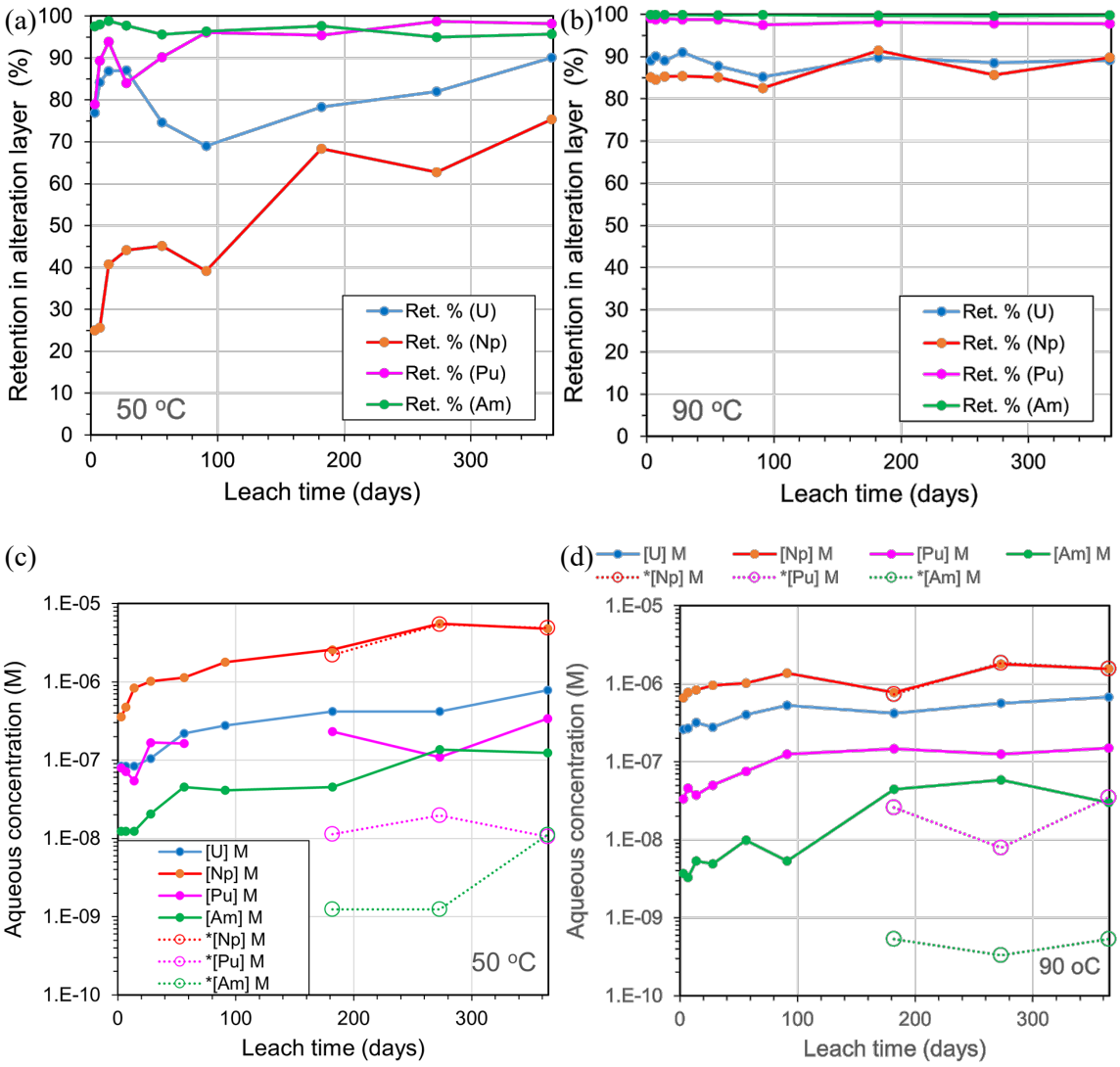

Fig. 5-1: Cumulative percentages of U, Np, Pu and Am retained in the alteration layer during aqueous corrosion of actinide-doped R7T7 glasses in static tests at 50 °C (a) and 90 °C (b) at S/V = 50 m^{-1}

Corresponding aqueous concentrations are also given (c,d). Concentrations obtained after ultrafiltration are marked by an asterisk (*) in the legend. The plots were generated from the tabulated data of Vernaz & Godon (1991).

Tab. 5-1: Percentages retained in the alteration layer after 12.2 years corrosion in initially pure water for dose-relevant elements (U, Th, stable isotopes of fission products or actinide analogues)

Excerpt of data from Curti et al. (2006)

Element in glass (represented RN)	**MW**		**SON68**	
	Avg.	**±SD**	**Avg.**	**±SD**
Ba	-	-	99.89	0.02
Ce ($Pu^{III/IV}$)	99.4	0.2	99.9	0.02
Cs	95.7	0.6	87.8	0.9
La (An^{III})	97.6	2.6	99.91	0.02
Mn ($Tc^{IV/VII}$)	-	-	99.5	0.2
Mo	62.2	2.3	52.8	6.1
Nd (An^{III})	99.5	0.2	99.94	0.02
Ni	99.7	0.2	99.5	0.5
Pr (An^{III})	99.8	0.1	99.83	0.01
Sr	99.7	0.02	99.45	0.03
Th (An^{IV})	-	-	> 99.6	-
U ($An^{IV/VI}$)	-	-	> 99.8	-
Y (An^{III})	99.6	0.1	99.9	0.02
Zr	99.8	0.1	99.93	0.02

5.2.3 Trapping of radionuclides in secondary glass alteration solids

This section focusses on the short-range mobility of radionuclides once they have been released into solution, i.e. their re-entrapment in secondary solids precipitated on top of the corroding glass surface. It may be argued that soluble nuclides like ^{135}Cs, which cannot be incorporated into the lattice of common minerals, would be leached out almost completely during borosilicate glass alteration. Extensive release of Cs was observed e.g. in the experiments of Vernaz & Godon (1991), which were however obtained far from "silica saturation". The data presented in Tab. 5-1, obtained under "residual rate regime", show on the contrary strong retention of Cs, calling for an explanation.

Curti et al. (2009) investigated the distribution of Cs and other elements in the corroded MW glass after 12.2 years leaching, i.e. the same sample to which the MW data listed in Tab. 5-1 refer, using advanced synchrotron-based techniques. Micro X-ray fluorescence (m-XRF) maps at low micrometre resolution showed homogeneous intensity patterns, both in the pristine glass and in altered regions rich in secondary Mg-phyllosilicates. This is consistent with the results in Tab. 5-1, since no or only weak depletion of Cs in the corroded glass regions can be inferred from the XRF maps. A large number of micro X-ray absorption spectra were recorded in both regions, showing uniform oscillation patterns in the entire sample. The absence of Cs-Cs pairs in the absorption spectra allow to exclude the occurrence of pollucite, a zeolitic Cs-alumosilicate that has been observed occasionally as corrosion product of Al-rich glasses at alkaline pH (Ribet &

Gin 2004, Inagaki et al. 2006). The spectra point to a disordered coordinative environment around Cs^+, both in the pristine glass and the secondary phyllosilicate. It may be argued that Cs^+ ions, which are too large to fit in tetrahedral or octahedral sites of the Mg-phyllosilicate, may be adsorbed or exchanged in the interlayer of the phyllosilicates. Although the exact mechanisms of retention remain obscure, it is clear that Cs^+ is not leached out and is homogeneously retained, probably via sorption, in the alteration products of the MW glass.

In the same study it was shown that in the pristine (non-altered) glass, Ni^{2+} is either homogeneously distributed at low concentrations in the borosilicate glass matrix, or concentrated in discrete micro-inclusions identified as trevorite (a spinel with ideal formula Fe_2NiO_4). As for Cs, most of the nickel released during the glass corrosion process remained entrapped *in situ* in the phyllosilicate. The spectroscopic data suggest that part of the released Ni^{2+} substitutes for Mg^{2+} in the octahedral sites of the phyllosilicate, thus forming a solid solution. Another part of the released Ni^{2+} is apparently adsorbed on frayed edges or exchanged in the interlayer.

In a later study with the same corroded MW samples, Curti et al. (2012) studied the distribution of cerium in the pristine glass and secondary corrosion products. Cerium is used as analogue of Pu(III)/Pu(IV) due to similarities in the chemical and oxidation potentials. The distribution of Ce(III) and Ce(IV) in the altered glass after 12.2 years leaching was determined using a dedicated m-XRF based technique and XANES were collected at selected locations of the sample (Fig. 5-2a). The maps show that the Ce(IV) is the predominant species in the pristine (non-altered) glass, while Ce(III) predominates in the secondary phyllosilicate. This indicates that upon release from the glass, cerium underwent reductive precipitation and was entrapped as Ce(III) in the secondary Mg-phyllosilicate. Micro-XANES spectra collected at different locations in the altered and non-altered glass domains (Fig. 5-2b) fully confirmed this interpretation. The source of reductant in these experiments was probably Fe(II) dissolved by the steel vessel used in the experiments.

Based on the aforementioned chemical analogy between Pu and Ce, these results suggest that in a typical reducing repository environment Pu^{IV} released from an Mg-rich glass would readily re-precipitate and be immobilized *in situ* as trivalent Pu shortly after being dissolved from the waste.

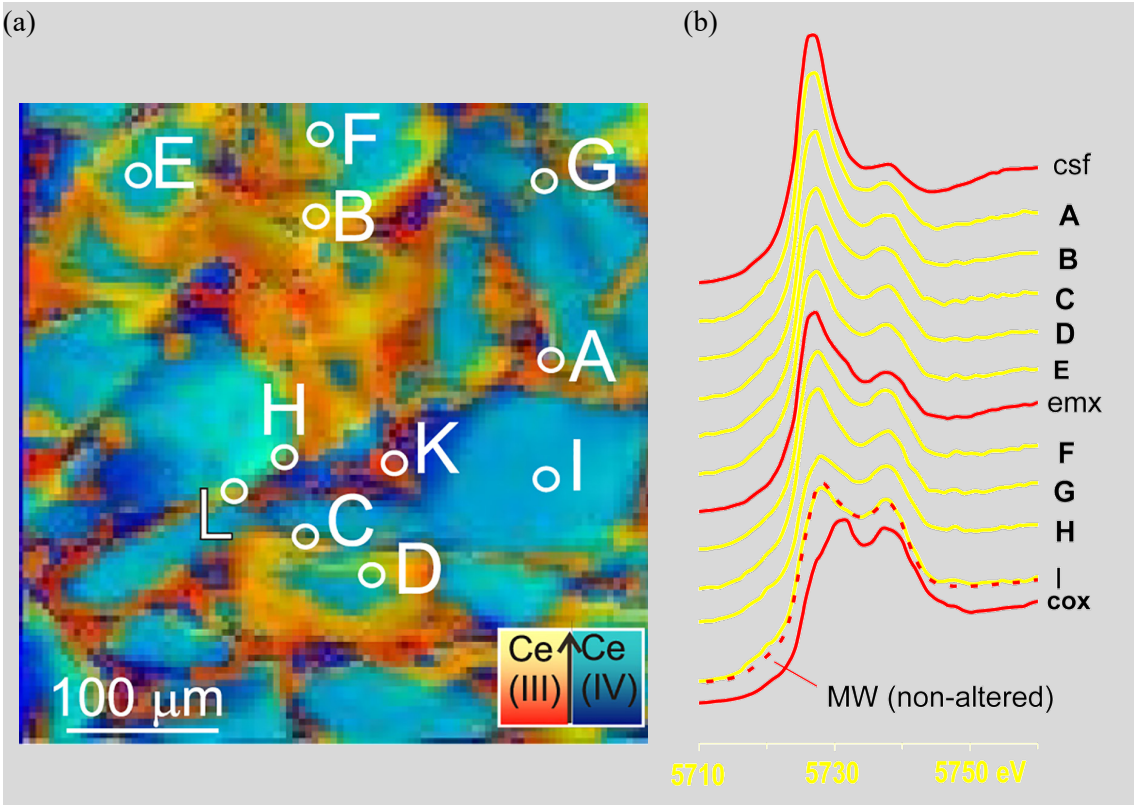

Fig. 5-2: Bicolor map showing (a) the distribution of Ce(III) (orange-red), Ce(IV) (turquoise-blue) and total Ce (brightness) in altered MW glass powder after 12 years leaching in deionised water, (b) micro-XANES spectra, with letters corresponding to selected sample locations

Reference spectra are shown in red: csf = $Ce^{III}_2(SO_4)_3$, cox = $Ce^{IV}O_2$, emx = equimolar mixture of the two reference compounds, dotted line = pristine MW glass. Taken from Curti et al. (2012) and printed with permission from Elsevier.

5.3 Concluding remarks

Although only few experiments have been carried out to date to investigate the fate of radionuclides released from corroding glass, the available data indicate consistently that most radionuclides (and particularly tri/tetravalent actinides) are retained either in the gel layer or in surface precipitates. Caesium has been also shown to be retained quite efficiently in the alteration layer of the MW and SON68 glasses. Some actinides (Pu, Am, Cm) may form radiocolloids, which however cannot migrate to the geosphere thanks to colloid filtration, if compacted bentonite is selected as sealing material.

6 Vitrified waste dissolution models

6.1 Preliminary remarks

Models to predict the kinetics of borosilicate glass corrosion have been developed since the early seventies of the past century. The first ones aimed at classifying generically the reactivity of the glass in water as a function of its bulk composition, giving rise to a ranking in "durability" of the glass in water. The term "durability" stands for the short-term dissolution far from "silica saturation" as observed in simple leach tests after limited experimental times and high solution volume to glass mass ratios. Paul (1977) developed the progenitor of this type of models. His basic idea was to correlate the observed dissolution rates with the free energy of hydration of the major oxide constituents of the glass. Using tabulated values of the free energy of oxides, he defined fictive equilibrium constants for simple glass compositions (e.g. Na_2SiO_3, $CaSiO_3$, $ZnSiO_3$, $Zr_2Si_2O_6$). From that, he calculated pH-dependent "solubility constants" of the glass in terms of the equilibrium activities of the basic silica species (H_4SiO_4 and $H_3SiO_4^-$). Although a thermodynamic solubility cannot exist for glass (since it is a metastable phase) this model was able to explain common empirical observations, e.g. that Ca-silicate glass is more resistant to aqueous leaching compared to Na-silicate glass, or that the addition of even small amounts of ZrO_2 to a glass formulation greatly improves its chemical resistance. The model was later refined and applied successfully to a large number of glass formulations (Jantzen & Plodinec 1984). Its major value was and still is to offer a quick toolkit to roughly evaluate the expected aqueous corrosion of a given glass composition in the absence of leach data. For the purpose of radioactive waste repository assessments, such models are however of limited value, since the major concern is the long-term evolution of the glass dissolution rates (i.e. close to "silica saturation" at the *residual rate* regime).

The first model capable of predicting quantitatively dissolution rates as a function of aqueous chemistry and leaching time was the so-called *affinity law* model (Grambow 1985). This model dominated for many years thanks to its capability to predict quite precisely the short-term *evolution* of glass dissolution kinetics in low S/V static leaching tests, carried out without additives over a time scale of 1 – 2 years at most. With increasing complexity and duration of glass leaching experiments, in which key parameters were varied "in isolation", it became however clear that the *affinity law* alone is not sufficient to predict long-term dissolution rates. As more and more experimental evidence accumulated, it became evident that the diffusion properties of the gel layer are a major factor controlling the long-term kinetics of borosilicate glasses, finally leading to the IDA model (Section 3.3). Because gel properties are a complex function of glass composition, aqueous solution speciation, pH, temperature and added materials (clay, Fe/Fe corrosion products, cement) the incorporation of passivation effects in a kinetic model proved to be an arduous task. Nevertheless, attempts to combine many relevant factors in a kinetic model applicable in the context of radioactive waste disposal and tailored for R7T7-type glasses have been made (GRAAL model, see Frugier et al. 2008 and Section 6.4).

This chapter is not intended to be a comprehensive review of kinetic models of nuclear waste glass dissolution. We will focus on few models applicable to a disposal context similar to that foreseen in Switzerland. Models developed specifically for largely different glass compositions and repository designs will not be discussed. Section 6.2 is devoted to the *affinity law* and an illustration of its shortcomings. This is followed by a presentation of PSI's in-house GLADIS model (Section 6.3), an early attempt to integrate the *affinity law* with the effect of silica sequestration and diffusion through a clay buffer. The model was tested successfully against laboratory data simulating a small-scale setup similar to the Swiss HLW repository concept.

Section 6.4 provides a succinct description of the currently most evolved model (GRAAL), developed at CEA Marcoule. The chapter is completed by some general-purpose remarks (Section 6.5).

6.2 The "affinity law" model

According to many experiments conducted at low to moderate S/V and short leaching times (< 1 – 2 y), the corrosion rate of borosilicate glasses appears to depend on dissolved silica concentration in the bulk solution. Data analysis indicated that the rates measured based on congruently dissolved elements (B, Li) was inversely proportional to the dissolved silica concentration in the bulk solution. From this evidence, Grambow (1985) derived a first-order kinetic law that allowed describing the strong decrease in glass corrosion rates observed in the initial stages of glass alteration. For a typical borosilicate glass such as SON68 and MW, the highest rate measured in pure water (the so-called *forward rate*) was in the order of 1 g m^{-2} d^{-1} at 90 °C. As the Si solution concentration increased due to release of soluble components from the glass, the corrosion rate decreased to an asymptotic minimum value (*residual rate*), at which dissolved silica reaches a stationary concentration (the so-called "saturation" concentration, C_{sat}). Typically, *forward rate* and *residual rate* were found to differ by 3-4 orders of magnitude. According to this model, at any dissolved silica concentration C_{Si} the glass corrosion rate r [g m^{-2} d^{-1}] is defined by the following empirical equation (Vernaz et al. 2001):

$$r = r_0 \left(1 - \frac{C_{Si}}{C^*}\right) \tag{1}$$

where r_0 is the glass corrosion rate in pure water (*forward rate*) and C^* is a theoretical Si concentration slightly exceeding C_{sat}, at which the rate reaches a minimum persistent value (*residual rate*, r_{fin}) Note that r_0 and C^* are purely empirical, glass-composition dependent parameters that must be extrapolated from a series of dedicated rate measurements at different silica concentrations. C^* represents a maximum hypothetical concentration, at which glass corrosion would cease completely, which is never attained[16]. Instead, a slightly lower "saturation" concentration C_{sat} is reached, which is not exceeded at further reaction progress and determines the *residual rate* (r_{fin}) according to:

$$r_{fin} = r_0 \left(1 - \frac{C_{sat}}{C^*}\right) \tag{2}$$

where r_0 is the *forward rate*, the initial corrosion rate measured in pure water. The kinetics described by Eqs. (1) and (2) are attributed to the decreasing chemical affinity, i.e. to the decreasing difference between the chemical potentials of silica in the glass and of silica effectively precipitating (recondensating) from solution. Since glass is thermodynamically unstable in water, a residual affinity, i.e. a small disequilibrium between a theoretical glass dissolution constant and an effective SiO_2 constant will persist until the glass is completely dissolved. This treatment follows the well-known description of irreversible mineral dissolution kinetics developed by Aagard & Helgeson (1982), according to which the affinity of a dissolved species j (silicic acid, H_4SiO_4, in our case) is given by:

[16] If C* were reached, then according to eq. (2) the glass dissolution rate would be zero, implying true thermodynamic equilibrium between glass and aqueous phase, which is not possible.

$$A_j = RT \ln \frac{Q_j}{K_j} \tag{3}$$

In the glass affinity model, the following approximations are made:

$$Q_j = K_{prec} = \frac{a_{H4SiO4(sat)}}{a_{H2O}^2} \tag{4a}$$

$$K_j = K_{glass} = \frac{a_{H4SiO4(*)}}{a_{H2O}^2} \tag{4b}$$

where K_{prec} is the equilibrium constant of the secondary SiO_2 precipitate at equilibrium with the aqueous solution (i.e. the thermodynamically stable product of the glass alteration reaction), K_{glass} is a fictive equilibrium constant describing the tendency of the glass to dissolve, and the a_{H4SiO4} are equilibrium activities of orthosilicic acid. The thermodynamic affinity at constant pH, temperature and pressure can be then expressed for the reaction SiO_2 (s) + 2 H_2O = H_4SiO_4(aq) as follows:

$$A_j \equiv \mathrm{RT} \ln \frac{Q_j}{K_j} = \mathrm{RT} \ln \frac{a_{H4SiO4(sat)}}{a_{H4SiO4(*)}} = \mathrm{RT} \ln \frac{C_{sat}}{C^*} \tag{5}$$

Since $C_{sat} < C^*$, it follows that $A_j < 0$, meaning that the glass dissolution reaction is spontaneous. In other words, the fact that the affinity is negative implies that the glass is metastable with respect to the secondary (precipitated) silica remaining as stable product at the end of the alteration reaction. C_{sat} and C^* are empirical parameters determined from experiments at constant pH, T and p for a specific glass composition.

Equations (1) and (2) suggest that the *residual rate* (r_{fin}) could be derived as a model output, after the determination of C_{sat} and C^*, without previous experimental determination of the *residual rate*. This would give a good predicting power to the affinity-law model. Unfortunately, such a procedure is not possible because, in practice, C_{sat} and C^* are so close that they cannot be discriminated. The problem is best illustrated with the help of Fig. 6-1, which shows a set of hypothetical measured silica concentrations and glass dissolution rates in linear and semi-logarithmic scale assuming that, after 1 year leaching time, a final rate of 0.01 g m^{-2} d^{-1} is measured. Let us further assume that the X-intercept of the linear interpolation yields a value for C^* of, say, 1.00 ± 0.05 mM and that the corresponding (measured) Si "saturation" concentration is 0.99 ± 0.10 mM (implying a fairly good analytical uncertainty of ± 10%). It is evident that, in spite of the good precision of both parameters, their values are indistinguishable. Rearranging equation (2), one obtains:

$$C_{sat} = C^* \left(1 - \frac{r_{fin}}{r_0}\right) \tag{6}$$

After 1 year leach time eq. (6) yields C_{sat} = 0.99 ± 0.05 mM, using $r_{fin} = 10^{-2}$ g m^{-2} d^{-1} and taking into account the uncertainty of C*. Suppose now that the experiment continues for another year, during which a further drop in the glass dissolution rate is observed down to 10^{-4} g m^{-2} d^{-1} (blue portion of model curve). Repeating the calculation, now using the new *residual rate*, yields C_{sat} = 0.9999 ± 0.05 mM, which is practically within the same uncertainty range previously calculated.

A further chemical analysis of the silica concentration (open circle in Fig. 6-1), would yield a concentration that is indistinguishable within the analytical uncertainty from the previous determination after 1 year.

This example shows that the resolution of C_{sat} and C^* is not sufficient to apply successfully eq. (2) and derive from it an unknown *residual rate*. The model can only be applied using eq. (1) at several times during the experiment to extract C*, then letting the experiment proceed for sufficient time until a true residual rate regime has been established and apply eq. (6) to derive C_{sat}. In other words, r_{fin} (the relevant quantity for safety assessment purposes) is not predictable but a required input parameter of the model, from which only C_{sat} can be extracted. With the affinity model, there is no way to determine the residual rate other than by direct experiment; a theoretical prediction is not possible. The consequence of the previous elaborate discussion is that, in order to apply the "affinity" law, one has to determine first the residual rate of any specific glass of interest experimentally, under the desired conditions.

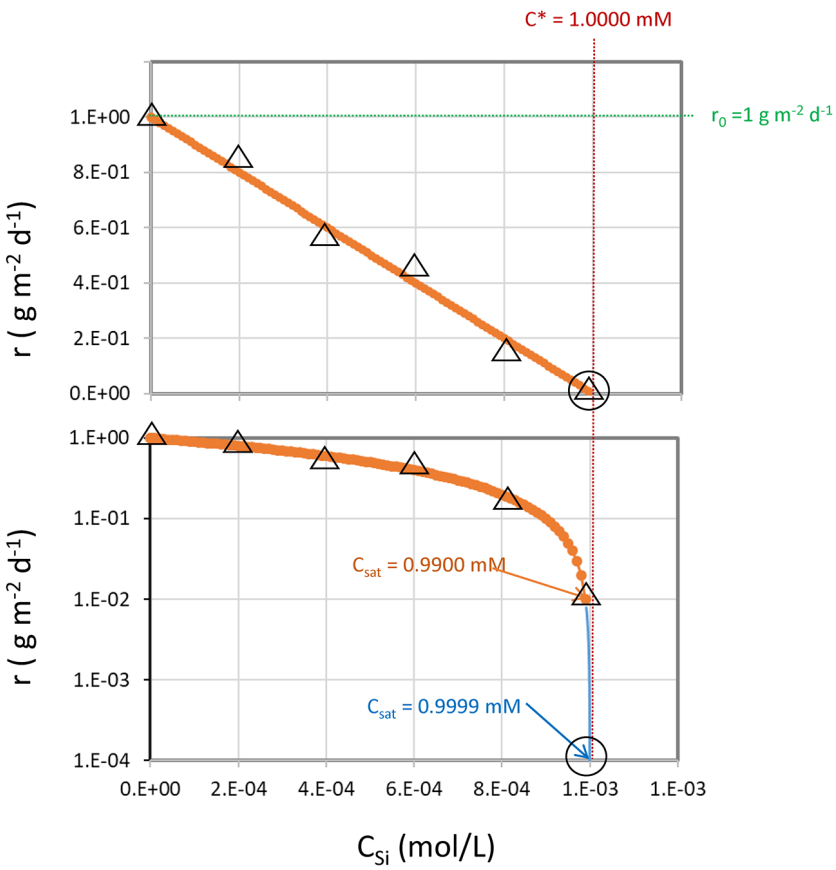

Fig. 6-1: Example of practical application of the "affinity law": derivation of empirical parameters from hypothetical experimental data (open triangles and large open circle) with linear scale (top figure) and with logarithmic scale (lower figure) for the rate *r*

See discussion in text for explanations.

6.3 The GLADIS model

An early attempt to develop a model capable of predicting glass dissolution in a repository-like environment was made in the early nineties by Curti & Smith (1991). The model couples the glass dissolution kinetics, as expressed by the "affinity law" in equation (2), with diffusion and reversible sorption of silica through a surrounding clay buffer. The model is implemented in cylindrical geometry, with the glass form surrounded by an annulus of clay buffer material. It calculates time-dependent diffusion profiles of silica through the clay, with implicit calculation of the activity of silicic acid at constant pH, assuming any background Si concentration in the initial pore water. The corrosion rate at any time is then derived from the time function of the silicic acid activity at the glass/clay interface. Also included in the model are an empirical retention factor of Si in the glass alteration layer (which has to be determined experimentally) and a fragmentation factor of the glass to take into account the increase in exposed surface area caused by cooling-induced cracking of the vitrified waste after its fabrication.

The model was implemented in FORTRAN and can be applied to both laboratory and repository scales, assuming homogeneous properties of the materials and neglecting any effects of differential glass corrosion. The code includes an in-built verification by comparing the numerical results with an algebraic solution predicting the final stationary glass corrosion rate, r_{ss}. It is important to realize that the final stationary rate, r_{ss}, calculated by GLADIS is always larger than the *residual rate*. This is simply a consequence of the open system conditions imposed in the model, as dissolved silica is allowed to diffuse out of the bentonite (in this sense, the model is conservative).

The GLADIS model was tested successfully against dedicated laboratory experiments carried out at CEA Marcoule, as described in detail in Section 4.4.2. From the model, optimised K_d values between 0.005 and 0.5 m^3/kg were derived for Si sorption on the clay, that are consistent with published data (Fig. 4-11). As an example of application of the GLADIS model to the scale and geometry of the Swiss HLW repository, calculations reported by Curti 2003 (op. cit., Fig. 3-1) are reproduced in Fig. 6-2. The results indicate that weak to moderate sorption of Si on bentonite ($K_d \leq 0.05$ m^3/kg) would have only a minor penalizing effect on the "lifetime" of the vitrified waste. In contrast, assuming a ten-fold larger (but still realistic) distribution coefficient (K_d = 0.05 m^3/kg) would greatly accelerate the degradation of the glass, particularly in the first ten thousand years after canister failure. These calculations are now obsolete, since (a) direct contact between bentonite and glass is highly unlikely and (b) the meanwhile quantifiable effect of Fe and its corrosion products are not taken into account.

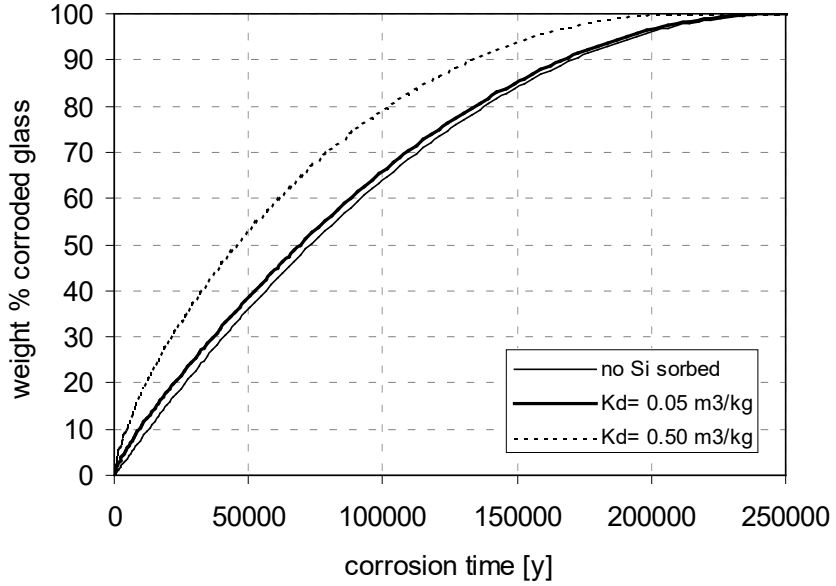

Fig. 6-2: Effect of Si sorption by clay minerals on the performance of borosilicate waste forms in a repository environment

Calculations were performed with the GLADIS code, based on a parameter set optimised for conditions applying to a deep repository, but neglecting the effects of Fe and Fe corrosion products.

GLADIS was specifically developed for modelling glass in direct contact with clay. However, the code could be in principle adapted to the contact with a porous corroded canister, by specifying appropriate porosity and sorption coefficient values of silica on Fe Fe/ corrosion products.

6.4 The GRAAL model

GRAAL (Glass Reactivity with Allowance for the Alteration Layer Model), developed by the CEA Marcoule group (Frugier et al. 2008, Minet et al. 2010), is probably the most evolved glass dissolution model. As expressed by the full model name, it includes, in addition to the pH and temperature-dependent "affinity law", dynamic effects related to the passivation of the gel layer. According to the authors, the aim of the model is "*to describe the glass alteration kinetics up to and including the final residual rate regime*". It is intended to provide a long-term source term function for radionuclide release from vitrified waste consistent with the mechanisms defined in the mechanistic IDA model (Section 3.3). GRAAL is thus potentially applicable to a repository context.

In the presentation of the GRAAL model, Frugier et al. (2008) first reviewed the underlying mechanisms governing the glass corrosion process and evaluated their relative importance for the long-term evolution. They identified five sequential stages of kinetic evolution, characterised by distinct microscopic mechanisms at the glass water interface:

I. *Interdiffusion*: exchange of cationic network modifiers, typically Na^+, with protons or other cationic species from solution

II. *Initial rate regime*: initial (Si, B, Al)-O network dissolution in the absence of alteration layer effects, defined in the model as a function of pH and temperature.

III. *Rate drop regime*: transient kinetic phase between initial and *residual rate* regime controlled by both "affinity law" and passivation effects in the gel, called in the paper "Passivating Reactive Interface" (PRI).

IV. *Residual rate regime*: long-term regime driven by steady state *residual rates*, determined by S/V ratio in combination with kinetic inhibition by diffusion through the gel layer

V. *Resumption regime*: sudden increase of glass corrosion kinetics driven by specific changes in solution chemistry, notably pH increase in the alkaline region and massive zeolite/C-S-H precipitation.

The GRAAL model is tailored to the SON68 glass and takes into account processes II, III and IV, as well as the precipitation of secondary phases, which are considered to be fully permeable. Stage I is neglected since it is active only at very short term and has thus no influence on the overall corrosion kinetics of the glass in the long term, while Stage V is not included since it is relevant only under particular conditions (e.g. cementitious environments, Al-rich glasses). The model includes equations predicting the growth or dissolution of the PRI (which represents the gel layer) as a function of corrosion time. Such equations are coupled to stationary diffusion of chemical species through the PRI. A single diffusion coefficient ($D = 10^{-22}$ m^2 s^{-1}) is used to describe the diffusion of water and solutes from the bulk solution towards the pristine glass surface and that of mobile species such as boron towards the bulk solution. The "affinity law" is applied at the outer boundary of the PRI (i.e. the PRI/bulk water interface). This means that the PRI dissolves there at the rate specified by the "affinity law", as long as the silica concentration in the bulk water is below C_{sat}. At the inner side of the PRI (pristine glass/PRI interface) mobile elements such as B and Li start to diffuse according to the preset diffusion coefficient, thus increasing the "penetration depth" of the PRI. The balance of the aforementioned processes at the two interfaces defines the thickness of the PRI, e(t), at any time. The quantity e(t), the thickness of the gel layer, is however not a measure of the total corrosion of the glass. This is given by the model output as $E(t)$, the total dissolved PRI thickness at time t, from which a linear glass corrosion rate $L = dE/dt$ (m d^{-1}) can be calculated. The normalized glass corrosion rate as usually given in glass corrosion studies, r (g m^{-2} d^{-1}), can then be readily derived by multiplying L with the density of the glass.

Minet et al. (2010) carried out validation tests and a sensitivity analysis by comparing the GRAAL predictions (with parameters calibrated for SON68) with a series of experimental data. In general, the results of static and dynamic corrosion tests were satisfactory. In the same study, an attempt was made to apply the model to (French) repository conditions. The vitrified waste was modelled as a cylindrical, fractured block surrounded by a chemical inert diffusion barrier permeated by a pore solution flowing with a Darcy velocity of 10^{-11} m s^{-1}. The inflowing solution is assumed to be silica-free. The results of the calculations, carried out at 90 °C, predict a *residual rate* of 6×10^{-15} m s^{-1} (corresponding to 1.4×10^{-6} g m^{-2} d^{-1}) reached already after about 1 year. According to Minet et al. (2010) this indicates that "*precipitation [of silica at the barrier/glass interface] is the driving mechanism of glass alteration, much more than silicon diffusion through the barrier*." The calculated *residual rate* (1.4×10^{-6} g m^{-2} d^{-1}) is however surprisingly low, as it is about two orders of magnitude slower than the dissolution rate measured in long-term corrosion tests for SON68 at 90 °C (2×10^{-4} g m^{-2} d$^{-1,}$ cf. Curti at al. 2006). Minet et al. (2010) do not comment this discrepancy. Moreover, the calculations do not take into account the strong effects of environmental materials (sorption of silica on clay, steel and its corrosion products), which are known to profoundly affect the glass alteration kinetics. In the opinion of the author of this report, the value of these calculations for safety assessment purposes is rather limited.

6.5 Concluding remarks

Up to the end of the past century, the kinetics of nuclear waste glass corrosion in aqueous media has been quantified with the help of a first order kinetic equation, the so-called "affinity law". The equation assumes that the dissolution rate of the borosilicate glass matrix is inversely proportional to the silica concentration in the aqueous solution. With increasing silica concentration, the glass dissolution rate decreases down to a limiting *residual rate*, sustained by the difference between the chemical potentials of silica in the glass and a SiO_2 phase condensing in the surface alteration layer. The model requires empirical parameters (*forward rate*, *residual rate* and a hypothetical silica concentration C^*) that can only be obtained from experiments for a specific glass composition.

In the first decade of this century, experimental evidence has accumulated that the diffusion properties of the growing alteration layer must be taken into account, in addition to the affinity term, in order to correctly predict long-term glass dissolution rates. This has given rise to a plethora of studies attempting to understand and quantify the complex processes taking place in such layers. The most evolved model currently available (GRAAL) combines both mechanisms, however it is not sufficiently advanced yet to take into account quantitatively the effects of clay, Fe and Fe corrosion products in a repository environment.

Even after implementation of environmental effects, models coupling glass corrosion with near-field chemistry will unavoidably be affected by large uncertainties, due to the large number of coupled properties involved (e.g. porosity changes in barrier materials, reactive surface areas of dissolving/precipitating secondary phases, to cite just two). Therefore, although glass corrosion models remain the method of choice to verify hypothetic dissolution mechanisms against the results of laboratory experiments, they seem to be inadequate to generate reliable source term functions for safety assessments. For safety assessment calculations, it appears more reasonable to use constant glass dissolution rates encompassing a realistic range, based on the best available knowledge. Such a strategy has been always preferred for the Swiss safety assessment, and is pursued in SGT-3. An update of recommended glass dissolution rates is presented in the next chapter.

7 Recommended parameters for safety assessment

7.1 HLW/SF repository layout

Nagra proposed a combined repository at the site of Nördlich Lägern in the Northern part of Switzlerand. Construction plans for the proposed HLW/SF repository section foresee waste disposal in a system of parallel (sub)horizontal drifts within the Opalinus Clay formation at depths of ca. 850 m below ground level. During construction, the emplacement drifts of ca. 3.5 m inner diameter will be supported by pre-fabricated segmental liners. Fig. 7-1 (Nagra 2022a) shows a schematic representation of such a combined repository, including the visualization of main repository, access tunnel, test/pilot facilities and vertical construction/ventilation shafts.

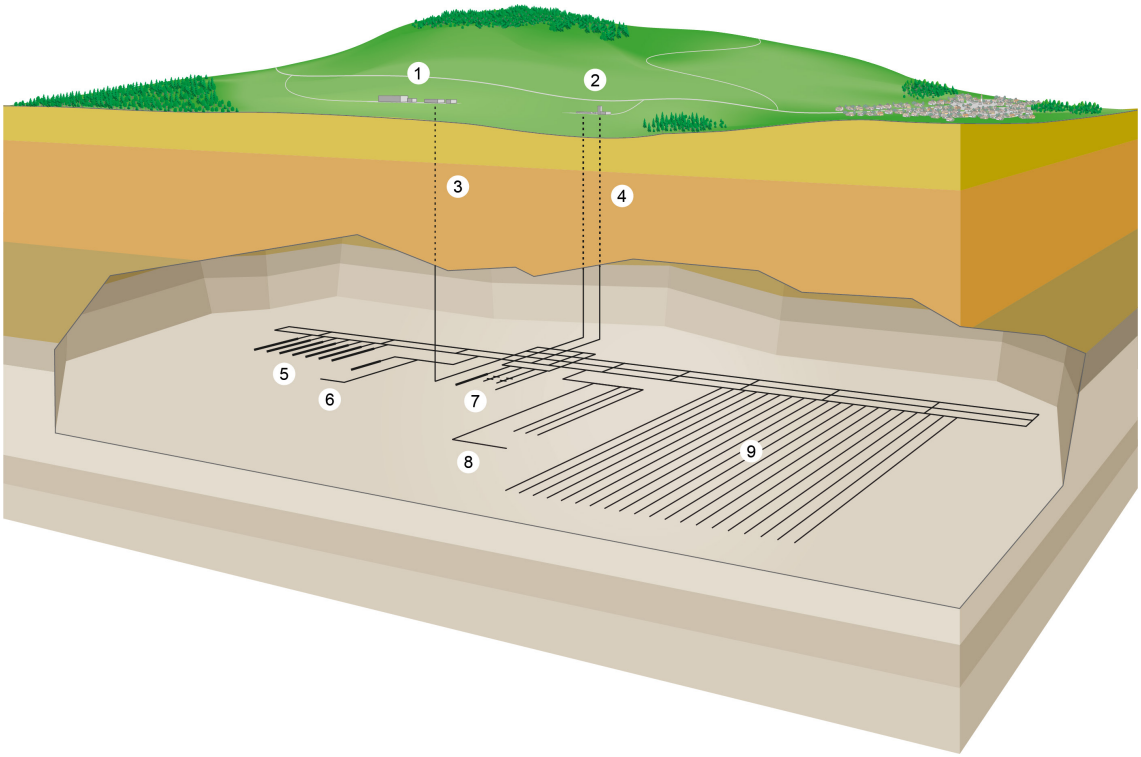

Fig. 7-1: Illustration of a combined repository for SF/HLW and for L/ILW

Legend: 1) Surface facility, 2) Auxiliary access facility, 3) Access shaft (main access), 4) Operations and ventilation shafts (auxiliary accesses), 5) Main repository L/ILW, 6) Pilot facility L/ILW, 7) Underground geological investigations/test areas, 8) Pilot facility HLW, 9) Main repository HLW

Nagra (2022a)

Two waste sorts will be hosted in the HLW repository section: spent fuel (irradiated fuel rods) and vitrified high-level waste. Both types of waste will be encapsulated into 14 cm-thick carbon steel canisters. The waste canisters will be placed sequentially on pedestals of highly compacted bentonite at the centre of the drifts, which will be progressively backfilled with compacted granular bentonite (reference dry density 1'450 $kg \cdot m^{-3}$).

Vitrified high-level waste is the product of the treatment and reprocessing of spent fuel, aiming at extracting fissionable U and Pu for re-use in nuclear power plants. The used fuel is first dissolved into a highly radioactive liquid. After a complex extraction procedure, the liquor is then evaporated, calcined and mixed at high temperatures with borosilicate glass forming additives to produce a homogeneous molten glass. The melt is poured into stainless steel flasks and allowed to solidify before sealing by welding. During cooling, the glass monolith undergoes unavoidable thermal stress fragmentation, causing an increase of the geometric surface area by a factor of 15 (Nagra 2014d, Tab. A3.45b, p. A91). Fig. 7-2 shows the safety barrier system foreseen for vitrified waste in the Swiss HLW/SF repository.

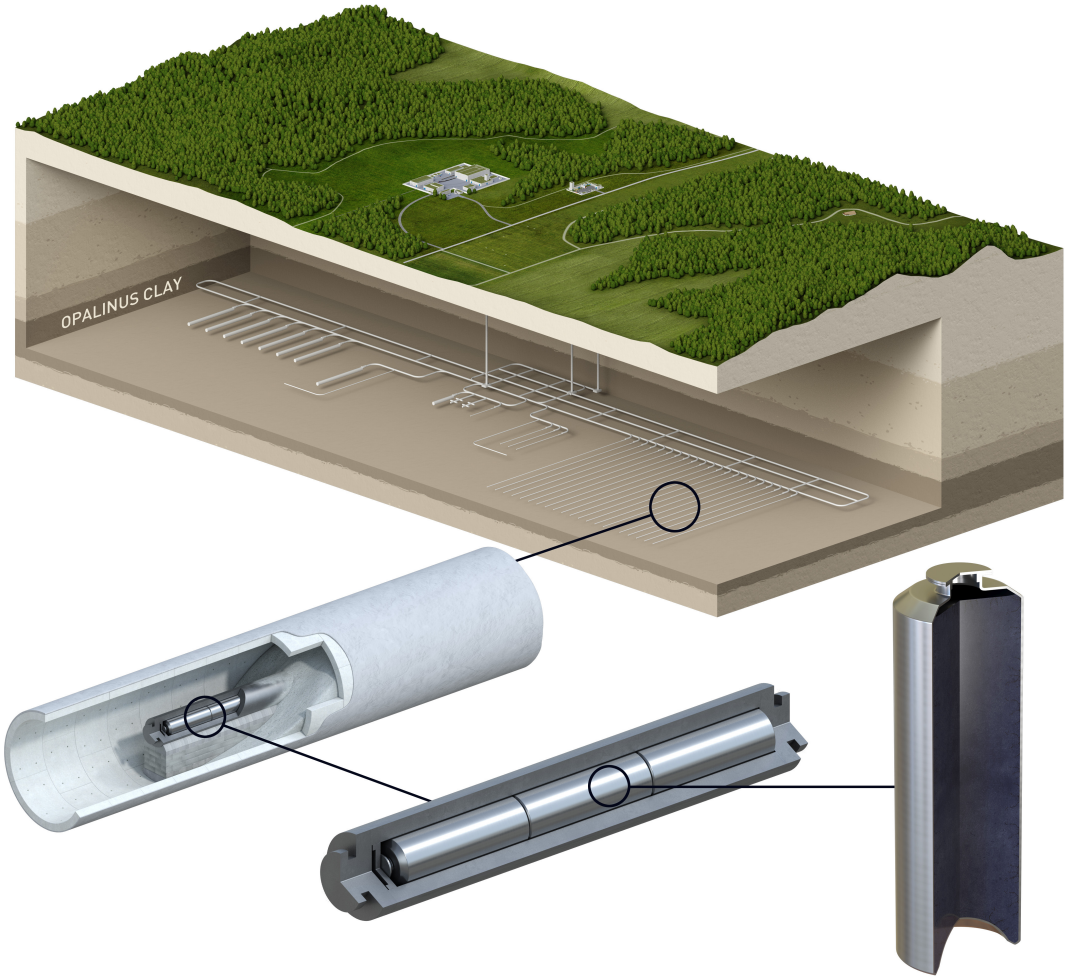

Fig. 7-2: The system of safety barriers for vitrified high-level waste

7.2 Safety assessment model

Dose rate calculations for safety assessments require source term functions for the release of radionuclides. For both spent fuel matrix and vitrified waste, such functions must rely on state-of-the-art knowledge of the dissolution kinetics of the waste materials and their dependencies on chemical-physical parameters. In the case of radioactive waste immobilized in borosilicate glass, there is meanwhile a large body of knowledge available, including models describing the large variation of dissolution rates as a function of solutes concentration, passivation properties of the alteration layer and the effect of engineered barrier materials (see Chapter 6).

The models used for the Swiss HLW safety assessment are documented in Nagra (2002, 2014c) and Nagra(in prep.). In these models, dissolution rates of either spent fuel or glass are assumed to remain constant during the entire evolution, i.e. there is no explicit coupling of SF or glass corrosion rates with chemical-physical parameters implemented. This means that all uncertainties and time-dependent variations of the dissolution rates are taken into account by "bracketing". i.e. by choosing an appropriate range of constant rates with different degrees of conservatism in separate calculations. Other national programs resort to more deterministic source term functions for glass dissolution. For instance, in performance assessments for the Hanford site vitrified low level waste (U.S.) a pH-dependent source term function based on the affinity law is used (Ryan & Freedman 2016).

In the Swiss safety assessment the STRENG code (Grindrod et al. 1990), integrated in the STMAN 5 package (Robinson 2022), is used to describe the release of radionuclides from the glass matrix at a pre-defined constant rate. The release of radionuclides is assumed to be congruent, i.e. there is no retention in the alteration layer. All radionuclides released from the dissolving glass are first directly transferred to an aqueous solution volume (the so-called "reservoir") representing the water-filled voids within the loaded canister. Possible mitigating effects are conservatively neglected: e.g. transport resistances within the fractured glass body, void volume reduction due to canister collapse and formation of high molar volume steel corrosion products, unsaturated conditions arising from hydrogen production and water consumption following anaerobic corrosion of steel. Moreover, the physical presence of the corroded canister is not taken into account. Dissolved radionuclides thus directly diffuse out into the pore space of compacted bentonite, where they undergo retardation according to element-specific sorption coefficients (K_d-approach). In the "reservoir", radionuclide concentrations are allowed to increase up to element-specific solubility limits (for most dose-relevant nuclides) or indefinitely for few very soluble nuclides (e.g. ^{135}Cs). In the STRENG model, radionuclide mobility is therefore limited "only" by the solubility limitation and by other "upstream" processes, namely slow diffusion and retardation through sorption on the bentonite buffer and Opalinus Clay host-rock, expressed by sorption coefficients (K_d).

In the case of spent fuel, an Instant Release Fraction (IRF) is defined for segregated, soluble nuclides promptly released on contact with aqueous solution (^{135}Cs, ^{129}I, ^{36}Cl), in addition to matrix dissolution. No such prompt release fraction is assumed in the case of vitrified waste, as no clear evidence for a preferential sudden release of specific radionuclides was found to date. Borosilicate glass is a much more homogeneous material than spent fuel. The heterogeneities in glass are usually less soluble than the glass itself, except for the so-called "yellow phase" which could in principle lead to a preferential release of ^{93}Mo. The data available on molybdenum release from the Swiss reference glasses however, rather point to congruent release (see NL(B)-NL(Mo) correlation in Fig. 4-1). In summary, it can be concluded that STRENG provides a strongly simplified, however conservative source-term model of the glass dissolution and radionuclide release process.

Another difference between spent fuel and vitrified waste source functions is that the former is defined as fractional release rate (mass fraction dissolved per unit time) whereas vitrified waste dissolution rates are surface normalised (mass of glass dissolved per unit time and unit exposed surface area). The reason for the different treatment arises from fundamental problems in quantifying the reactive surface area of spent fuels (Hanson & Stout 2004), due to technical challenges in characterization techniques and the high activity/heterogeneity of this material. Such problems are less critical in the case of glass, as this material is much more homogeneous and the water-accessible surface area of the cylindrical waste form (including the increase due to cooling-induced fracturing) can be well simulated with non-radioactive glass simulants.

7.3 Selection of glass dissolution rates

In this section, updated glass dissolution rates recommended for use in safety assessment calculations are derived (Tab. 7-1) and discussed. The recommended rates refer specifically to vitrified waste compositions and environmental conditions applying to the Swiss HLW repository. They rely mainly on recent experimental studies carried out with inactive and actinide doped SON68 and with inactive MW borosilicate glass. These two glasses correspond to the chemical specifications provided by ORANO and Sellafield LTd. for vitrified waste returned to Switzerland from the La Hague and Sellafield reprocessing plants, respectively. For the present update, new experimental results on the effects of self-irradiation and the presence of large amounts Fe and Fe corrosion products in close vicinity to the glass were taken into account.

Data obtained from leach experiments carried out with radioactive glasses doped with actinides (Mougnaud 2017, Tribet et al. 2021) indicate that the effect of *cumulative alpha dose* may lead to a significant increase of the residual rate (Section 4.3.3.3). The data of Mougnaud (2017), obtained from ^{244}Cm-doped glass having experienced a cumulative dose representative of canister failure times (third column in Tab. 4-3) indicate dissolution rates of about 6×10^{-4} g m^{-2} d^{-1} after 600 days leaching time in pure water at 90 °C. This rate is about 5 times faster than the residual rates determined under the same conditions for inactive SON68 glass and a ^{239}Pu-doped glass with unrealistically low cumulative dose (see Section 4.3.3.3 and Fig. 4-7 for details). Based on these findings, it is concluded that the effect of cumulative α-dose on glass dissolution kinetics is significant and cannot be ignored, although it cannot be excluded that the rate measured for the ^{244}C-doped glass is still a transient and would decrease at longer corrosion times.

Prior to SGT-3, data on the influence of iron on glass corrosion were scarce and not conclusive. Meanwhile, a number of dedicated studies with sufficiently long leach times confirm that both metallic iron and iron oxides enhance glass dissolution persistently via removal of silica from solution, either through adsorption or precipitation of Fe-silicates (see Section 4.4.3). These processes lead to a dual penalizing effect: (i) a considerable increase in both short-term and residual glass dissolution rate; and (ii) a delay in the attainment of the residual rate regime. Both effects correlate with the amount and specific surface of accessible Fe/Fe-oxides and apparently overprint the effect of self-irradiation (cf. Fig. 4-5 and Fig. 4-6). Because of the large amounts of iron stored in the carbon steel canister foreseen in the Swiss HLW repository and given the small physical separation from the vitrified waste, this effect needs to be considered in the present update. On the contrary, since bentonite intrusion in the failed canister is unlikely, the similar penalizing effect of clay on glass dissolution needs not to be taken into account.

In SGT-2, reference glass corrosion rates of 2.0×10^{-4} and 1.5×10^{-3} g m^{-2} d^{-1} were recommended for French and U.K. vitrified waste, respectively (Bradbury et al. 2014, Tab. 8-2). These rates were selected based on the results of long-term leach experiments carried out with inactive simulants (SON68 and MW) only in initially pure water at 90 °C and did not account for the effects of alpha dose and Fe corrosion products (Curti 2003, Curti et al. 2006). Because the effect of Fe appears to "overprint" the effect self-irradiation, it was decided to use the best so far

available leach data obtained in the presence of Fe to define reference corrosion rate of the French glass for SGT-3. A rate of 1×10^{-3} g m^{-2} d^{-1} was selected based on the experiment GSM1 of Rébiscoul et al. (2015). This experiment was carried out at 50°C with COx water, using SON68 glass separated from the magnetite by a thin diffusion filter and a H_2/Ar atmosphere. It is judged to best represent the Swiss repository layout and conditions. The data indicate that a *residual rate* regime with a rate of 1×10^{-3} g m^{-2} d^{-1} was attained after about 100 days and maintained until the end of the experiment at about 1'200 days leaching time (Fig. 4-16b).

Data of similar quality and obtained under comparable experimental conditions unfortunately do not exist for the MW glass. Therefore, the reference corrosion rate for MW was not updated and the former SGT-2 value of 1.5×10^{-3} g m^{-2} d^{-1} was retained. The option to increase the MW rate proportionally to the ratio of rates determined for SGT-2 rates (i.e. by the factor $7.5 = 1.5 \times 10^{-3}$ g m^{-2} d^{-1}/ 2×10^{-4} g m^{-2} d^{-1}) was rejected because there is no basis to justify such extrapolation. There is indeed no experimental evidence that observed differences in residual rates obtained in experiments in pure water at 90 °C could be transferred to different experimental conditions (reduced temperature and presence of magnetite and clay).

In contrast, a differentiation between French and U.K. glass was maintained for the selection of pessimistic rates, since these are now based on *forward rates* calculated at repository-relevant temperatures. Forward rates demonstrably obey an Arrhenius type dependence (Section 4.3.2), making temperature extrapolations justified. Jollivet et al. (2012) determined for SON68 leached in COx clay water at the same temperature a *forward rate* 5.5 times higher (9.3×10^{-2} g m^{-2} d^{-1}, see Tab. 4-1). This value is adopted as pessimistic dissolution rate for SON68 in the Swiss safety case based on the similarities between COx water and bentonite pore water compositions and pH. The corresponding pessimistic rate for MW (1.7×10^{-1} g m^{-2} d^{-1}) was then derived with the help of the Arrhenius relation presented in Fig. 4-3, according to which the forward rate of MW glass in clay water should be 1.83 times higher than for SON68. This extrapolation can be justified by the fact that the experimentally determined slope of the Arrhenius plot (i.e. the temperature dependency of the forward rate) is the same for glass leached in distilled water and clay water (see Fig. 3 in Jollivet et al. 2012).

For the optimistic rates, the values selected in SGT-2, i.e. 2.0×10^{-5} g m^{-2} d^{-1} for SON68 and 1.5×10^{-4} g m^{-2} d^{-1} for MW, were retained. Although there is no direct experimental evidence for such low glass dissolution rates, a justification based on evidence from natural analogue can be provided. The rationale for this choice is that most of the glass dissolution will occur inside the fractured glass body, where the glass itself will presumably impose pH and environmental conditions of the glass dissolution process. In other words, the influence of the external environment will be negligible in the interior of the glass. This is shown by the differential corrosion in an ancient, fractured Roman glass body that remained buried during 1'800 years in seawater-saturated mud sediments (Verney-Carron et al. 2008). These authors (see Section 4.4.5) demonstrated that surface normalized glass dissolution rates were much lower in the internal parts of the fractured glass body compared to the periphery and determined very low corrosion rates ($< 10^{-6}$ g m^{-2} d^{-1}).

The recommended rates are summarized in Tab. 7-1. The main changes with respect to the selection for SGT-2 (Tab. 8-2 in Bradbury et al. 2014) are:

- an increase by a factor 5 for the SON68 *reference rate* and by 70% for the pessimistc rate of MW
- a slightly smaller pessimistic rate for SON68

All other rates listed in Tab. 7-1 remain equal to the SGT-2 values.

Tab. 7-1: Recommended glass dissolution rates in [g m^{-2} d^{-1}] for SGT-3 safety analysis calculations, compared to old values (SGT-2, in grey)

	Optimistic	**Reference**	**Pessimistic**	
SON68	2.0×10^{-5}	1.0×10^{-3}	9.3×10^{-2}	SGT-3
	2.0×10^{-5}	2.0×10^{-4}	1.0×10^{-1}	SGT-2
MW	1.5×10^{-4}	1.5×10^{-3}	1.7×10^{-1}	SGT-3
	1.5×10^{-4}	1.5×10^{-3}	2.0×10^{-1}	SGT-2

The reference rates are best estimates based on the geochemical conditions corresponding to Nagra's reference evolution scenario. Specifically, the selected reference rates are consistent with the high cumulative alpha doses and the large amounts of steel and Fe corrosion present after canister breaching. Higher rates arising from resumption phenomena due to pH increase (pH > 11) can be excluded due to the absence of cementitious materials in the proximity of the waste. Pessimistic rates are intentionally selected to be unrealistically high, however still possible for the specific glass, in order to allow calculating "worst case" scenarios in safety assessment calculations. Finally, the optimistic rates take into account evidence from archaeological analogues (buried Roman glass block, see Verney-Carron et al. 2008) that glass dissolution in the internal part of the fractured glass body will be slower, due to self-driven physical and chemical processes and because of the absence of penalizing materials (Fe, clay) in the direct vicinity. An overview of processes and mechanisms considered in the selection procedure of glass dissolution rates is given in Tab. 7-2, while Tab. 7-3 gives an account of the simplifying assumptions made in the Swiss safety assessment model concerning vitrified waste dissolution and radionuclide release.

Tab. 7-2: Processes and mechanisms considered in the selection procedure of glass dissolution rates for safety assessment calculations

Effect of process/mechanism	**Evidence**	**References**	**Evaluation of assumption**	**Applied to glass ...**	**Applied to rate ....**
Enhancement of glass dissolution due to Si sorption/precipitation on Fe and Fe corrosion products can occur	Persistent high corrosion rates observed in presence of magnetite after > 3 years	Rébiscoul et al. (2015)	Conservative, since rate could decrease at later times	SON68	Reference
Enhancement of glass dissolution due to Si sorption/precipitation on bentonite can be neglected	Large physical separation between glass and bentonite buffer should prevent interaction between the two materials	-	Realistic	all glasses	All rates
Enhancement of glass dissolution due to long-term self-irradiation (cumulative alpha dose) can occur	Recent data prove that high alpha dose leads to higher glass dissolution rates compared to annealed twin sample. Data for glass with realistic cumulative dose at canister failure time point to increased residual rate	Tribet et al. (2021) Mougnaud (2017)	Conservative, since rate could decrease at later times due to gel passivation	SON68	Reference
Radiolysis of groundwater does not affect vitrified waste dissolution in Swiss repository	Alpha radiolysis is weak at canister failure times	Bradbury et al. (2014)	Realistic	SON68MW	All rates
Temperature dependence of forward dissolution rate	Arrhenius behaviour repeatedly proved for many glasses	Pierce et al. (2008) Jollivet et al. (2012)	Realistic	All “Swiss” glasses	Pessimistic
Enhancement of forward rate in clay water	Forward rate of SON68 was shown to increase by a factor of 5 at all temperatures between 30 and 90 °C when pure water replaced by Callovo-Oxfordian clay water	Jollivet et al. (2012)	Realistic	SON68	Pessimistic

Tab. 7-2: Cont.

Effect of process/mechanism	Evidence	References	Evaluation of assumption	Applied to glass ...	Applied to rate ....
Reduction of rate due to internal transport resistance within the vitrified waste	Clogging of fractures and slow diffusion was shown to reduce internal dissolution of archaeological glass	Verney-Carron et al. (2008)	Realistic, since pH 11 threshold will not be exceeded due to absence of cementitious materials	All "Swiss" glasses	Optimistic
Resumption of glass corrosion rates can be excluded	Sudden increase in glass corrosion rate is frequently observed at pH >11 or with Al-rich glasses favouring zeolite formation	Gin et al. (2015) Fournier et al. (2014)	Realistic, as all "Swiss" glasses have low Al_2O_3 contents and pH > 11 can be excluded	All "Swiss" glasses	Reference, optimistic

* No data on compositional variations available for ORANO glasses

Tab. 7-3: Simplifying model assumptions related to glass dissolution considered in the safety assessment code STRENG

Grindrod et al. (1990)

Process assumption	References	Explanations
Glass corrosion rate assumed to remain constant during all the waste dissolution process	Grindrod et al. (1990)	The lack of coupling with chemically or physically decrease or resumption of the glass dissolution rate is compensated through parameter variations in sensitivity analyses
RN are supposed to be released from the glass at the same rate as mobile glass tracers (congruent release)	Grindrod et al. (1990)	This is a conservative assumption, as available data indicate high retention factors for all nuclides in glass alteration layer (Curti et al. 2006)
Precipitation of radionuclides in the water filled canister/waste interface volume	Grindrod et al. (1990)	This “compensates” the previous conservative assumption. Radionuclides dissolved congruently may rapidly reach element-specific solubility limits and thus reduce their mobility
Exposed glass surface area of increased by a factor of 15 to simulate thermally induced cracking of the glass monolith	Nagra (2014c)	Realistic assumption based on confidential data from reprocessing plants

8 References

Aagard, P. & Helgeson, H.C. (1982): Thermodynamic and kinetic constraints on reaction rates among minerals and aqueous solutions. I. Theoretical considerations. Am. J. Sci. 282, 237-285

Abraitis, P.K., Livens, F.R., Monteith, J.E., Small, J.S., Trivedi, D.P., Vaughan, D.J. & Wogelius R.A. (2000): The kinetics and mechanisms of simulated British Magnox waste glass dissolution as a function of pH, silicic acid activity, and time in low temperature aqueous systems. Appl. Geochem. 15, 1399-1416

Advocat Th., Crovisier J.L., Vernaz E., Ehret G. & Charpentier H. (1991): Hydrolysis of R7T7 nuclear waste glass in dilute media: mechanisms and rate as a function of pH. In: Scientific Basis for Nuclear Waste Management XIV, T.A. Abrajano Jr. and L.H. Johnson, eds., Mat. Res. Soc. Symp. Proc. Vol. 212, 57-64

Advocat, Th. (1991): Les mécanismes de corrosion en phase aqueuse du verre nucléaire R7T7. Approche expérimentale, Essai de modélisation thermodynamique et cinétique. Ph.D. thesis, Univ. Louis Pasteur, Strasbourg

Advocat, Th., Jollivet, P., Crovisier, J.L. & del Nero, M. (2001): Long-term alteration mechanisms in water for SON68 radioactive borosilicate glass. J. Nucl. Mat. 298, 55-62

Alexander, G.B., Heston, W.M. & Iler, R.K. (1954): The solubility of amorphous silica in water. Phys. Chem. 58, 453-455

Anderson, G.M. (2005): Thermodynamics of Natural Systems, 2nd edition, Cambridge University Press, New York, 648 p.

Andriambololona, Z., Godon, N. & Vernaz, E. (1992): R7T7 Glass alteration in the presence of mortar: effect of the cement grade. Mat. Res. Soc. Symp. Proc. Vol. 257, 151-158

Aréna, H., Godon, N., Rébiscoul, D., Frugier, R., Podor, R., Garcès, E., Cabie, M. & Mestre, J.P. (2017): Impact of iron and magnesium on glass alteration: characterization of the secondary phases and determination of their solubility constants. Appl. Geochem. 82, 119-133

Aréna, H., Rébiscoul, D., Podor, R., Garcès, E., Cabie, M., Mestre, J.P. & Godon, N. (2018): Impact of Fe, Mg and Ca elements on glass alteration: Interconnected processes. Geochim. Cosmochim. Acta 239, 420-445

Aschwanden, L., Camesi, L., Gaucher, E., Gimmi, T., Jenni, A., Kiczka, M, Mäder, U., Mazurek, M., Rufer, D., Waber, H.N., Wersin, P., Zwahlen, C. & Traber, D. (2022): TBO Stadel-3-1: Data Report, Dossier VIII: Rock properties, porewater characterisation and natural Tracer Profiles. Nagra Arbeitsbericht NAB 22-01

Backhouse, D.J., Fisher, A.J., Neeway, J.J., Corkhill, C.L., Hyatt, N.C.& Hand, R.J. (2018): Corrosion of the International Simple Glass under acidic to hyperalkaline conditions. Materials Degradation 2:29

Berner, U.R. (1992): Evolution of pore water chemistry during degradation of cement in a radioactive waste repository environment. Proc. Waste Manag. 12, 201-219

Boizot, B., Petite, G., Ghaleb, D., Pellerin, N., Fayon, F., Reynard, B. & Calas, G. (2000): Migration and segregation of sodium under β-irradiation in nuclear glasses. Nuclear Instruments and Methods in Physics Research B 166-167, 500-504

Bradbury, M., Berner, U., Curti, E., Hummel, W., Kosakowski, G. & Thoenen, T. (2014): The Long Term Geochemical Evolution of the Nearfield of the HLW Repository. Nagra Technical Report NTB 12-01

Bunker, B.C. (1994): Molecular mechanisms for corrosion of silica and silicate glasses. J. Non-Cryst. Solids 179, 300-308

Bunker, B.C., Tallant, D.R., Headley, T.J., Turner, G.L. & Kirkpatrick, R.J. (1987): The structure of leached sodium borosilicate glass. Phys. Chem. Glasses 29(3), 106-120

Cailleteau, C., Angeli, F., Devreux, F., Gin, S., Jestin, J., Jollivet, P. & Spalla O. (2008): Insight into silicate-glass corrosion mechanisms. Nature Materials 7, 978-983

Cloet, V., Lothenbach, B., Lurà, P., Kosakowski, G., Curti, E., Wieland, E., Lanyon, G.W., Diomidis, N. & Leupin, O. (2019): Cementitious backfill for a highlevel waste repository: impact of repository-induced effects. Nagra Arbeitsbericht NAB 18-41

Corkhill, C., Cassingham, N.J., Heath, P.G. & Hyatt, N.C. (2013): Dissolution of UK High-Level Waste Glass Under Simulated Hyperalkaline Conditions of a Colocated Geological Disposal Facility. International Journal of Applied Glass Science, 4 (4), 341-356

Crovisier, J.-L., Advocat, T. & Dussossoy, J.-L. (2003): Nature and role of natural alteration gels formed on the surface of ancient volcanic glasses (Natural analogs of waste containment glasses) J. Nucl. Mat. 321, 91-109

Curti, E. & Smith, P.A. (1991): Enhancement of borosilicate glass dissolution by silica sorption and diffusion in compacted bentonite: a model study. In: Scientific Basis for Nuclear Waste Management XIV, Mat. Res. Soc. Proc. 212, 31–39, Materials Research Society

Curti, E. (2003): Glass dissolution parameters: update for "Entsorgungsnachweis". Nagra Technical Report NTB 02-21

Curti, E. (2018): The JSS database on glass corrosion kinetics. Technical Note TM-44-18-04, Paul Scherrer Institut, Villigen, Switzerland

Curti, E. (2022): Bentonite Pore Waters (BPW) for the Sectoral Plan, phase SGT-3: model development, testing and final calculations. Nagra Work Report NAB 22-43. Nagra, Wettingen, Switzerland

Curti, E., Aimoz, L. & Kitamura, A. (2013): Selenium uptake onto natural pyrite. J. Radioanal. Nucl. Chem. 295, 1655-1665

Curti, E., Crovisier, J.L., Karpoff, A.M. & Morvan, G. (2006): Long-term corrosion of two nuclear waste reference glasses (MW and SON68): a kinetic and mineral alteration study. Appl. Geochem. 21, 1152-1168

Curti, E., Dähn, R., Farges, F. & Vespa, M. (2009): Na, Mg, Ni and Cs distribution and speciation after long-term alteration of a simulated nuclear waste glass: a micro-XAS/XRF/XRD and wet chemical study. Geochim. Cosmochim. Acta 73, 2283-2298

Curti, E., Godon, N. & Vernaz, E.Y. (1993): Enhancement of the glass corrosion in the presence of clay minerals: testing experimental results with an integrated glass dissolution model. In: Scientific Basis for Nuclear Waste Management XVI, Mat. Res. Soc. Proc. 294, 163-170, Materials Research Society

Curti, E., Grolimund, D. & Borca, C.N. (2012): A micro-XAS/XRF and thermodynamic study of $Ce^{III/IV}$ speciation after long-term aqueous alteration of simulated nuclear waste glass: Relevance for predicting Pu behavior? Appl. Geochem. 27, 56-63

De Cannière, P., Moors, H., Dierckx, A., Gasiaux, F., Aertsen, M., Put M. & Van Iseghem, P. (1998): Diffusion and Sorption of ^{32}Si-labelled Silica in the Boom Clay. Radiochim. Acta 82, 191-196

De Echave, T. (2018): Étude des mécanismes d'altération des verres nucléaires sous radiolyse alpha et en conditions environnementales, Ph.D. thesis, École doctorale I2S, Université de Montpellier (France)

De Echave, T., Tribet, M., Gin, S. & Jégou, C. (2019): Influence of iron on the alteration of the SON68 nuclear glass in the Callovo-Oxfordian groundwater. Appl. Geochem. 100, 268-278

Dietzel, A. (1942): Die Kationenfeldstärken und ihre Beziehungen zu Entglasungsvorgängen, zur Verbindungsbildung und zu den Schmelzpunkten von Silicaten, Z. Elektrochem. 48, 9-23

Eikenberg, J. (1990): On the problem of silica solubility at high pH. Nagra Technical Report NTB 90-36

Feng, X., Bates, J.K., Buck, E.R., Bradley, C.R & Gong, M. (1993): Long-term comparison of dissolution behavior between fully radioactive and simulated nuclear waste glasses. Nuclear Technol. 104, 193-206

Ferrand, K., Klinkenberg, M., Caes, S., Poonoosamy, J., Van Renterghem, W., Barthel, J., Lemmens, K., Bosbach, D. & Brandt, F. (2021): Dissolution Kinetics of International Simple Glass and Formation of Secondary Phases at very High Surface Area to Solution Ratio in Young Cement Water. Materials 2021, 14, 1254

Ferrand, K., Liu, S. & Lemmens, K. (2014): The effect of Ordinary Portland Cement on nuclear waste glass dissolution. Procedia Materials Science 7, 223-229

Ferrand, K., Liu, S. & Lemmens, K. (2018) Integrated leach tests with simulated HLW glass in contact with ordinary Portland cement paste. Topical Report SCK•CEN/30198860, SCK-CEN, Mol, Belgium

Ferrand, K., Sanheng, L. & Lemmens, K. (2013): The interaction between nuclear waste glass and ordinary Portland cement. Int. J. Appl. Glass Sci. 4(4), 328-340

Fournier, M., Frugier, P. and Gin, S. (2014): Resumption of alteration at high temperature and pH: rates measurements and comparison with initial rates. Procedia Mat. Sci. 7, 202-208

Frugier, P., Gin, S., Minet, Y., Chave, T., Bonin, B., Godon, N., Lartigue, J.-E., Jollivet, P., Ayral, A., De Windt, L. & Santarini, G. (2008): SON68 nuclear glass dissolution kinetics: Current state of knowledge and basis of the new GRAAL model. J. Nucl. Mat. 380, 8-21

Frugier, P., Martin, C., Ribet, I., Advocat, T. & Gin, S. (2005): The Effect of Composition on the Leaching of three Nuclear Waste Glasses: R7T7, AVM and VRZ. J. Nucl. Mater. 346, 194-207

Geisler, Th., Janssen, A., Scheiter, D., Stephan, Th., Berndt, J. & Putnis, A. (2010): Aqueous corrosion of borosilicate glass under acidic conditions: a new corrosion mechanism. J. Non-Cryst. Solids 356 (28-30), 1458-1465

Geisler, Th., Nagel, Th., Kilburn, M.R., Janssen, A., Icenhower, J.P., Fonseca, R.O.C., Grange, M. & Nemchin, A.A. (2015): The mechanism of borosilicate glass corrosion revisited. Geochim. Cosmochim. Acta 158, 112-129

Gin, S., Abdelouas, A., Criscenti, L.J., Ebert, W.L., Ferrand, K., Geisler, Th., Harrison, M.T., Inagaki, Y., Mitsui, S., Mueller, K.T., Marra, J.C., Pantano, C.G., Pierce, E.M., Ryan, J.V., Schofield, J.M., Steefel, C.I. & Vienna, J.D. (2013b) An international initiative on long-term behavior of high-level nuclear waste glass. Materials Today 16(6), 243-248

Gin, S., Beaufort, D., Godon, N., Vernaz, E. & Thomassin, J.H. (1992): Experimental alteration of R7T7 glass in salt brines at 90 °C and 150 °C. Appl. Clay Sci. 7, 87-96

Gin, S., Collin, M., Jollivet, P., Fournier, M., Minet, Y., Dupuy, L., Mahadevan, T., Kerisit, S. & Du, J. (2018) Dynamics of self-reorganization explains passivation of silicate glasses. Nat. Commun. 9, 2169

Gin, S., Delaye, J.-M., Angeli, F. & Schuller, S. (2021): Aqueous alteration of silicate glass: state of knowledge and perspectives. npj Materials Degradation 5:42

Gin, S., Frugier, P., Jollivet, P., Bruguier, F. & Curti, E. (2013a): New Insight into the Residual Rate of Borosilicate Glasses: Effect of S/V and Glass Composition. International Journal of Applied Glass Science 4(4), 371-382

Gin, S., Guo, X., Delaye, J.-M., Angeli, F., Damodaran, K., Testud,V., Du, J., Kerisit, S. & Kim, S.H. (2020a): Insights into the mechanisms controlling the residual corrosion rate of borosilicate glasses. npj Materials Degradation 4:41

Gin, S., Jollivet, P., Fournier, M., Berthon, C., Zhaoying, W., Mitroshkov, A., Zhu, Z. & Ryan, J.V. (2015): The fate of silicon during glass corrosion under alkaline conditions: A mechanistic and kinetic study with the International Simple Glass, Geochim. Cosmochim. Acta 151, 68-85

Gin, S., Jollivet, P., Mestre, J.P., Jullien, M. & Pozo, C. (2001b): French SON 68 nuclear glass alteration mechanisms on contact with clay media. Appl. Geochem. 16, 861-881

Gin, S., Jollivet, P., Tribet, M., Peuget, S. & Schuller, S. (2017): Radionuclides containment in nuclear glasses: an overview. Radiochim. Acta 105(11), 927-959

Gin, S., Mir, A.H., Jan, A., Delaye, J.M., Chauvet, E., De Puydt, Y., Gourgiotis, A. & Kerisit, S. (2020b): A General Mechanism for Gel Layer Formation on Borosilicate Glass under Aqueous Corrosion. Journal of Physical Chemistry C 124, 5132-5144

Gin, S., Neill, L., Fournier, M., Frugier, P., Ducasse, T., Tribet, M., Abdelouas, A., Parruzot, B., Neeway, J. & Wall, N. (2016): The controversial role of inter-diffusion in glass alteration, Chemical Geology 440, 115-123

Gin, S., Ribet, I. & Couillard, M. (2001a): Role and properties of the gel formed during nuclear glass alteration: importance of gel formation conditions. J. Nucl. Mat. 298, 1-10

Godon, N. (1988): Effet des matériaux d'environnement sur l'altération du verre nucléaire R7T7 – influence des argiles, Ph. D. thesis, Univ. Orléans, France

Godon, N. (2004): Dossier de référence sur le comportement à long terme des verres nucléaires. Rapport Technique DTCD/2004/06, Direction de l'énergie nucléaire, Commissariat à l'énergie atomique (CEA), Bagnols-sur-Cèze (France)

Godon, N., Gin, S., Rébiscoul, D. & Frugier, P. (2013): SON68 glass alteration enhanced by magnetite. Procedia Earth and Planetary Science 7, 300-303

Godon, N. & Vernaz, E. (1989): R7T7 Nuclear Waste Glass Behavior in Moist Clay: Role of the Clay Mass/Glass Surface Area Ratio. In: Scientific Basis for Nuclear Waste Management XIII, Mater. Res. Soc. Symp. Proc. 176, 319-325

Goldschmidt, V.M. (1926): Geochemische Verteilungsgesetze der Eleente, Skrifter Norske Videnskaps Akad. (Oslo), I. Math. Naturwiss. K1(8), 7-156

Grambow, B. (1985): A general rate equation for nuclear waste glass corrosion. In: Scientific Basis for Nuclear Waste Management VIII, Mat. Res. Soc. Proc. 44, pp.15–27, Boston: Materials Research Society

Greenberg, S. A. & Sinclair, D. (1955): The polymerisation of silicic acid. J. Am. Chem. Soc. 59, 435-440

Grindrod, P., Williams, M., Grogan, H. & Impey, M. (1990): STRENG, A source term model for vitrified high level waste. Nagra Technical Report NTB 90-48

Gutzow, I.S. & Schmelzer, J.W.P. (2013): The Vitreous State - Thermodynamics, Structure, Rheology, and Crystallization, 2nd Edition, Springer, Heidelberg, p. 553

Hanson, B.D. & Stout, R.B. (2004): Re-examining the Dissolution of Spent Fuel: A Comparison of Different Methods for Calculating Rates. Proc. of Spring Material Research Society Meeting San Francisco, April 12-16, 2004, UCRL-PROC-205539, Lawrence Livermore National Laboratory (LLNL), Livermore, CA 94550, United States

Hellmann, R., Cotte, S., Cadel, E., Malladi, S., Karlsson, L.S., Lozano-Perez, S., Cabié, M. & Seyeux, A. (2015): Nanometre-scale evidence for interfacial dissolution–reprecipitation control of silicate glass corrosion. Nature Materials 14, 307-311

Hopf, J., Eskelsen, J.R., Chiu, M., Ievlev, A.V., Ovchinnikova, O.S., Leonard, D. & Pierce, E.M. (2018): Toward an understanding of surface layer formation, growth, and transformation at the glass-fluid interface. Geochim et Cosmochim. Acta 229, 65-84

Inagaki, Y., Shinkai, A., Idemistu, K., Arima, T., Yoshikawa, H. & Yui, M. (2006): Aqueous alteration of Japanese simulated waste glass P0798: effects of alteration-phase formation on alteration rate and cesium retention. J. Nucl. Mater. 354, 171-184

IRSN (2014): Projet de stockage Cigéo. Ouvrages de fermeture. Rapport IRN N°2014-00006. Institut de Radioprotection et de Sûreté Nucléaire (IRSN), Fontenay-aux-Roses, France

Jacques, D. & Mallants, D. (2011): Evolution of concrete pore water and solid phase composition during leaching with different types of water. Report NIROND-TR 2008-24 E, NIROND-TR report 2008–24 E Version 2. ONDRAF/NIRAS. Avenue des Arts 14, BE-1210 Brussels

Jantzen, C.M. & Plodinec, M.J. (1984): Thermodynamic model of natural, medieval and nuclear waste glass durability. J. Non-Cryst. Solids 67, 207-233

Jollivet, P., Gin, S. & Schumacher, S. (2012): Forward dissolution rate of silicate glasses of nuclear interest in, clay-equilibrated groundwater, Chemical Geology 330-331, 207-217

JSS (1984a): JSS-Project Phase I: Static leaching in distilled water, silicate water and simulated groundwater at 90 °C with and without granite. Studsviks Final Report. JSS Report 84-01, SKB, Stockholm, Sweden

JSS (1984b): JSS-Project Phase I, EIR Final Report of JSS glass corrosion programme Phase I. JSS Report 84-02, SKB, Stockholm, Sweden

JSS (1984c): JSS-Project Phase I, JSS Report 84-03, SKB, Stockholm, Sweden

JSS (1985): JSS-Project Phase II, Final report of work performed at Studsvik Energiteknik AB and at Swiss Federal Institute for Reactor Research. JSS Report 85-01, SKB, Stockholm, Sweden

JSS (1986): JSS-Project Phase III, Final report JSS project phase III: Static corrosion of radioactive glass at 40 °C and corrosion of radioactive glass under dynamic conditions. JSS Report 86-01, SKB, Stockholm, Sweden

JSS (1987a): JSS-Project Phase IV, Final Report: Experimental and modelling studies of HLW glass dissolution in repository environments. JSS Report 87-01, SKB, Stockholm, Sweden

JSS (1987b): JSS-Project Phase IV, Grambow B. : Nuclear Waste Glass Dissolution: JSS Report 87-02, SKB, Stockholm, Sweden

JSS (1988a): JSS-Project Phase V, Jercinovic M.J: and Ewing R.C.: Basaltic glasses from Iceland and the deep sea: Natural analogues to borosilicate waste-form glass. JSS Report 88-01, SKB, Stockholm, Sweden

JSS (1988b): JSS-Project Phase V, Testing and modelling of the corrosion of simulated nuclear waste glass powders in a waste package environment. JSS Report 88-02, SKB, Stockholm, Sweden

Khodokovskiy, I.L. & Mishin, I.V. (1971): Solubility products of calcium molybdateand calcium tungstate; ratio of powellite to scheelite mineralization under hydrothermal conditions, International Geology Review, 13:5, 760-768

King, F. (2008): Corrosion of carbon steel under anaerobic conditions in a repository for SF and HLW in Opalinus Clay. Nagra Technical Report NTB 08-12

Kursten, B., Cornelis, B., Labat, S. & Van Iseghem, P. (1997): Completion of the corrosion programme in Boom Clay – in situ experiments. European Atomic Energy Community's shared cost programme (1990-94) on 'Management and storage of radioactive waste' Task 3, EUR 17105 EN, European Commission

Lemmens, K. (2001): The effect of clay on the dissolution of nuclear waste glass. J. Nucl. Mat. 298 (1-2), 11-18

Lemmens, K., Cachoir, Ch., Valcke, E., Ferrand, K., Aertsen, M. & Mennecart, Th., (2007): The strategy of the Belgian nuclear research centre in the area of high-level waste form compatibility research. Proc. 11th Int. Conference on Environmental Remediation and Radioactive Waste Management (ICEM 2007), September 2-6 2007, Bruges, Belgium

Liu, S., Ferrand, K. & Lemmens, K. (2015): Transport- and surface reaction-controlled SON68 glass dissolution at 30 °C and 70 °C and pH 13.7. Appl. Geochem. 61, 302311

Lu, X., Reiser, J.T., Parruzot, B., Deng, L., Gussev, I.M., Neuefeind, J.C., Graham, T.R., Liu, H., Ryan, J.V., Kim, S.H., Washton, N., Lang, M., Du, J. & Vienna, J.D. (2021) Effects of Al:Si and (Al + Na):Si ratios on the properties of the international simple glass, part II: Structure. J. Am. Ceram. Soc. 104, 183-207

Lukscheiter, B. & Nesovic, M. (1996): Development of glasses for the vitrification of high level liquid waste (HLLW) in a Joule heated ceramic melter) Waste Management 16(7), 571-578

Lutze, W., Müller, R. & Montserrat, W. (1988): Chemical Corrosion of Cogema Glass R7T7 in High Saline Brines - Part II. Scientific Basis for Nuclear Waste Management XII, R.C. Ewing & W. Lutze, eds., MRS Proceedings Vol.127: 81, 575-584

Mäder, U. (2009): Reference pore water for the Opalinus Clay and «Brown Dogger» for the provisional safety-analysis in the framework of the sectoral plan – interim results (SGT-ZE). Nagra Arbeitsbericht NAB 09-14

Mann, C., Ferrand, K., Liu, S., Eskelsen, J.R., Pierce, E., Lemmens, K. & Corkhill, C. (2019): Influence of young cement water on the corrosion of the International Simple Glass. NPJ Mater. Degrad. 2019 (5), 1-9

Matzke, H.J. (1988): Radiation damage effects in nuclear materials. Nuclear Instruments and Methods in Physics Research B32, 455-470.

Matzke, H.J. & Vernaz, E. (1993): Thermal and physicochemical properties important for the long term behavior of nuclear waste glasses. Journal of Nuclear Materials 201, 295-309

Mazurek, M., Aschwanden, L., Camesi, L., Gimmi, T., Jenni, A., Kiczka, M, Mäder, U., Rufer, D., Waber, H.N., Wanner, P, Wersin, P. & Traber, D. (2021): TBO Bülach-1-1: Data Report, Dossier VIII: Rock Properties, Porewater Characterisation and Natural Tracer Profiles. Nagra Arbeitsbericht NAB 20-08

McGrail, B.P., Ebert, W.L., Bakel, A.J. & Peeler, D. K. (1997): Measurement of kinetic rate law parameters on a Na-Ca-Al borosilicate glass for low-activity waste. J. Nucl. Mater. 249, 175-189

McVay, G.L. & Pederson, L.R. (1981): Effect of gamma radiation on glass leaching. J. Am. Ceram. Soc. 64(3), 154-158

Mendel, J.E. (1986): The Fixation of High-Level Wastes in Glasses. Phil. Trans. R. Soc. Lond. A 319, 49-62

Mendoza, C., Peuget, S., Charpentier, T., Moskura, M., Caraballa, R., Bouty, O., Mir, A.H., Monnet, I., Grygiel, C. & Jégou, C. (2014): Oxide glass structure evolution under swift heavy ion irradiation. Nucl. Instrum. Methods Phys. Res. Sect. B: Beam Interact. Mater. At. 325, 54-65

Mercado-Depierre, S., Angeli F., Frizon, F. & Gin, S. (2013): Antagonist effects of calcium on borosilicate glass alteration. J. Nucl. Mat. 441, 402-410

Michelin, A., Burger, E., Rébiscoul, D., Neff, D., Bruguier, F., Drouet, E., Dillmann, P. & Gin, S. (2013): Silicate glass alteration enhanced by iron: origin and long-term implications, Environ. Sci. Technol. 47, 750-756

Michelin, A., Leroy, E., Neff, D., Dynes, J.J., Dillmann, P. & Gin, S. (2015): Archeological slag from Glinet: An example of silicate glass altered in an anoxic iron-rich environment. Chemical Geology 413, 28-43

Minet, Y., Bonin, B., Gin, S. & Frugier, P. (2010): Analytic implementation of the GRAAL model: Application to a R7T7-type glass package in a geological disposal environment. J. Nucl. Mat. 404, 178-20

Mougnaud, S. (2017): Effets de l'irradiation sur l'évolution de la pellicule d'altération formée lors de la lixiviation des verres borosilicatés nucléaires. Ph.D. thesis, Université Paris-Saclay, HAL Id: tel-01510825, https://tel.archives-ouvertes.fr/tel-01510825

Mougnaud, S., Tribet, M., Renault, J.P., Gin, S., Peuget, S., Podor, R. & Jégou, C. (2018): Heavy ion radiation ageing impact on long-term glass alteration behavior. J. Nucl. Mater. 510, 168-177

Mougnaud, S., Tribet, M., Renault, J.P., Jollivet, P., Panczer, G., Charpentier, T. & Jégou, C. (2016): Effect of low dose electron beam irradiation on the alteration layer formed during nuclear glass leaching: J. Nucl. Mater. 482 53-62

Muller, I.S., McKeown, D.A. & Pegg, I.L. (2014): Structural Behavior of Tc and I ions in Nuclear Waste Glass. Procedia Materials Science 7, 53-59

Nagra (2014a): Modellhaftes Inventar für radioaktive Materialien MIRAM 14. Nagra Technischer Bericht NTB 14-04 (Hauptbericht)

Nagra (2014b): Modellhaftes Inventar für radioaktive Materialien MIRAM 14. Nagra Technischer Bericht NTB 14-04 (Beilage 1, Abfallsortenreports)

Nagra (2014c): Provisional Safety Analyses for SGT Stage 2 - Models, Codes and General Modelling Approach. Nagra Technical Report NTB 14-09

Nagra (2014d): Charakteristische Dosisintervalle und Unterlagen zur Bewertung der Barrierensysteme. Nagra Technischer Bericht NTB 14-03

Nagra (2016): ENSI-Nachforderung zum Indikator «Tiefenlage im Hinblick auf bautechnische Machbarkeit» in SGT Etappe 2. Prüfung der Lager- und Barrierenkonzepte. Nagra Arbeitsbericht NAB 16-42

Nagra (2022a): Entsorgungsprogramm 2021 der Entsorgungspflichtigen. Nagra Technischer Bericht NTB 21-01

Nagra (2023): Modellhaftes Inventar für radioaktive Materialien MIRAM RBG. Nagra Technischer Bericht NTB 22-05 (Hauptbericht)

Nagra (in prep): Safety assessment methodology. Nagra Technical Report NTB 24-19

NEA (2010): National Programmes in Chemical Partitioning - A Status Report, Nuclear Energy Agency (NEA), Organisation for Economic Co-operation and Development (OECD), NEA report No. 5425, ISBN 978-92-64-99096-8.

Neeway, J.J., Abdelouas, A., Ribet, S., El Mendili, Y., Schumacher, S. & Grambow, B. (2015): Effect of Callovo-Oxfordian clay rock on the dissolution rate of the SON68 simulated nuclear waste glass. J. Nucl. Mat. 459, 291-300

Ojovan, M.I., Lee, W.E. & Kalmykov, S.N. (2019): An Introduction to Nuclear Waste Immobilisation, Chapter 19 (Immobilisation of Radioactive Wastes in Glass), third edition, Elsevier

Parruzot, B., Jollivet, P., Rébiscoul, D. & Gin, S. (2015): Long-term alteration of basaltic glass: Mechanisms and rates. Geochim. Cosmochim. Acta 154, 28-48

Paul, A. (1977): Chemical durability of glasses; a thermodynamic approach. J. Mater. Sci. 12, 2246-2268

Perea, D.E., Schreiber, D.K., Ryan, J.V., Wirth, M.G., Deng, L., Lu, X., Du, J. & Vienna, J.D. (2020): Tomographic mapping of the nanoscale water-filled pore structure in corroded borosilicate glass. npj Materials Degradation 4:8

Peuget, S., Delaye, J.M. & Jégou, C. (2014): Specific outcomes of the research on the radiation stability of the French nuclear glass towards alpha decay accumulation. J. Nucl. Mat. 444, 76-91

Peuget, S., Tribet, M., Mougnaud, S., Miro, S. & Jégou, C. (2018): Radiation effects in ISG glass: from structural changes to long term aqueous behavior. npj Mater. Degrad. 2018, 2, 23

Pierce, E.M., Rodriguez, E.A., Calligan, L.J., Shaw, W.J. & McGrail, B.P. (2008): An experimental study of the dissolution rates of simulated aluminoborosilicate waste glasses as a function of pH and temperature under dilute conditions. Appl. Geochem. 23, 2559-2573

Pirlet, V. (2001): Overview of actinides (Np, Pu, Am) and Tc release from waste glasses: influence of solution composition. J. Nucl. Mat. 298, 47-94

Plodinec, M.J. (2000): Borosilicate glasses for nuclear waste immobilisation, Glass Tech. 41(6), 186-192

Putnis, A. & Putnis, Ch.V. (2007): The mechanism of reequilibration of solids in the presence of a fluid phase. J. Solid State Chem. 180, 1783-1786

Rébiscoul, D., Tormos, V., Godon, N., Mestre, J.-P., Cabie, M., Amiard, G., Foy E., Frugier, P. & Gin, S. (2015): Reactive transport processes occurring during nuclear glass alteration in presence of magnetite. Applied Geochemistry 58, 26-37

Reiser J.T., Lu X., Parruzot, B., Liu, H., Subramani, T., Kaya H., Kissinger, R.M., Crum, J.V., Ryan, J.V., Navrotsky, A., Kim, S.H. & Vienna, J.D. (2021): Effects of Al:Si and (Al + Na): Si ratios on the properties of the international simple glass, part I: Physical properties. J. Am. Ceram. Soc. 104,167-182

Ribet, S. & Gin, S. (2004): Role of neoformed phases on the mechanisms controlling the resumption of SON68 glass alteration in alkaline media. J. Nucl. Mat. 324, 152-164

Riley, B.J., Schweiger, M.J., Kim, D.-S., Lukens Jr., W.W, Williams, B.D., Iovin, C., Rodriguez, C.P., Overman, N.R., Bowden, M.E., Dixon, D.R., Crum, J.V., McCloy, J.S. & Kruger, A.A. (2014): Iodine solubility in a low-activity waste borosilicate glass at 1000 °C, J. Nucl. Mat. 452, 178-188

Robinson (2022): STMAN 5: User guide and theoretical backbround for version 5.10. Nagra Arbeitsbericht NAB 22-10

Rolland, S., Wiss, T., Janssen, A., Blondel, A. & Toulhoat, P. (2013): ^{99}Tc- and ^{239}Pu-Doped Glass Leaching Experiments: Residual Alteration Rate and Radionuclide Behavior. Int. J. Applied Glass Sci. (4)4, 296-306

Rosenflanz, A., Frey, M., Endres, B., Anderson, T., Richards, E. & Schardt, C. (2004): Bulk glasses and ultrahard nanoceramics based on alumina and rare-earth oxides. Nature, 430(7001):761-764

Ryan, J.V. & Freedman, V.L.(2016): A Strategy for Maintenance of the Long-Term Performance Assessment of Immobilized Low-Activity Waste Glass. Report RPT-IGTP-001, Rev.1 and PNNL-23503, Rev 1, United States Department of Energy (DOE), Oak Ridge, TN 37831-0062, U.S.A.

Spitsyn, V.I. & Savich, I.A. (1952): Solubility of calcium molybdate, Zhur. Obshch. Khirmi (U.S.S.R.) 22(8), 1323

Strachan, D.M., Turcotte, R.P. & Barnes, B.O. (1982): MCC-1: A Standard Leach Test for Nuclear Waste Forms, Nuclear Technology, 56:2, 306-312

Strachan, D.M. (2017): Glass dissolution as a function of pH and its implications for understanding mechanisms and future experiments. Geochimica et Cosmochimica Acta 219, 111v123

Strachan, D.M., Pederson, L.R. & Lokken, R.O. (1985): Results from the long-term interaction and modelling of SRL-131 glass with aqueous solutions. Report PNL-5654, Pacific Northwest Laboratory, Battelle, U.S

Techer, I., Advocat, T., Lancelot, J. & Liotard, J. M. (2000): Basaltic glass: alteration mechanisms and analogy with nuclear waste glasses. J. Nucl. Mat. 282, 40-46

Techer, I., Lancelot, J., Clauer, N., Liotard, J. M. & Advocat, T. (2001): Alteration of a basaltic glass in an argillaceous medium: the Salagou dike of the Lodève Permian Basin (France).Analogy with an underground nuclear waste repository. Geochim. Cosmochim. Acta 65, 1071-1086

Thien, B.M.J., Godon, N., Ballestero, A., Gin, S. & Ayral, A. (2012): The dual effect of Mg on the long-term alteration rate of AVM nuclear waste glasses. J. Nucl. Mat. 427, 297-310

Thien, B.M.J., Godon, N., Hubert, F., Angéli, F., Gin, S. & Ayral, A. (2010): Structural identification of a trioctahedral smectite formed by the aqueous alteration of a nuclear glass. Applied Clay Science 49, 135-141

Tribet, M., Marques, C., Mougnaud, S., Broudic, V., Jégou, Ch. & Peuget, S. (2021) Alpha dose rate and decay dose impacts on the long-term alteration of HLW nuclear glasses, npj Materials Degradation 5:36

Tribet, M., Mir, A.H., Gillet, C., Jégou, C., Mougnaud, S., Hinks, A., Donnelly, S.E. & Peuget, S. (2020): New Insights about the Importance of the Alteration Layer/Glass Interface. J. Phys. Chem. C, 124, 10032-10044

Utton, C.A., Hand, R.J., Hyatt, N.C., Swanton, S.W. & Williams, S.J. (2013): Formation of alteration products during dissolution of vitrified ILW an a high-pH calcium-rich solution. J. Nucl. Mat. 442, 33-45

Utton, C.A., Swanton, S.W., Schofield, J., Hand, R.J., Clacher, A. & Hyatt, N.C. (2012): Chemical durability of vitrified wasteforms: effects of pH and solution composition. Mineralogical Magazine, Vol. 76(8), 2919-2930

Valcke, E. (2007): Integrated in situ corrosion test on α-active high-level waste (SF/HLW) glass – Phase 2 (CORALUS-2). European Commission, Contract No FIKW-CT-2000-0001. Final Report.Vernaz, E.Y. & Dussossoy, J.L. (1992): Current state of knowledge of nuclear waste glass corrosion mechanisms: the case of R7T7 glass, Appl. Geochem., Suppl. Issue No. 1, 13-22

Vernaz, E.Y., Gin, S., Jégou, Ch. & Ribet, I. (2001): Present understanding of R7T7 glass alteration kinetics and their impact on long-term behavior modeling. J. Nucl. Mat. 298, 27-36

Vernaz, E.Y. & Godon, N. (1991): Leaching of actinides from nuclear waste glass: French experience. Mat. Res. Soc. Symp. Proc. Vol. 257, 37-48

Verney-Carron, A., Gin, S. & Libourel, G. (2008): A fractured roman glass block altered for 1800 years in seawater: Analogy with nuclear waste glass in a deep geological repository. Geochim. Cosmochim. Acta 72, 5372-5385

Vienna, J.D., Neeway, J.J., Ryan, J.V. & Kerisit, S.N. (2018): Impacts of glass composition, pH, and temperature on glass forward dissolution rate. npj Materials Degradation 2:22

Vogel, W. (1979): Glaschemie, 2nd edition, VEB Deutscher Verlag für Grundstoffindustrie, Leipzig

Warren, B.E. (1933): X-ray diffraction of vitreous silica. Z. kristallogr. Mineral. Petrogr. 86, 349

Weber, W.J., Ewing, R.C., Angell, C.A., Arnold, G.W., Cormack, A.N., Delaye, J.M., Griscom, D.L., Hobbs, L.W., Navrotsky, A., Price, D.L., Stoneham, A.M. & Weinberg, M.C. (1997): Radiation effects in glasses used for immobilization of high-level waste and plutonium disposition, J. Mater. Res. 12(8), 1946-1978

Werme, L., Björner, I.K., Bart, G., Zwicky, H.U., Grambow, B., Lutze, W., Ewing, R.C. & Magrabi, C. (1990): Chemical corrosion of highly radioactive borosilicate nuclear waste glass under simulated repository conditions, J. Mater. Res. 5 (5), 1130–1146

Wicks, G.G. (1986): Nuclear Waste Vitrification – The Geology Connection. J. Non-Crystalline Solids 84, 241-250

Wicks, G.G., Lodding, A.R. & Molecke, M.A. (1993): Aqueous alteration of nuclear waste glasses and metal package components, MRS Bulletin XVIII(9), 32-39

Wyrzykowski, M., Lurà, P. & Martin, L. (2019): Cementitious backfill for a high level waste repository: Assessment of the mechanical feasibility of the concept. Nagra Arbeitsbericht NAB 19-47

Zachariasen, W.J. (1932): The atomic arrangement in glass. J. Am. Ceram. Soc. 54, 3841-3851

Zwicky, H.U., Graber, Th. & Keil R. (1992): Versuche zur Bestimmung der Langzeitkorrosionsrate von Alkaliborosilicatglass: Zwischenbericht, TM-43-92-26, Paul Scherrer Institut

Zwicky, H.U., Grambow, B., Magrabi, C., Aerne, E.T., Bradley, R., Barnes, B., Graber, Th., Mohos, M. & Werme, L.O. (1989): Corrosion behaviour of British Magnox Waste glass in pure water. Mat. Res. Soc. Symp. Proc. Vol. 127, 129-136